# Single-ion and exchange anisotropy effects and multiferroic behavior in high-symmetry tetramer single-molecule magnets

Richard A. Klemm[1,*] and Dmitri V. Efremov[2,†]
[1]*Department of Physics, University of Central Florida, Orlando, Florida 32816, USA*
[2]*Institut für Theoretische Physik, Technische Universität Dresden, 01062 Dresden, Germany*
(Received 26 April 2007; revised manuscript received 29 February 2008; published 12 May 2008)

We study single-ion and exchange anisotropy effects in equal-spin $s_1$ tetramer single-molecule magnets exhibiting $T_d$, $D_{4h}$, $D_{2d}$, $C_{4h}$, $C_{4v}$, or $S_4$ ionic site point group symmetry. We first write the group-invariant quadratic single-ion and symmetric anisotropic exchange Hamiltonians in the appropriate local coordinates. We then rewrite these local Hamiltonians in the molecular or laboratory representation, along with the group-invariant Dzyaloshinskii-Moriya (DM) and isotropic Heisenberg, biquadratic, and three-center quartic Hamiltonians. Using our exact, compact forms for the single-ion spin matrix elements, we analytically evaluate the eigenstate energies to first order in the microscopic anisotropy interactions, corresponding to the strong exchange limit, and provide tables of simple formulas for the anisotropy energies of the lowest four eigenstate manifolds of ferromagnetic (FM) and antiferromagnetic (AFM) tetramers with arbitrary $s_1$. For AFM tetramers, we illustrate the first-order level-crossing inductions for $s_1=1/2$, 1, and $3/2$, and obtain preliminary estimates of the microscopic parameters in a $Ni_4$ from fits to magnetization data, indicating the presence of strong symmetric anisotropic exchange interactions. Accurate analytic expressions for the thermodynamics, electron paramagnetic resonance absorption, and inelastic neutron scattering cross section are given, allowing for a determination of three of the microscopic anisotropy interactions from the second excited state manifold of FM tetramers. We also predict that tetramers with symmetries $S_4$ and $D_{2d}$ should exhibit both DM interactions and multiferroic states, and we illustrate our predictions for $s_1=1/2$ and 1.

DOI: 10.1103/PhysRevB.77.184410 PACS number(s): 75.10.Jm, 75.30.Gw, 75.50.Xx, 75.75.+a

## I. INTRODUCTION

Single molecule magnets (SMM's) have been a topic of great interest for more than a decade[1] because of their potential uses in quantum computing and/or magnetic storage,[2] which are possible due to magnetic quantum tunneling (MQT) and entangled states. In fits to a wealth of data, the Hamiltonian within a SMM cluster was assumed to be the Heisenberg exchange interaction plus weaker total (global or giant) spin anisotropy interactions, with a fixed overall total spin quantum number $s$.[1] MQT and entanglement were only studied in this simple model.

The simplest SMM clusters are dimers.[3–5] Two antiferromagnetic (AFM) dimers, an $Fe_2$, $[Fe(salen)Cl]_2$, where salen is $N,N'$-ethylenebis(salicylideneiminato), and a $Ni_2$, $Na_2Ni_2(C_2O_4)_3(H_2O)_2$, appear to have substantial single-ion anisotropy without any appreciable total spin anisotropy.[4–7] Although the most common SMM clusters have ferromagnetic (FM) intramolecular interactions and contain $n \geqslant 8$ magnetic ions,[8,9] a number of intermediate-sized FM SMM clusters with $n=4$ and rather simple molecular structures were recently studied. Fits to electron paramagnetic resonance (EPR) $Ni_4$ data assuming a fixed $s$ were also problematic, suggesting single-ion or exchange anisotropy in that tetramer, as well.[10,11] The $Cu_4$ tetramer $Cu_4OCl_6(TPPO)_4$, where TPPO is triphenylphosphine oxide, has four spin $1/2$ ions on the corners of a regular tetrahedron, with a $s=2$ ground state and approximate $T_d$ symmetry.[12–14] In this case, there are no single-ion anisotropy effects, but anisotropic symmetric exchange interactions were thought to be responsible for the zero-field energy splittings.[12,15] The $Co_4$, $Co_4(hmp)_4(MeOH)_4Cl_4$, where hmp is hydroxymethylpyridyl, and $Cr_4$, $[Cr_4S(O_2CCH_3)_8(H_2O)_4](NO_3)_2\cdot H_2O$, compounds have $s=6$ ground states with spin $3/2$ ions on the corners of tetrahedrons.[16,17] Those compounds have $S_4$ and approximate $D_{2d}$ symmetry, respectively.[16,17] A number of high symmetry $s=4$ ground state $Ni_4$ structures with spin 1 ions were reported.[18–22] Two of these, $[Ni(hmp)(ROH)Cl]_4$, where $R$ is an alkyl group, such as methyl, ethyl, or 3,3-dimethyl-1-butyl, and hmp is 2-hydroxymethylpyridyl, form tetramers with precise $S_4$ group symmetry.[21,22] Two others, $Ni_4(ROH)L_4$, where $R$ is methyl or ethyl and $H_2L$ is salicylidene-2-ethanolamine, had approximate $S_4$ symmetry, although the precise symmetry was only $C_1$.[18] Several planar $Mn_4$ compounds with the $Mn^{+3}$ spin 2 ions on the corners of squares were made, with overall $s=8$ tetramer ground states.[23] Although two of these complexes had only approximate $S_4$ symmetry, one of these complexes, $Mn_4Cl_4(L')_4$, where $H_2L'$ is 4-$t$-butyl-salicylidene-2-ethanolamine, had perfect $S_4$ symmetry.[23] Inelastic neutron scattering (INS) experiments provided strong evidence for single-ion anisotropy in $Co_4$ and $Ni_4$ with approximate $S_4$ symmetry.[17,18]

We note that *ab initio* calculations of the intracluster spin-spin interactions in SMM clusters have not been always successful in accurately calculating even the strongest intracluster isotropic Heisenberg interactions and have been incapable of calculating any of the local anisotropic spin-spin interactions within a SMM cluster.[24–26] To accurately obtain the Heisenberg interactions, it seems one needs to extend the local spin-density approximation to include on-site repulsions with strength $U$, which would have to be phenomenologically introduced to fit the lowest two energy level manifolds in zero applied magnetic field.[26–30]

 

Further descriptions of magnetic clusters are based upon two concepts. The simplest and most common one is to treat the SMM cluster as having a fixed total spin value, and to describe its properties solely in terms of anisotropies of the total spin. The various anisotropy parameters in the model are chosen phenomenologically for each individual experiment on the same material, so we denote this approach phenomenological. The second approach is to project the magnetism within the cluster onto its constituent localized individual spins, with local anisotropies of the individual spins arising from their individual local environments, and anisotropic Heisenberg interactions between the individual spins. We characterize this individual spin approach as microscopic in order to distinguish it from the phenomenological one. Our description of a microscopic model is analogous to the standard model of quantum chromodynamics for the interactions of quarks and gluons within a hadron.

Recently, there have been microscopic treatments of dimers,[4,5] trimers, and tetramers, including Zeeman $g$-tensor anisotropy, single-ion anisotropy, and anisotropic exchange interactions.[31] Most of those treatments and their recent extensions to more general systems expressed the single-spin matrix elements only in terms of Wigner $3j$, $6j$, and $9j$ symbols.[31,32] While such treatments are very helpful in fitting experimental data, more compact analytic forms are desirable to study microscopic models of FM SMM clusters, in which the MQT and entanglement issues crucial for quantum computing can be understood. We constructed the quadratic single-ion and anisotropic near-neighbor (NN) and next-nearest-neighbor (NNN) exchange SMM cluster Hamiltonians from the respective local axial and azimuthal vector groups for equal-spin tetramer SMM clusters with ionic site point group (ISPG) symmetries $g=T_d$, $D_{4h}$, $D_{2d}$, $C_{4h}$, $C_{4v}$, and $S_4$, and we found compact analytic expressions for the single-spin matrix elements of four general spins. We then impose the ISPG symmetry operations for each $g$. The resulting Hamiltonian in the molecular representation contains both site-independent and site-dependent single-ion and exchange anisotropy interactions for each $g$. We then show that for ISPG $D_{2d}$ and $S_4$ symmetries, the antisymmetric exchange interactions lead to nonvanishing spin currents that may be accompanied by electric polarizations, leading to multiferroic effects. We evaluate the magnetization, specific heat, EPR transitions, and INS cross section in the self-consistent Hartree approximation (or strong-exchange limit) and provide a procedure for extracting three of the effective site-independent microscopic parameters using EPR. We also show analytically how to include the effects of weak biquadratic and three-center quartic isotropic exchange.

An outline of the paper is as follows. In Sec. II, we discuss the six structures and the general quadratic spin Hamiltonian. In Sec. III, we write the single-ion and symmetric anisotropic exchange Hamiltonians in terms of local coordinates, and the antisymmetric exchange Hamiltonian in molecular coordinates. In Sec. IV, we impose the operations of the six ISPG symmetries and discuss the effects of antisymmetric anisotropic exchange interactions and the related electric polarizations in lower symmetry systems. In Sec. V, the resulting ISPG-invariant Hamiltonians are written in the molecular representation, and the isotropic biquadratic and three-center quartic exchange interactions are introduced. Section VI contains the eigenstates of the full Hamiltonian to first order in the anisotropy and NN biquadratic and three-center quartic exchange interactions. These eigenstates are used to obtain the level-crossing inductions for AFM tetramers, and particular examples with $s_1=1/2$, 1, and $3/2$ are presented. In Sec. VI, we also evaluate quantitatively some effects of antisymmetric anisotropic exchange and provide our related predictions for multiferroic behavior. In Sec. VII, the self-consistent Hartree approximation is used to provide simple but accurate results for the thermodynamics, EPR resonant inductions, and INS cross sections and describe how EPR experiments in the excited states of FM tetramers can provide a measure of some of the microscopic anisotropy interaction strengths. Finally, in Sec. VIII, we discuss the significance of our results and provide preliminary fits to the magnetization data on an AFM $Ni_4$ tetramer, and in Sec. IX, we present our conclusions.

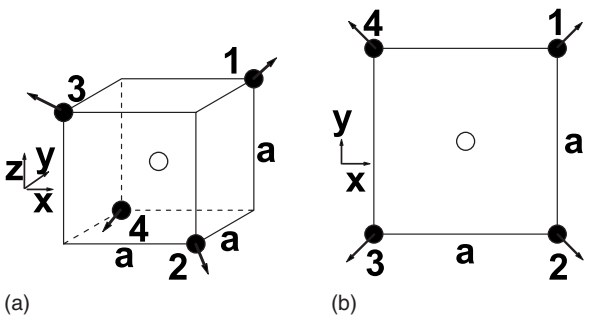


FIG. 1. $T_d$ (left) and $D_{4h}$ (right) ion sites (filled). Circle, origin; arrows, local axial $\hat{z}_n^{T_d}$ (left) and azimuthal $\hat{x}_n^{D_{4h}}$ (right) single-ion vectors. The axial vectors $\hat{z}_n^{D_{4h}}=\hat{z}$, normal to the ionic plane.

## II. STRUCTURES AND BARE HAMILTONIAN

For SMM clusters with ISPG $g=T_d$ or $D_{4h}$, we assume that the four equal-spin $s_1$ ions sit on opposite corners of a cube or square of side $a$, as pictured in Fig. 1. For clusters with $g=D_{2d}$ and $S_4$, we take the ions to sit on opposite corners of a tetragonal prism with sides $(a,a,c)$, as in Fig. 2. The ions for $g=C_{4h}$ and $C_{4v}$ also sit on the corners of a square of side $a$, as pictured in Fig. 3, but the attached

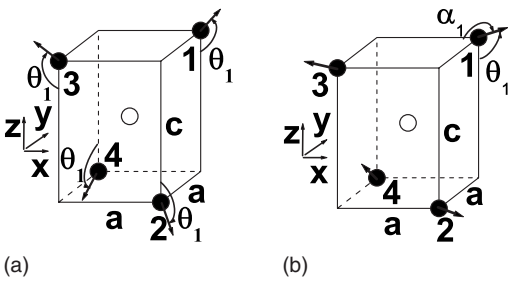


FIG. 2. $D_{2d}$ (left) and $S_4$ (right) ion sites (filled). Circle, origin; arrows, local axial single-ion vectors. The $g=D_{2d}$ and $S_4$ axial vectors $\hat{z}_1^g$ make the angles $\theta_1^g$ with the $z$ axis, and the $S_4$ axial vector $\hat{z}_1^{S_4}$ also makes an angle $\alpha_1$ with the $x$ axis, where $\cos\alpha_1=\sin\theta_1^{S_4}\cos\phi_1^{S_4}$.

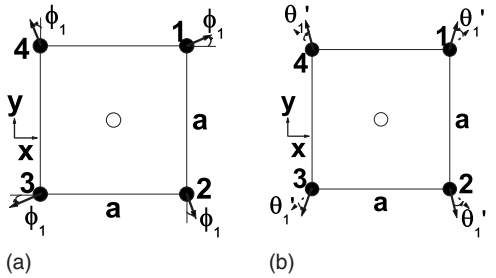


FIG. 3. $C_{4h}$ (left) and $C_{4v}$ (right) ion sites (filled). Circle, origin; arrows, local azimuthal $\hat{\boldsymbol{x}}_n^{C_{4h}}$ (left) and axial $\hat{\boldsymbol{z}}_n^{C_{4v}}$ (right) single-ion vectors. The axial vectors $\hat{\boldsymbol{z}}_n^{C_{4h}}=\hat{\boldsymbol{z}}$. The $C_{4v}$ axial vectors each make the angle $\theta_1=\pi/2-\theta_1'$ with the $z$ axis. The dotted arrows (equivalent to the $D_{4h}$ azimuthal single-ion vectors $\hat{\boldsymbol{x}}_n^{D_{4h}}$) are their projections in the $xy$ plane.

ligands have symmetries different from that of the simpler $D_{4h}$ case pictured in Fig. 1.[33] In each case, we take the origin to be at the geometric center, so that $\Sigma_{n=1}^4 \boldsymbol{r}_n=0$, where the relative ion site vectors are

$$\boldsymbol{r}_n=\frac{a}{\sqrt{2}}\left[\sin\left(\frac{(2n-1)\pi}{4}\right)\hat{\boldsymbol{x}}+\cos\left(\frac{(2n-1)\pi}{4}\right)\hat{\boldsymbol{y}}\right]-\frac{c}{2}(-1)^n\hat{\boldsymbol{z}}. \tag{1}$$

Tetrahedrons with $g=T_d$ and $c/a=1$, approximately as in $Cu_4$,[12] are a four-spin example of the equivalent-neighbor model.[34] In squares with $g=D_{4h}$, $C_{4h}$, or $C_{4v}$, $c=0$. The high $D_{4h}$ symmetry is approximately exhibited by the square $Nd_4$ compound, $Nd_4(OR)_{12}$, where $R$ is 2,2-dimethyl-1-propyl, in which the $Nd^{+3}$ ions have equal total angular momentum $j=9/2$.[35,36] We note that the $Mn_4$ clusters with approximate or exact $S_4$ symmetry also have $c=0$.[23] In tetragonal prisms with $g=D_{2d}$ or $S_4$, $c/a>1$, approximately as in $Co_4$,[17] or $c/a<1$, as in some $Mn_4$ and $Ni_4$.[19,23] For a comparison with the planar symmetries $g=C_{4h}$, $D_{4h}$, and $D_{4v}$, we assume for $g=D_{2d}$ and $S_4$ that $c/a<1$, so that there are four NN bonds and two NNN bonds. For each $g$, $\hat{\boldsymbol{x}}$, $\hat{\boldsymbol{y}}$, and $\hat{\boldsymbol{z}}$ are the molecular (or laboratory) unit coordinate axis vectors.

The most general Hamiltonian quadratic in the four individual spin operators $\boldsymbol{S}_n$ may be written for ISPG $g$ as

$$\mathcal{H}^g=-\mu_B\sum_{n=1}^4 \boldsymbol{B}\cdot\overleftrightarrow{\boldsymbol{g}}_n^g\cdot\boldsymbol{S}_n+\sum_{n,n'=1}^4 \boldsymbol{S}_n\cdot\overleftrightarrow{\boldsymbol{D}}_{n,n'}^g\cdot\boldsymbol{S}_{n'}, \tag{2}$$

where $\mu_B$ is the Bohr magneton and $\boldsymbol{B}=B(\sin\theta\cos\phi,\sin\theta\sin\phi,\cos\theta)$ is the magnetic induction at an arbitrary direction $(\theta,\phi)$ relative to the molecular coordinates $(\hat{\boldsymbol{x}},\hat{\boldsymbol{y}},\hat{\boldsymbol{z}})$.[31,37]

For simplicity, we take $\overleftrightarrow{\boldsymbol{g}}_n^g$ to be diagonal, isotropic, and site independent, so that the Zeeman interaction may be written in terms of a single gyromagnetic ratio $\gamma\approx 2\mu_B$. Thus, in the following, $g$ only refers to the ISPG. We separate $\overleftrightarrow{\boldsymbol{D}}_{n,n'}^g$ into its symmetric and antisymmetric parts, $\overleftrightarrow{\boldsymbol{D}}_{n,n'}^g=\overleftrightarrow{\boldsymbol{D}}_{n,n'}^{g,s}+\overleftrightarrow{\boldsymbol{D}}_{n,n'}^{g,a}$, respectively. For $n'=n$, the single-ion $\overleftrightarrow{\boldsymbol{D}}_{n,n}^g$ is necessarily symmetric, so $\overleftrightarrow{\boldsymbol{D}}_{n,n}^{g,a}=0$. For each $g$, the four $\overleftrightarrow{\boldsymbol{D}}_{n,n}^{g,s}$ contain the local single-ion structural information, and the six distinct symmetric $\overleftrightarrow{\boldsymbol{D}}_{n,n'}^{g,s}$ contain the local symmetric exchange structural information, which lead to the isotropic, or Heisenberg, exchange interactions, and the remaining symmetric anisotropic exchange interactions. The six distinct antisymmetric $\overleftrightarrow{\boldsymbol{D}}_{n,n'}^{g,a}$ contain additional local structural information, which lead to the Dzyaloshinskii-Moriya (DM) interactions.[38,39] Physically, the symmetric anisotropic exchange interactions also contain the intracluster dipole-dipole interactions, which can even be larger in magnitude than the terms originating from actual anisotropic exchange.[37,40]

As is well known, each of the symmetric rank-3 tensors (or matrices) $\overleftrightarrow{\boldsymbol{D}}_{n,n'}^g$ can be diagonalized by three rotations: a rotation by the angle $\phi_{n,n'}^g$ about the molecular $z$ axis, then a rotation by the angle $\theta_{n,n'}^g$ about the rotated $\tilde{x}$ axis, followed by a rotation by the angle $\psi_{n,n'}^g$ about the rotated $\tilde{z}$ axis.[41] This necessarily leads to the three principal axes $\hat{\tilde{\boldsymbol{x}}}_{n,n'}^g$, $\hat{\tilde{\boldsymbol{y}}}_{n,n'}^g$, and $\hat{\tilde{\boldsymbol{z}}}_{n,n'}^g$. For the single-ion axes with $n'=n$, we denote these principal axes to be $\hat{\tilde{\boldsymbol{x}}}_n^g$, $\hat{\tilde{\boldsymbol{y}}}_n^g$, and $\hat{\tilde{\boldsymbol{z}}}_n^g$, respectively, which are explicitly written in Sec. III. The nonvanishing matrix elements in these locally diagonalized symmetric matrices $\overleftrightarrow{\tilde{\boldsymbol{D}}}_{n,n'}^{g,s}$ are $\tilde{D}_{n,n',xx}^{g,s}$, $\tilde{D}_{n,n',yy}^{g,s}$, and $\tilde{D}_{n,n',zz}^{g,s}$. The local environmental information is contained in these diagonalized matrix elements and in the local principal axis basis, so that in the absence of ISPG symmetry, each of them would, in principle, be different from one another.

Although an antisymmetric exchange matrix $\overleftrightarrow{\boldsymbol{D}}_{n,n'}^{g,a}$ can generally be diagonalized by a unitary transformation, it contains at most three independent real parameters that can be incorporated into the components of a three-vector, $\boldsymbol{d}_{n,n'}^g$, with an effective spin-spin interaction of the form $\boldsymbol{d}_{n,n'}^g\cdot(\boldsymbol{S}_n\times\boldsymbol{S}_{n'})$.[38,39] This is easiest to write in the molecular representation.

For the six high-symmetry clusters under study, we analyze the effects of ISPG symmetry on the single-ion and anisotropic exchange parts of $\mathcal{H}^g$. The ISPG symmetries further restrict the number of independent parameters.

## III. SINGLE-ION AND EXCHANGE HAMILTONIANS

To take account of the ISPG $g$ symmetries, it is useful to write the single-ion and symmetric anisotropic exchange interactions in terms of the local coordinates of the individual spins. In this section, we write the local Hamiltonian for these interactions and the cluster Hamiltonian for the antisymmetric exchange interactions. In Sec. IV, we then impose the ISPG symmetries on these interactions for $g=C_{4h}$, $D_{4h}$, $C_{4v}$, $S_4$, $D_{2d}$, and $T_d$, respectively.

### A. Single-ion Hamiltonian

For the single-ion anisotropy, the single-ion principal axis basis for the $n$th site is $\{\hat{\tilde{\boldsymbol{x}}}_n^g,\hat{\tilde{\boldsymbol{y}}}_n^g,\hat{\tilde{\boldsymbol{z}}}_n^g\}$ for each $g$. These basis elements are the vectors that diagonalize the single-ion ma-

trix from $\overleftrightarrow{\boldsymbol{D}}^{g}_{n,n}$ to $\overleftrightarrow{\tilde{\boldsymbol{D}}}^{g}_{n,n}$.[41] Since we repeatedly employ these vectors, we write them here for simplicity of presentation. The diagonalized vector set elements may be written in the molecular $(\hat{\boldsymbol{x}},\hat{\boldsymbol{y}},\hat{\boldsymbol{z}})$ representation as

$$\hat{\tilde{\boldsymbol{x}}}^{g}_{n}=\begin{pmatrix}\cos\phi^{g}_{n}\cos\psi^{g}_{n}-\cos\theta^{g}_{n}\sin\phi^{g}_{n}\sin\psi^{g}_{n}\\ \sin\phi^{g}_{n}\cos\psi^{g}_{n}+\cos\theta^{g}_{n}\cos\phi^{g}_{n}\sin\psi^{g}_{n}\\ \sin\theta^{g}_{n}\sin\psi^{g}_{n}\end{pmatrix}, \tag{3}$$

$$\hat{\tilde{\boldsymbol{y}}}^{g}_{n}=\begin{pmatrix}-\cos\phi^{g}_{n}\sin\psi^{g}_{n}-\cos\theta^{g}_{n}\sin\phi^{g}_{n}\cos\psi^{g}_{n}\\ -\sin\phi^{g}_{n}\sin\psi^{g}_{n}+\cos\theta^{g}_{n}\cos\phi^{g}_{n}\cos\psi^{g}_{n}\\ \sin\theta^{g}_{n}\cos\psi^{g}_{n}\end{pmatrix}, \tag{4}$$

$$\hat{\tilde{\boldsymbol{z}}}^{g}_{n}=\begin{pmatrix}\sin\theta^{g}_{n}\sin\phi^{g}_{n}\\ -\sin\theta^{g}_{n}\cos\phi^{g}_{n}\\ \cos\theta^{g}_{n}\end{pmatrix}, \tag{5}$$

which satisfy $\hat{\tilde{\boldsymbol{x}}}^{g}_{n}\times\hat{\tilde{\boldsymbol{y}}}^{g}_{n}=\hat{\tilde{\boldsymbol{z}}}^{g}_{n}$. We then write the most general quadratic single-ion anisotropy interaction as

$$\mathcal{H}^{g,\ell}_{si}=-\sum_{n=1}^{4}\{J^{g}_{a,n}(\boldsymbol{S}_{n}\cdot\hat{\tilde{\boldsymbol{z}}}^{g}_{n})^{2}+J^{g}_{e,n}[(\boldsymbol{S}_{n}\cdot\hat{\tilde{\boldsymbol{x}}}^{g}_{n})^{2}-(\boldsymbol{S}_{n}\cdot\hat{\tilde{\boldsymbol{y}}}^{g}_{n})^{2}]\} \tag{6}$$

in terms of the single-ion principal axis basis and the site-dependent axial and azimuthal interactions,

$$J^{g}_{a,n}=(\tilde{D}^{g,s}_{n,n,xx}+\tilde{D}^{g,s}_{n,n,yy})/2-\tilde{D}^{g,s}_{n,n,zz}, \tag{7}$$

$$J^{g}_{e,n}=(\tilde{D}^{g,s}_{n,n,yy}-\tilde{D}^{g,s}_{n,n,xx})/2, \tag{8}$$

respectively, which are analogous in notation to that for homoionic dimers.[4,5] In Eq. (6), we dropped the irrelevant constant $s_1(s_1+1)\Sigma_{n=1}^{4}\mathrm{Tr}\,\overleftrightarrow{\tilde{\boldsymbol{D}}}^{g,s}_{n,n}$.

### B. Symmetric exchange Hamiltonian

In addition to the single-ion interactions, the other microscopic quadratic interactions are the exchange interactions, which include the intracluster dipole-dipole interactions.[40] The intercluster dipole-dipole interactions can lead to low-$T$ hysteresis in the phenomenological total spin model,[42] but are generally much weaker than the intracluster ones in the microscopic individual spin model, due to the larger distances involved. Hence, we neglect those and all other intercluster interactions, such as those mediated by phonons.

As for the single-ion interactions, diagonalization of $\overleftrightarrow{\boldsymbol{D}}^{g,s}_{n,n'}$ leads to $\overleftrightarrow{\tilde{\boldsymbol{D}}}^{g,s}_{n,n'}$ and the principal axis bases $\{\hat{\tilde{\boldsymbol{x}}}^{g}_{n,n'},\hat{\tilde{\boldsymbol{y}}}^{g}_{n,n'},\hat{\tilde{\boldsymbol{z}}}^{g}_{n,n'}\}$, given by Eqs. (3)–(5) with the subscript $n$ replaced by $n,n'$, where $n'\neq n$. The bare quadratic Hamiltonian $\mathcal{H}^{g}_{0}$ is given by the Zeeman and the isotropic part of the exchange interactions,

$$\mathcal{H}^{g}_{0}=-\gamma\boldsymbol{B}\cdot\boldsymbol{S}-\sum_{n,n'=1}^{4}J_{g,n,n'}\boldsymbol{S}_{n}\cdot\boldsymbol{S}_{n'}, \tag{9}$$

where $n'\neq n$ and

$$J_{g,n,n'}=-\mathrm{Tr}\,\overleftrightarrow{\tilde{\boldsymbol{D}}}^{g,s}_{n,n'}. \tag{10}$$

For these isotropic terms, we may impose the ISPG symmetries by inspection. For $g=D_{2d}$, $S_4$, $C_{4v}$, $C_{4h}$, and $D_{4h}$ symmetries,

$$J_{g}=2J_{g,n,n+1}, \tag{11}$$

$$J'_{g}=2J_{g,n,n+2} \tag{12}$$

are independent of $n$. For our $c/a<1$ convention, $-J_g$ and $-J'_g$ are the NN and NNN Heisenberg (isotropic) exchange interactions. Equation (9) can then be rewritten as

$$\mathcal{H}^{g}_{0}=-\frac{J_{g}}{2}\boldsymbol{S}^{2}-\gamma\boldsymbol{B}\cdot\boldsymbol{S}-\frac{(J'_{g}-J_{g})}{2}(\boldsymbol{S}^{2}_{13}+\boldsymbol{S}^{2}_{24}), \tag{13}$$

where $\boldsymbol{S}_{13}=\boldsymbol{S}_1+\boldsymbol{S}_3$, $\boldsymbol{S}_{24}=\boldsymbol{S}_2+\boldsymbol{S}_4$, and $\boldsymbol{S}=\boldsymbol{S}_{13}+\boldsymbol{S}_{24}$ is the total spin operator,[36] and we dropped the irrelevant overall constant $2J'_{g}s_1(s_1+1)$. In Eq. (13), $J'_{T_d}=J_{T_d}$, but for $g=D_{2d}$, $S_4$, $D_{4h}$, $C_{4h}$, and $C_{4v}$, $J'_{g}\neq J_{g}$.

In terms of the individual spin operators, the symmetric anisotropic exchange Hamiltonian $\mathcal{H}^{g,\ell}_{ae}$ is then given by

$$\begin{aligned}\mathcal{H}^{g,\ell}_{ae}=-\sum_{q=1}^{2}\sum_{n=1}^{6-2q}\{&J^{f,g}_{n,n+q}(\boldsymbol{S}_{n}\cdot\hat{\tilde{\boldsymbol{z}}}^{g}_{n,n+q})(\boldsymbol{S}_{n+q}\cdot\hat{\tilde{\boldsymbol{z}}}^{g}_{n,n+q})\\&+J^{c,g}_{n,n+q}[(\boldsymbol{S}_{n}\cdot\hat{\tilde{\boldsymbol{x}}}^{g}_{n,n+q})(\boldsymbol{S}_{n+q}\cdot\hat{\tilde{\boldsymbol{x}}}^{g}_{n,n+q})\\&-(\boldsymbol{S}_{n}\cdot\hat{\tilde{\boldsymbol{y}}}^{g}_{n,n+q})(\boldsymbol{S}_{n+q}\cdot\hat{\tilde{\boldsymbol{y}}}^{g}_{n,n+q})]\},\end{aligned} \tag{14}$$

where we define $\boldsymbol{S}_5\equiv\boldsymbol{S}_1$, as if the four spins were on a ring. In Eq. (14), the axial and azimuthal interaction strengths are

$$J^{f,g}_{n,n'}=\tilde{D}^{g,s}_{n,n',xx}+\tilde{D}^{g,s}_{n,n',yy}-2\tilde{D}^{g,s}_{n,n',zz}, \tag{15}$$

$$J^{c,g}_{n,n'}=\tilde{D}^{g,s}_{n,n',yy}-\tilde{D}^{g,s}_{n,n',xx}, \tag{16}$$

as for the single-ion interaction strengths. The subscripts $a,e$ and superscripts $f,c$ correspond to our dimer notation.[5]

### C. Antisymmetric anisotropic exchange Hamiltonian

As noted above, we write the antisymmetric anisotropic exchange, or DM,[38,39] Hamiltonian $\mathcal{H}^{g}_{DM}$ in the following molecular representation:[37]

$$\mathcal{H}^{g}_{DM}=\sum_{q=1}^{2}\sum_{n=1}^{6-2q}\boldsymbol{d}^{g}_{n,n+q}\cdot(\boldsymbol{S}_{n}\times\boldsymbol{S}_{n+q}). \tag{17}$$

We note that in these molecular coordinates, the DM interaction three-vectors $\boldsymbol{d}^{g}_{n,n+q}$ explicitly depend on the exchange bond indices $n,n+q$ for each ISPG $g$. We then employ the ISPG symmetries to relate them to one another.

The rules for the directions of the $\boldsymbol{d}^{g}_{n,n+q}$ were given by Moriya[38] and were employed for a dimer example by Ben-

cini and Gatteschi.[37] The Moriya rules are as follows: (1) $\boldsymbol{d}^g_{n,n'}$ vanishes if a center of inversion connects $\boldsymbol{r}_n$ and $\boldsymbol{r}_{n'}$. (2) When a mirror plane contains $\boldsymbol{r}_n$ and $\boldsymbol{r}_{n'}$, $\boldsymbol{d}^g_{n,n'}$ is normal to the mirror plane. (3) When a mirror plane is the perpendicular bisector of $\boldsymbol{r}_n-\boldsymbol{r}_{n'}$, $\boldsymbol{d}^g_{n,n'}$ lies in the mirror plane. (4) When a twofold rotation axis is the perpendicular bisector of $\boldsymbol{r}_n-\boldsymbol{r}_{n'}$, then $\boldsymbol{d}^g_{n,n'}$ is orthogonal to the rotation axis. (5) When $\boldsymbol{r}_n-\boldsymbol{r}_{n'}$ is an $r$-fold rotation axis with $r>2$, then $\boldsymbol{d}^g_{n,n'}$ is parallel to $\boldsymbol{r}_n-\boldsymbol{r}_{n'}$. As noted above, we shall incorporate these rules in the molecular representation. For example, in $NaV_2O_5$, the lack of inversion symmetry between interacting spins has been shown to lead to a DM interaction.[43]

## IV. GROUP SYMMETRY INVARIANCE

### A. General considerations

In this section, we impose the set of allowed ISPG $g$ symmetry operations on the full Hamiltonian $\mathcal{H}^g$. For the six $g$ cases under study, the set $\mathcal{O}^g$ of ISPG operations greatly reduces the number of single-ion and symmetric anisotropic exchange parameters. As we shall see, for each $g$, these reduce the single-ion and symmetric anisotropic exchange interaction strength set to

$$\{J^g_j\} \equiv \{J^g_a, J^g_e, J^g_{f,q}, J^g_{c,q}\}, \tag{18}$$

for $q=1$ and 2, which are independent of the site index $n$. That is, for each $g$, there are at most two single-ion, two NN, and two NNN symmetric anisotropic exchange interaction strengths. In addition, for these six $g$ cases, the ISPG operations further limit the number of vector set parameters to

$$\mu^g_1 = \{\theta^g_1, \phi^g_1, \psi^g_1\}, \tag{19}$$

$$\mu^g_{1p} = \{\theta^g_{1p}, \phi^g_{1p}, \psi^g_{1p}\}, \tag{20}$$

where $p=q+1=2$ and 3, and we used the notation $\theta^g_1=\theta^g_{1,1}$, $\theta^g_{1p}=\theta^g_{1,p}$, etc. Some of these parameters may further be restricted. In addition, however, the molecular single-ion and anisotropic exchange Hamiltonians contain both site-independent and site-dependent terms.

For $\mathcal{H}^g_{DM}$, we first impose the Moriya rules on each anisotropic exchange pair,[37,38] and then impose the required group symmetries on the six pairs. For the six $g$ cases under study, the ISPG symmetries place restrictions on $\boldsymbol{d}^g_{n,n+q}$, leading to the anisotropic exchange parameter set

$$d^g = \{d^g_z, d^g_{x1}, d^g_{y1}, d^g_{x2}, d^g_{y2}\}. \tag{21}$$

For each of the six $g$ cases, the NNN DM parameter set has at least one more restriction than does the NN DM parameter set. Some $g$ symmetries lead to site-dependent signs of the elements of $d^g$.

### B. Imposing the group symmetries

In Appendix A, we describe the complete set of unitary matrices $\mathcal{O}=\{\mathcal{O}_\lambda\}$ for $\lambda=1,\ldots,26$ representing the combined ISPG symmetry operations for $g=C_{4h}$, $D_{4h}$, $C_{4v}$, $S_4$, $D_{2d}$, and $T_d$. For each $g$, the $\lambda$th element $\mathcal{O}^g_\lambda$ of the allowed subset of symmetry operations $\mathcal{O}^g$ commutes with the Hamiltonian, which implies $\mathcal{H}=\mathcal{O}^g_\lambda\mathcal{H}(\mathcal{O}^g_\lambda)^T$, where $(\mathcal{O}^g_\lambda)^{-1}=(\mathcal{O}^g_\lambda)^T$. For a particular $g$ and $\lambda$, $\mathcal{O}^g_\lambda \boldsymbol{r}_n=\boldsymbol{r}_{n'(g,\lambda)}$. We therefore take $\boldsymbol{S}_n=\boldsymbol{S}(\boldsymbol{r}_n)$, so that $\mathcal{O}^g_\lambda \boldsymbol{S}_n=\boldsymbol{S}(\mathcal{O}^g_\lambda \boldsymbol{r}_n)=\boldsymbol{S}(\boldsymbol{r}_{n'(g,\lambda)})=\boldsymbol{S}_{n'(g,\lambda)}$.

We use the simple case of $C_{4h}$ symmetry to illustrate how the symmetry operations are imposed. For $g=C_{4h}$, besides the trivial identity operation, the allowed ISPG operations are clockwise and counterclockwise rotations of $\pi/2$ about the $z$ axis and reflections in the $xy$ plane.[33] These operations are represented respectively by the subset of matrices $\mathcal{O}^{C_{4h}}=\{\mathcal{O}_1,\mathcal{O}_2,\mathcal{O}_6\}$. We first consider the axial part of $\mathcal{H}^{C_{4h},\ell}_{si}$, and set

$$\sum_{n=1}^{4} J^{C_{4h}}_{a,n}(\boldsymbol{S}_n\cdot\hat{\boldsymbol{z}}^{C_{4h}}_n)^2 = \sum_{n=1}^{4} J^{C_{4h}}_{a,n}\mathcal{O}_1(\boldsymbol{S}_n\cdot\hat{\boldsymbol{z}}^{C_{4h}}_n)^2\mathcal{O}_1^T = \sum_{n=1}^{4} J^{C_{4h}}_{a,n}\mathcal{O}_1\boldsymbol{S}_n\cdot(\hat{\boldsymbol{z}}^{C_{4h}}_n)^T\mathcal{O}_1^T\mathcal{O}_1\hat{\boldsymbol{z}}^{C_{4h}}_n\cdot\boldsymbol{S}_n^T\mathcal{O}_1^T, \tag{22}$$

and employ the properties of $\mathcal{O}_1$ that

$$\mathcal{O}_1\boldsymbol{S}_n = \boldsymbol{S}_{n+1}, \tag{23}$$

$$(\hat{\boldsymbol{z}}^{C_{4h}}_n)^T\mathcal{O}_1^T = (-\sin\theta^{C_{4h}}_n\cos\phi^{C_{4h}}_n, -\sin\theta^{C_{4h}}_n\sin\phi^{C_{4h}}_n, \cos\theta^{C_{4h}}_n). \tag{24}$$

Substituting these into the right-hand side of Eq. (22), setting $n\rightarrow n+1$ in the left-hand side, and equating coefficients of $S_{n+1,\alpha}S_{n+1,\beta}$ for $\alpha,\beta=x,y,z$ leads to

$$J^{C_{4h}}_{a,n} = J^{C_{4h}}_{a,n+1} = J^{C_{4h}}_a, \tag{25}$$

$$\theta^{C_{4h}}_n = \theta^{C_{4h}}_{n+1} = \theta^{C_{4h}}_1, \tag{26}$$

$$\phi^{C_{4h}}_n = \phi^{C_{4h}}_{n+1} + \frac{\pi}{2}. \tag{27}$$

There are no further restrictions from $\mathcal{O}_2$. Then, by imposing $\mathcal{O}_6$ symmetry, we have $\mathcal{O}_6\boldsymbol{S}_n=\boldsymbol{S}_n$ and either $\theta^{C_{4h}}_1=\pi/2$ or $\theta^{C_{4h}}_1=0$, both of which lead to an invariance of this part of the Hamiltonian under $\mathcal{O}_6$. We therefore take the easy-axis case, $\theta^{C_{4h}}_1=0$. Carrying out similar transformations on the azimuthal single-ion Hamiltonian leads to

$$J^{C_{4h}}_{e,n} = J^{C_{4h}}_e, \tag{28}$$

$$\chi^{C_{4h}}_n = \phi^{C_{4h}}_n + \psi^{C_{4h}}_n = \chi^{C_{4h}}_{n+1} + \frac{\pi}{2}. \tag{29}$$

We could then choose $\psi^{C_{4h}}_1=0$, leaving one free angle parameter $\phi^{C_{4h}}_1$, as listed in Table I, plus the two interaction strengths $J^{C_{4h}}_a$ and $J^{C_{4h}}_e$.

The symmetric anisotropic exchange Hamiltonian $\mathcal{H}^{C_{4h},\ell}_{ae}$ can be made invariant under the elements of $\mathcal{O}^{C_{4h}}$ in a very similar fashion. The ISPG operations for the other five $g$ symmetries are listed in Appendix A, along with the associated matrices. Our results for the single-ion, symmetric anisotropic exchange, and DM interaction parameters are compiled in Tables I–III.

TABLE I. Lists of the single-ion parameters sets $\mu_1^g$.

| $g$ | $\theta_1^g$ | $\phi_1^g$ | $\psi_1^g$ |
|---|---|---|---|
| $C_{4h}$ | 0 | $\phi_1^g$ | 0 |
| $D_{4h}$ | 0 | $\frac{\pi}{4}$ | 0 |
| $C_{4v}, D_{2d}$ | $\theta_1^g$ | $\frac{3\pi}{4}$ | $-\frac{\pi}{2}$ |
| $S_4$ | $\theta_1^{S_4}$ | $\phi_1^{S_4}$ | $\psi_1^{S_4}$ |
| $T_d$ | $\tan^{-1}\sqrt{2}$ | $\frac{3\pi}{2}$ | 0 |

### C. Induced electric polarizations

As shown by Katsura *et al.*,[44] the spin-orbit interactions between spins at sites $n$ and $n'$ can induce an electric polarization

$$\boldsymbol{P}_{n,n'} \sim \hat{\boldsymbol{r}}_{n,n'} \times (\boldsymbol{S}_n \times \boldsymbol{S}_{n'}), \tag{30}$$

where $\hat{\boldsymbol{r}}_{n,n'}$ is a unit vector directed from site $n$ to site $n'$. In our model, the thermodynamic quantum mechanical ensemble expectations of such polarizations vanish in the absence of DM interactions, but nonvanishing in-plane vector components $\boldsymbol{d}_q^g$ of the $d^g$ DM interaction parameter sets allow them to become finite. Tetramers with the rather low molecular group symmetries $S_4$ and $D_{2d}$ have no overall center of inversion symmetry and contain a complex set of DM interactions. Depending on the polarizability of the attached ligand groups, this may lead to a combined spin-induced electric polarization

$$\boldsymbol{P}_s \propto \frac{1}{2} \sum_{n,n'=1}^{4} \hat{\boldsymbol{r}}_{n,n'} \times \langle \boldsymbol{S}_n \times \boldsymbol{S}_{n'} \rangle, \tag{31}$$

where $\langle \ldots \rangle$ represents the expectation of the quantum mechanical ensemble in the presence of the full Hamiltonian, including the relevant DM interactions.

Besides the direct DM interactions, we predict the possibility of dual, or induced, DM interactions. Although $\boldsymbol{d}_q^g$ DM interactions between individual spin pairs are allowed in tetramers with the lowest $C_{4h}$ and $D_{4h}$ symmetries studied, the group symmetry causes the dipole moments on opposite sides of their square geometries to cancel each other. Although we have not studied this point in detail, tetramers with these symmetries can, in principle, be made to exhibit additional effective DM interactions by the application of an electric field $\boldsymbol{E} \neq 0$.[44,45] Thus, in tetramers with $S_4$, $D_{2d}$, or lower symmetry, a multiferroic effect can occur,[45] in which both DM interactions and $\boldsymbol{P}_s \neq 0$. More generally, multiferroic effects arise in systems such as some dimers, trimers, and tetramers that generally do not have a center of inversion at the midpoints of $\boldsymbol{r}_{n,n'}$.[5]

TABLE II. Lists of the relevant NN ($p=2$) and NNN ($p=3$) parameters sets $\mu_{1p}^g$.

| $g$ | $\theta_{1p}^g$ | $\phi_{1p}^g$ | $\psi_{1p}^g$ |
|---|---|---|---|
| $C_{4h}$ | 0 | $\phi_{1p}^{C_{4h}}$ | 0 |
| $D_{4h}$ | 0 | $\frac{\pi}{4}$ | 0 |
| $C_{4v}$ | 0 | $\frac{(p-2)\pi}{4}$ | 0 |
| $S_4$ | $\theta_{1p}^{S_4}$ | $\phi_{1p}^{S_4}$ | $\psi_{1p}^{S_4}$ |
| $D_{2d}$ | $\theta_{12}^{D_{2d}}\delta_{p,2}+\frac{\pi}{2}\delta_{p,3}$ | $\frac{(-1)^p\pi}{2(p-1)}$ | $\frac{(p-2)\pi}{2}$ |

## V. HAMILTONIAN IN THE MOLECULAR REPRESENTATION

### A. Molecular single-ion Hamiltonian

To make contact with experiment, we use the ISPG symmetries to rewrite $\mathcal{H}_{si}^{g,\ell}$ in the molecular $(\hat{\boldsymbol{x}}, \hat{\boldsymbol{y}}, \hat{\boldsymbol{z}})$ representation,

$$\mathcal{H}_{si}^g = -\sum_n \left[ J_z^g S_{n,z}^2 + (-1)^n J_{xy}^g (S_{n,x}^2 - S_{n,y}^2) + \sum_{\alpha \neq \beta} K_{\alpha\beta}^g(n) S_{n,\alpha} S_{n,\beta} \right], \tag{32}$$

where $\alpha, \beta = x, y, z$, and we subtracted an irrelevant constant. $\mathcal{H}_{si}^g$ contains the site-independent interaction strength $J_z^g$ and the site-dependent interaction strengths $(-1)^n J_{xy}^g$ and $K_{\alpha\beta}^g(n)$, which are written in terms of the parameter sets $\mu_1^g$ in Appendix B. Most important is the result that for $T_d$ symmetry,

$$J_z^{T_d} = 0. \tag{33}$$

The first-order contributions to the eigenstate energies from the site-dependent interaction strengths $(-1)^n J_{xy}^g$ and $K_{\alpha\beta}^g(n)$ vanish. Hence, these interactions only contribute to the eigenstate energies to second and higher orders in the interaction strengths $J_a^g$ and $J_e^g$. For $C_{4v}$, $D_{2d}$, and $S_4$, the effective axial site-independent interaction strength $J_z^g$ arises from a combination of the local axial and azimuthal interaction strengths $J_a^g$ and $J_e^g$. For $g \neq T_d$, $J_z^g$ can be large, even if the ISPG is nearly $T_d$.

TABLE III. List of the DM parameter sets $d^g$.

| $g$ | $d_z^g$ | $d_{x1}^g$ | $d_{y1}^g$ | $d_{x2}^g$ | $d_{y2}^g$ |
|---|---|---|---|---|---|
| $C_{4h}, D_{4h}$ | $d_z^g$ | 0 | 0 | 0 | 0 |
| $S_4$ | $d_z^{S_4}$ | $d_{x1}^{S_4}$ | $d_{y1}^{S_4}$ | $d_{x2}^{S_4}$ | $d_{y2}^{S_4}$ |
| $D_{2d}$ | $d_z^{D_{2d}}$ | 0 | $d_{y1}^{D_{2d}}$ | $d_{x2}^{D_{2d}}$ | 0 |
| $T_d, C_{4v}$ | 0 | 0 | 0 | 0 | 0 |

### B. Symmetric anisotropic exchange in the molecular representation

We then construct the group-invariant symmetric anisotropic exchange Hamiltonian in the molecular coordinates for the six ISPG $g$ symmetries. For $g=D_{2d}$ and $S_4$, there are renormalizations of the isotropic exchange interactions, modifying $\mathcal{H}_0^g$ to

$$\mathcal{H}_0^{g,r} = -\frac{\tilde{J}_g}{2}\boldsymbol{S}^2 - \boldsymbol{\gamma B}\cdot\boldsymbol{S} - \frac{(\tilde{J}'_g - \tilde{J}_g)}{2}(\boldsymbol{S}_{13}^2 + \boldsymbol{S}_{24}^2), \quad (34)$$

where

$$\tilde{J}_g = J_g + \delta J_g, \quad (35)$$

$$\tilde{J}'_g = J'_g + \delta J'_g, \quad (36)$$

where $J_g$ and $J'_g$ are given by Eqs. (11) and (12), and $\delta J_g$ and $\delta J'_g$ are given in terms of the parameters sets $\mu_{1p}^g$ in Appendix C. For the three planar ISPG symmetries, $g=C_{4h}$, $D_{4h}$, and $C_{4v}$, $\delta J_g=\delta J'_g=0$. For $T_d$ symmetry, there are no group-satisfying azimuthal symmetric exchange vectors, so $J_{c,q}^{T_d}=0$ for $q=1$ and 2. However, the axial vectors parallel to $\boldsymbol{r}_{n,n'}$ satisfy all of the $T_d$ ISPG symmetries, so that the $J_{f,q}^{T_d}$ could exist, provided that $J_{f,1}^{T_d}=J_{f,2}^{T_d}$. However, the requirement $\tilde{J}_{T_d}=\tilde{J}'_{T_d}$ to preserve the $T_d$ symmetry of the renormalized Heisenberg interactions forces $J_{f,2}^{T_d}=J_{f,1}^{T_d}/2$. Hence, we must conclude that $J_{f,q}^{T_d}=0$ for $q=1$ and 2 and $\delta J_{T_d}=\delta J'_{T_d}=0$.

$\mathcal{H}_{ae}^{g,\ell}$ also leads to additional interactions $\delta\mathcal{H}_{ae}^g$ in the molecular frame,

$$\delta\mathcal{H}_{ae}^g = \sum_{q=1}^{2}\sum_{n=1}^{6-2q}\Bigg[J_{q,z}^g S_{n,z}S_{n+q,z} + (-1)^{n+1} \times\Bigg(J_{q,xy}^g[S_{n,x}S_{n+q,x} - S_{n,y}S_{n+q,y}] + \sum_{\alpha\neq\beta} K_{q,\alpha\beta}^g(n)S_{n,\alpha}S_{n+q,\beta}\Bigg)\Bigg], \quad (37)$$

where $\alpha,\beta=x,y,z$. As for the single-ion interactions in the molecular representation, the site-independent symmetric exchange interaction strengths $J_{q,z}^g$ contribute to the eigenstate energies to first order, but the first-order contributions to the eigenstate energies from the site-dependent interactions vanish. Both the site-independent and site-dependent symmetric exchange interaction strengths are given in terms of the parameter sets $\mu_{1p}^g$ in Appendix C.

### C. Antisymmetric exchange Hamiltonian

In Secs. IV and V, we already evaluated the antisymmetric exchange Hamiltonians in the molecular representation, and the parameter sets are listed in Table III. These six $\mathcal{H}_{DM}^g$ may be combined as

$$\mathcal{H}_{DM}^g = \sum_{q=1}^{2}\sum_{n=1}^{6-2q}(\boldsymbol{S}_n \times \boldsymbol{S}_{n+q})\cdot[d_z^g(n)\delta_{q,1}\hat{\boldsymbol{z}} + \boldsymbol{d}_q^g \sin(n\pi/2) + (\hat{\boldsymbol{z}}\times\boldsymbol{d}_q^g)\cos(n\pi/2)], \quad (38)$$

where the scalar $d_z^g(n)$ and the two two-vectors $\boldsymbol{d}_q^g$ all vanish for $g=C_{4v}$ and $T_d$, but for the other four ISPG symmetries are given in Appendix C.

We note that both site-dependent and site-independent DM interactions give rise to second-order eigenstate energy corrections and can only be neglected in fits to experiment for tetramers with symmetries very close to $T_d, C_{4v}$, or higher. In Appendix D, we give $\mathcal{H}_{DM}^g$ for the lower symmetry $C_{2v}^{13}$ tetramers.

### D. Biquadratic and three-center quartic isotropic exchange interactions

In the previous sections, we listed the quadratic single-ion and anisotropic exchange interactions for the six high-symmetry tetramer ISPG's under study. However, in the lower-symmetry AFM tetramers $\{Ni_4Mo_{12}\}$, with $C_{1v}$ symmetry,[46] and $Ni_4$ and $Co_4$ $[2\times2]$ grids (or rhombuses), with approximate $C_{2v}^{13}$ symmetry,[47–49] fits to magnetization data were facilitated by the inclusion of biquadratic interactions.[46–48] In the former case, the powder fits assumed field-dependent interaction parameters, but the single-ion interactions were assumed to have $T_d$ symmetry, which vanish to first order in their strength, and the anisotropic exchange interactions were neglected. In the latter $C_{2v}^{13}$ case, the authors neglected the NN DM interactions given in the Appendixes. Subsequently, Kostyuchenko argued for $T_d$ symmetry that AFM three-center isotropic quartic interactions should be comparable in magnitude to the AFM biquadratic interactions, and provided a fit to the midpoints of the level-crossing magnetization behavior on $\{Ni_4Mo_{12}\}$, without making the assumption of a strong field dependence of the Heisenberg interaction strength.[50] Here, we calculate the effects of three-center quartic isotropic interactions for the six ISPG $g$ symmetries under study and provide preliminary fits to the AFM $\{Ni_4Mo_{12}\}$ magnetization data, including the first-order anisotropy interactions, which can fit the widths of the transitions as well as the midpoints. More complete fits to those experiments and to experiments on the grid SMM's will be presented elsewhere.[51] Such fits are greatly aided by an analytic treatment of biquadratic and three-center isotropic quartic exchange.

For tetramers with the six $g$ symmetries under study, the isotropic biquadratic and three-center quartic Hamiltonians $\mathcal{H}_{\rm b}^g$ and $\mathcal{H}_{\rm t}^g$, respectively, may be written as

$$\mathcal{H}_{\rm b}^g = \sum_{q=1}^{2}\mathcal{H}_{{\rm b},q}^g, \quad (39)$$

$$\mathcal{H}_{{\rm b},q}^g = -J_{{\rm b},q}^g\sum_{n=1}^{6-2q}(\boldsymbol{S}_n\cdot\boldsymbol{S}_{n+q})^2, \quad (40)$$

$$\mathcal{H}_{\rm t}^g = \sum_{q=1}^{2} \mathcal{H}_{{\rm t},q}^g, \tag{41}$$

$$\mathcal{H}_{{\rm t},1}^g = -J_{{\rm t},1}^g \sum_{\substack{n=1 \\ \text{odd}}}^{4} \sum_{\substack{n'=1 \\ \text{even}}}^{4} (\boldsymbol{S}_n \cdot \boldsymbol{S}_{n+1})(\boldsymbol{S}_{n'} \cdot \boldsymbol{S}_{n'+1}), \tag{42}$$

$$\mathcal{H}_{{\rm t},2}^g = -J_{{\rm t},2}^g \sum_{n=1}^{4} \sum_{n'=1}^{2} (\boldsymbol{S}_n \cdot \boldsymbol{S}_{n+1})(\boldsymbol{S}_{n'} \cdot \boldsymbol{S}_{n'+2}). \tag{43}$$

For $g=T_d$, we take $J_{{\rm b},1}^{T_d}=J_{{\rm b},2}^{T_d}$ and $J_{{\rm t},1}^{T_d}=J_{{\rm t},2}^{T_d}$; otherwise, $J_{{\rm b},2}^g \neq J_{{\rm b},1}^g$ and $J_{{\rm t},2}^g \neq J_{{\rm t},1}^g$. For the six $g$ symmetries, $\mathcal{H}_{\rm b}^g+\mathcal{H}_{\rm t}^g$ is invariant under all rotations and each of the elements of $\mathcal{O}^g$.

## VI. EIGENSTATES OF THE FULL HAMILTONIAN

### A. Induction representation

We assume a molecular Hamiltonian

$$\mathcal{H}^g = \mathcal{H}_0^{g,r} + \mathcal{H}_{si}^g + \delta\mathcal{H}_{ae}^g + \mathcal{H}_{DM}^g + \mathcal{H}_{\rm b}^g + \mathcal{H}_{\rm t}^g. \tag{44}$$

To take proper account of $\boldsymbol{B}$ in $\mathcal{H}_0^{g,r}$, we construct our SMM eigenstates in the induction representation by the rotation

$$\begin{pmatrix} \hat{\boldsymbol{x}} \\ \hat{\boldsymbol{y}} \\ \hat{\boldsymbol{z}} \end{pmatrix} = \begin{pmatrix} \cos\theta\cos\phi & -\sin\phi & \sin\theta\cos\phi \\ \cos\theta\sin\phi & \cos\phi & \sin\theta\sin\phi \\ -\sin\theta & 0 & \cos\theta \end{pmatrix} \begin{pmatrix} \hat{\boldsymbol{x}}' \\ \hat{\boldsymbol{y}}' \\ \hat{\boldsymbol{z}}' \end{pmatrix}, \tag{45}$$

so that $\boldsymbol{B}=B\hat{\boldsymbol{z}}'$.[5] A subsequent arbitrary rotation about $\hat{\boldsymbol{z}}'$ does not affect the eigenstates. We then set $\hbar=1$ and write

$$\boldsymbol{S}^2 |\psi_{s,m}^{s_{13},s_{24}}\rangle = s(s+1)|\psi_{s,m}^{s_{13},s_{24}}\rangle, \tag{46}$$

$$\boldsymbol{S}_{13}^2 |\psi_{s,m}^{s_{13},s_{24}}\rangle = s_{13}(s_{13}+1)|\psi_{s,m}^{s_{13},s_{24}}\rangle, \tag{47}$$

$$\boldsymbol{S}_{24}^2 |\psi_{s,m}^{s_{13},s_{24}}\rangle = s_{24}(s_{24}+1)|\psi_{s,m}^{s_{13},s_{24}}\rangle, \tag{48}$$

$$S_{z'} |\psi_{s,m}^{s_{13},s_{24}}\rangle = m|\psi_{s,m}^{s_{13},s_{24}}\rangle, \tag{49}$$

$$S_{\sigma'} |\psi_{s,m}^{s_{13},s_{24}}\rangle = A_s^{\sigma' m} |\psi_{s,m+\sigma'}^{s_{13},s_{24}}\rangle, \tag{50}$$

$$A_s^m = \sqrt{(s-m)(s+m+1)}, \tag{51}$$

where $S_{\sigma'}=S_{x'}+i\sigma' S_{y'}$ with $\sigma'=\pm 1$. For brevity, we define

$$\nu \equiv \{s,m,s_{13},s_{24}\}, \tag{52}$$

$$\bar{\nu} \equiv \{s,s_{13},s_{24}\}, \tag{53}$$

where $\bar{\nu}$ excludes $m$, and write $|\nu\rangle \equiv |\psi_{s,m}^{s_{13},s_{24}}\rangle$, where the additional dependence of $\nu$, $\bar{\nu}$, and $|\nu\rangle$ on the fixed single-spin value $s_1$ is taken to be understood. $\mathcal{H}_{{\rm b},2}^g$, $\mathcal{H}_{{\rm t},2}^g$, and $\mathcal{H}_0^{g,r}$ are diagonal in this representation, $\langle\nu'|\mathcal{H}_0^{g,r}+\mathcal{H}_{{\rm b},2}^g+\mathcal{H}_{{\rm t},2}^g|\nu\rangle = E_{\nu,0}^g \delta_{\nu,\nu'}$, where, based on Eqs. (46)–(49),

$$\delta_{\nu,\nu'} = \delta_{s,s'}\delta_{m,m'}\delta_{s_{13},s'_{13}}\delta_{s_{24},s'_{24}}, \tag{54}$$

$$E_{\nu,0}^g = -\frac{\tilde{J}_g}{2} s(s+1) - \gamma B m + \delta E_{\bar{\nu},0}^g, \tag{55}$$

$$\delta E_{\bar{\nu},0}^g = -\frac{1}{2}\sum_{n=1}^{2} \Bigg[ (\tilde{J}'_g - \tilde{J}_g) s_{n,n+2}(s_{n,n+2}+1) + \frac{J_{{\rm b},2}^g}{2}[-2s_1(s_1+1) + s_{n,n+2}(s_{n,n+2}+1)]^2 + \frac{J_{{\rm t},2}^g}{2}[-2s_1(s_1+1) + s_{n,n+2}(s_{n,n+2}+1)] \times \left( s(s+1) - \sum_{n'=1}^{2} s_{n',n'+2}(s_{n',n'+2}+1) \right) \Bigg], \tag{56}$$

where $\tilde{J}_g$ and $\tilde{J}'_g$ are given by Eqs. (35) and (36). Since $\mathcal{H}_0^{g,r}$, $\mathcal{H}_{{\rm b},2}^g$, and $\mathcal{H}_{{\rm t},2}^g$ are invariant under all rotations, $E_{\nu,0}^g$ is independent of $\theta$ and $\phi$.

### B. First-order eigenstates

In the induction representation, we write $\mathcal{H}_{si}^g+\delta\mathcal{H}_{ae}^g+\mathcal{H}_{DM}^g$ as $\mathcal{H}_{si}^{\prime;g}+\mathcal{H}_{ae}^{\prime,g}+\mathcal{H}_{DM}^{\prime,g}$. $\mathcal{H}_{{\rm b},1}^g$ and $\mathcal{H}_{{\rm t},1}^g$ are scalars, independent of the direction of $\boldsymbol{B}$. Since these Hamiltonian terms are not diagonal in the induction representation, we then make a standard first-order perturbation expansion, assuming the magnitude of each of their strengths to be small relative to $|\tilde{J}_g|$ and $|\tilde{J}'_g|$.[5] To do so, it is necessary to analytically evaluate the single-ion matrix elements, as they contain much of the interesting physics. Compact expressions for these matrix elements for general $(s_1,s_2,s_3,s_4)$ are given in Appendix E.

At arbitrary $\boldsymbol{B}$ angles $(\theta,\phi)$, the first-order corrections $E_{\nu,1}^g = \langle\nu|\mathcal{H}_{si}^{\prime;g}+\mathcal{H}_{ae}^{\prime,g}+\mathcal{H}_{DM}^{\prime,g}+\mathcal{H}_{{\rm b},1}^g+\mathcal{H}_{{\rm t},1}^g|\nu\rangle$ to the eigenstate energies for $g=C_{4h}$, $D_{4h}$, $C_{4v}$, $S_4$, $D_{2d}$, and $T_d$ symmetries are

$$E_{\nu,1}^g = \frac{\tilde{J}_z^{g,\bar{\nu}}}{2}[m^2 - s(s+1)] - \delta\tilde{J}_z^{g,\bar{\nu}} - \frac{[3m^2 - s(s+1)]}{2}\tilde{J}_z^{g,\bar{\nu}} \cos^2\theta, \tag{57}$$

$$\tilde{J}_z^{g,\bar{\nu}} = J_z^g a_{\bar{\nu}}^+ - J_{1,z}^g c_{\bar{\nu}}^- - \frac{1}{2} J_{2,z}^g a_{\bar{\nu}}^-, \tag{58}$$

$$\delta\tilde{J}_z^{g,\bar{\nu}} = J_z^g b_{\bar{\nu}}^+ - \frac{1}{4} J_{1,z}^g (b_{\bar{\nu}}^+ + b_{\bar{\nu}}^-) - \frac{1}{4} J_{2,z}^g b_{\bar{\nu}}^- + J_{{\rm b},1}^g \mathcal{B}_{\bar{\nu}} + J_{{\rm t},1}^g \mathcal{T}_{\bar{\nu}}, \tag{59}$$

where analytic expressions for $a_{\bar{\nu}}^{\pm}$, $b_{\bar{\nu}}^{\pm}$, $c_{\bar{\nu}}^-$, $\mathcal{B}_{\bar{\nu}}$, and $\mathcal{T}_{\bar{\nu}}$ for general $\bar{\nu}$ are given in Appendix F, along with Tables IV and V of their values for $s_1=1/2$ and 1 and Tables VI and VII and Tables VIII and IX of the simple analytic forms of $a_{\bar{\nu}}^{\pm}$, $b_{\bar{\nu}}^{\pm}$, and $c_{\bar{\nu}}^-$ for the lowest four eigenstate manifolds of FM and AFM tetramers, respectively. We note that all of these interaction coefficients are invariant under $s_{13} \leftrightarrow s_{24}$, as ex-

TABLE IV. Values of the first-order energy coefficients $a_{\bar{\nu}}^{\pm}$, $b_{\bar{\nu}}^{\pm}$, $c_{\bar{\nu}}^{-}$, $\mathcal{B}_{\bar{\nu}}$, and $\mathcal{T}_{\bar{\nu}}$ for $s_1=1/2$.

| $s$ | $s_{13}$ | $s_{24}$ | $a_{\bar{\nu}}^{+}$ | $a_{\bar{\nu}}^{-}$ | $b_{\bar{\nu}}^{+}$ | $b_{\bar{\nu}}^{-}$ | $c_{\bar{\nu}}^{-}$ | $\mathcal{B}_{\bar{\nu}}$ | $\mathcal{T}_{\bar{\nu}}$ |
|---|---|---|---|---|---|---|---|---|---|
| 2 | 1 | 1 | 0 | $\frac{1}{3}$ | 2 | $-\frac{2}{3}$ | $\frac{1}{6}$ | $\frac{1}{4}$ | $\frac{1}{4}$ |
| 1 | 1 | 1 | 0 | −1 | 2 | 2 | $-\frac{1}{2}$ | $\frac{5}{4}$ | $\frac{1}{4}$ |
| 1 | 1 | 0 | 0 | 1 | 2 | −2 | 0 | $\frac{3}{2}$ | −1 |
| 0 | 1 | 1 | 0 | $\frac{11}{3}$ | 2 | $\frac{2}{3}$ | $\frac{11}{6}$ | $\frac{7}{4}$ | $\frac{1}{4}$ |
| 0 | 0 | 0 | 2 | −1 | 2 | −2 | $\frac{1}{2}$ | $\frac{3}{4}$ | $-\frac{3}{4}$ |

pected. The DM and all site-dependent interactions vanish in this first-order perturbation. Second-order corrections to the eigenstate energies will be presented elsewhere.[51]

For all six $g$ ISPG's, $E_{\nu,1}^{g}$ has a form analogous to that of the equal-spin dimer in the absence of azimuthal single-ion and symmetric anisotropic exchange interactions.[5] For these high-symmetry tetramers, to first order in the anisotropy interactions, the azimuthal single-ion and anisotropic exchange interactions merely renormalize the respective effective site-independent axial interactions. Thus, to first order, we only have two effective isotropic exchange interactions, two biquadratic and two three-center quartic isotropic exchange interactions, and three effective anisotropy interactions, with respective strengths $\tilde{J}_g$, $\tilde{J}'_g$, $J_{\mathrm{b,q}}^{g}$, $J_{\mathrm{t,q}}^{g}$, $J_{z}^{g}$, and $J_{q,z}^{g}$, for $q=1$ and 2, which are fixed for a particular equal-spin $s_1$ SMM tetramer. Nevertheless, the first-order eigenstate energies $E_{\nu}^{g}=E_{\nu,0}^{g}+E_{\nu,1}^{g}$, given by Eqs. (55) and (57), contain these nine effective interaction strengths in ways that strongly depend on the quantum number set $\nu$ and on $\theta$. These different $\nu$ and $\theta$ dependencies can be employed to provide definitive measures of at least some of them.

### C. Type-I and type-II tetramers

There are at least two types of FM and AFM tetramers. To the extent that the single-ion, symmetric anisotropic exchange, and biquadratic and three-center quartic exchange interaction strengths are small relative to the difference in the Heisenberg interaction strengths, there are just two types of tetramers. The criterion is simply based on $\tilde{J}'_g-\tilde{J}_g$ in $\delta E_{\bar{\nu},0}^{g}$, which for this classification purpose we assume to be larger in magnitude than the magnitudes of all anisotropy and quartic interaction strengths. Type-I tetramers have $\tilde{J}'_g-\tilde{J}_g>0$, which can occur for either sign of $\tilde{J}_g$, provided $g\neq T_d$. For type I, the lowest energy state in each $s$ manifold occurs for the maximum values $s_{13},s_{24}=2s_1$. Thus, at low $T$, type-I tetramers behave as pairs of spin $2s_1$ dimers. Type-II tetramers with $\tilde{J}'_g-\tilde{J}_g<0$ are frustrated, with the lowest energy state in each $s$ manifold occurring for the minimal $s_{13}$ and $s_{24}$ values. For even $s$, these minima occur for $s_{13}$, $s_{24}=s/2$, but for odd $s$, the energy minimum is doubly degenerate, occurring at $s_{13}$, $s_{24}=(s\pm 1)/2$, $(s\mp 1)/2$. Hence, explicit formulas for the first-order eigenstate energy parameters $a_{\bar{\nu}}^{\pm}$, $b_{\bar{\nu}}^{\pm}$, $c_{\bar{\nu}}^{-}$, $\mathcal{B}_{\bar{\nu}}$, and $\mathcal{T}_{\bar{\nu}}$ with arbitrary $s$ in these three optimal $s_{13}$, $s_{24}$ cases are given in Appendixes G and H, respectively. For sufficiently strong $\tilde{J}'_g-\tilde{J}_g$, these formulas apply to the lowest energy eigenstate in each $s$ manifold. When $\tilde{J}'_g-\tilde{J}_g$ is small relative to the other interactions, multiple tetramer types can occur. Tables VI–IX are sufficient for easy full analyses of such cases for $s_1\leqslant 3/2$, and the lowest four $s$ manifolds for FM and AFM tetramers with arbitrary $s_1$.

TABLE V. Values of the first-order energy coefficients $a_{\bar{\nu}}^{\pm}$, $b_{\bar{\nu}}^{\pm}$, $c_{\bar{\nu}}^{-}$, $\mathcal{B}_{\bar{\nu}}$, and $\mathcal{T}_{\bar{\nu}}$ for $s_1=1$.

| $s$ | $s_{13}$ | $s_{24}$ | $a_{\bar{\nu}}^{+}$ | $a_{\bar{\nu}}^{-}$ | $b_{\bar{\nu}}^{+}$ | $b_{\bar{\nu}}^{-}$ | $c_{\bar{\nu}}^{-}$ | $\mathcal{B}_{\bar{\nu}}$ | $\mathcal{T}_{\bar{\nu}}$ |
|---|---|---|---|---|---|---|---|---|---|
| 4 | 2 | 2 | $\frac{1}{7}$ | $\frac{2}{7}$ | $\frac{24}{7}$ | $-\frac{8}{7}$ | $\frac{3}{14}$ | 4 | 4 |
| 3 | 2 | 2 | $\frac{1}{15}$ | $\frac{2}{15}$ | $\frac{24}{5}$ | $\frac{8}{5}$ | $\frac{1}{10}$ | 4 | 0 |
| 3 | 2 | 1 | $\frac{1}{15}$ | $\frac{2}{5}$ | $\frac{24}{5}$ | $-\frac{16}{5}$ | $\frac{8}{45}$ | $\frac{43}{9}$ | $-\frac{7}{9}$ |
| 2 | 2 | 2 | $-\frac{1}{7}$ | $-\frac{2}{7}$ | $\frac{124}{21}$ | $\frac{80}{21}$ | $-\frac{3}{14}$ | $\frac{23}{4}$ | $\frac{9}{4}$ |
| 2 | 2 | 1 | $\frac{1}{3}$ | 0 | 4 | 0 | $-\frac{1}{18}$ | $\frac{307}{36}$ | $-\frac{55}{36}$ |
| 2 | 2 | 0 | $\frac{1}{3}$ | $\frac{2}{3}$ | 4 | −4 | 0 | 7 | −3 |
| 2 | 1 | 1 | $-\frac{1}{3}$ | $\frac{2}{3}$ | $\frac{20}{3}$ | $-\frac{16}{3}$ | $\frac{1}{6}$ | $\frac{31}{4}$ | $-\frac{23}{4}$ |
| 1 | 2 | 2 | $-\frac{7}{5}$ | $-\frac{14}{5}$ | $\frac{36}{5}$ | $\frac{32}{5}$ | $-\frac{21}{10}$ | $\frac{31}{4}$ | $\frac{25}{4}$ |
| 1 | 2 | 1 | $\frac{3}{5}$ | $\frac{8}{5}$ | $\frac{68}{15}$ | $-\frac{32}{15}$ | $-\frac{9}{10}$ | $\frac{23}{4}$ | $-\frac{1}{12}$ |
| 1 | 1 | 1 | 1 | −2 | 4 | 0 | $-\frac{1}{2}$ | $\frac{15}{4}$ | $\frac{1}{4}$ |
| 1 | 1 | 0 | −1 | 2 | $\frac{20}{3}$ | $-\frac{20}{3}$ | 0 | 9 | $-\frac{23}{3}$ |
| 0 | 2 | 2 | 3 | 6 | $\frac{16}{3}$ | $\frac{8}{3}$ | $\frac{9}{2}$ | $\frac{32}{3}$ | $\frac{22}{3}$ |
| 0 | 1 | 1 | $-\frac{11}{3}$ | $\frac{22}{3}$ | $\frac{16}{3}$ | $-\frac{8}{3}$ | $\frac{11}{6}$ | 8 | −6 |
| 0 | 0 | 0 | $\frac{11}{3}$ | $-\frac{8}{3}$ | $\frac{16}{3}$ | $-\frac{16}{3}$ | $\frac{1}{2}$ | $\frac{16}{3}$ | $-\frac{16}{3}$ |

TABLE VI. Values of $a_{\bar{\nu}}^{\pm}$ for the ground and first three excited state manifolds for FM tetramers (or the highest four excited state manifolds of AFM tetramers), where $a_1(x)=2048x^6-9472x^5+17\,344x^4-15\,440x^3+6924x^2-1530x+135$. The quantum numbers are restricted by $0\leqslant s_{13}$, $s_{24}\leqslant 2s_1$, and $|s_{13}-s_{24}|\leqslant s\leqslant s_{13}+s_{24}$.

| $s,s_{13},s_{24}$ | $a_{\bar{\nu}}^{+}$ | $a_{\bar{\nu}}^{-}$ |
|---|---|---|
| $4s_1,2s_1,2s_1$ | $\frac{2s_1-1}{8s_1-1}$ | $\frac{2s_1}{8s_1-1}$ |
| $4s_1-1,2s_1,2s_1$ | $\frac{(2s_1-1)(4s_1-3)}{(4s_1-1)(8s_1-3)}$ | $\frac{2s_1(4s_1-3)}{(4s_1-1)(8s_1-3)}$ |
| $4s_1-1,2s_1,2s_1-1$ | $\frac{(2s_1-1)(4s_1-3)}{(4s_1-1)(8s_1-3)}$ | $\frac{2s_1}{8s_1-3}$ |
| $4s_1-2,2s_1,2s_1$ | $\frac{(2s_1-1)(32s_1^2-44s_1+3)}{(4s_1-1)(8s_1-1)(8s_1-5)}$ | $\frac{2s_1(32s_1^2-44s_1+3)}{(4s_1-1)(8s_1-1)(8s_1-5)}$ |
| $4s_1-2,2s_1,2s_1-1$ | $\frac{16s_1^3-36s_1^2+26s_1-3}{(2s_1-1)(4s_1-1)(8s_1-5)}$ | $\frac{4s_1(s_1-1)}{(2s_1-1)(8s_1-5)}$ |
| $4s_1-2,2s_1,2s_1-2$ | $\frac{16s_1^3-36s_1^2+26s_1-3}{(2s_1-1)(4s_1-1)(8s_1-5)}$ | $\frac{2(8s_1^3-6s_1^2+2s_1-1)}{(2s_1-1)(4s_1-1)(8s_1-5)}$ |
| $4s_1-2,2s_1-1,2s_1-1$ | $\frac{2s_1-3}{8s_1-5}$ | $\frac{2s_1}{8s_1-5}$ |
| $4s_1-3,2s_1,2s_1$ | $\frac{(2s_1-1)(8s_1-15)}{(8s_1-3)(8s_1-7)}$ | $\frac{2s_1(8s_1-15)}{(8s_1-3)(8s_1-7)}$ |
| $4s_1-3,2s_1,2s_1-1$ | $\frac{a_1(s_1)}{(4s_1-3)^2(2s_1-1)(4s_1-1)(8s_1-3)(8s_1-7)}$ | $\frac{4s_1(512s_1^5-1856s_1^4+2416s_1^3-1420s_1^2+399s_1-45)}{(4s_1-3)^2(2s_1-1)(4s_1-1)(8s_1-3)(8s_1-7)}$ |
| $4s_1-3,2s_1,2s_1-2$ | $\frac{16s_1^3-52s_1^2+58s_1-9}{(2s_1-1)(4s_1-3)(8s_1-7)}$ | $\frac{4s_1^3-7s_1^2+3s_1-1}{(2s_1-1)(4s_1-3)(8s_1-7)}$ |
| $4s_1-3,2s_1,2s_1-3$ | $\frac{(2s_1-1)(16s_1^2-48s_1+45)}{(4s_1-3)^2(8s_1-7)}$ | $\frac{2(16s_1^3-24s_1^2+15s_1-9)}{(4s_1-3)^2(8s_1-7)}$ |
| $4s_1-3,2s_1-1,2s_1-1$ | $\frac{(2s_1-3)(4s_1-5)}{(4s_1-3)(8s_1-7)}$ | $\frac{2s_1(4s_1-5)}{(4s_1-3)(8s_1-7)}$ |
| $4s_1-3,2s_1-1,2s_1-2$ | $\frac{32s_1^3-96s_1^2+70s_1-9}{(4s_1-1)(4s_1-3)(8s_1-7)}$ | $\frac{2(16s_1^3-16s_1^2+5s_1-2)}{(4s_1-1)(4s_1-3)(8s_1-7)}$ |

### D. Dzyaloshinskii-Moriya interactions and spin-induced polarizations

Although the first-order correction to the energy arising from the DM interactions vanishes, for $s_1=1/2$ and 1, it is not too difficult to diagonalize the Hamiltonian matrix exactly and, hence, to take precise account of the effects of the DM interactions. To focus on the effects of DM interactions, in Figs. 4–9, we omit the single-ion, symmetric anisotropic exchange interactions, and biquadratic and three-center quartic interactions, keeping only the AFM Heisenberg, Zeeman, and weak DM interactions. Although Katsura *et al.* derived the spin-induced polarization for large spin values, we have assumed that the same physics should apply for small spin values. In Fig. 4, we plotted $M/\gamma$ versus $\gamma B/|\tilde{J}_g|$ for $s_1=1/2$ AFM tetramers with $S_4$ symmetry with $\boldsymbol{B}\|(111)$, $T=0$, and $d/|\tilde{J}_g|=0.1$, where $d_z^g=d_{1y}^g=d_{2x}^g=d_{2y}^g=d$ and $d_{1x}^g=0$, in the limit $c=a$. We note that for $\tilde{J}_g<0$ and $\tilde{J}_g'/\tilde{J}_g=0.5$, the magnetization exhibits sharp steps close to the integral values $s=1$ and 2 of $\gamma B/|\tilde{J}_g|$, characteristic of type-I AFM tetramers. For $\tilde{J}_g<0$ and $\tilde{J}_g'/\tilde{J}_g=1.5$, the two steps are shifted to higher $B$ values, and the first step is broadened. This is a type-II AFM tetramer behavior for the DM interaction. In Fig. 5, the corresponding curves for the spin-induced polarization $|\boldsymbol{P}_s|$ are shown. In both cases, there is a sharp peak at the inflection point of the first magnetization step, at which the total spin value $s$ changes from 0 to 1. In addition, there is a discontinuity in slope at the position of each second magnetization step, at which $\boldsymbol{P}_s$ begins its rapid decrease to

TABLE VII. Values of $b_{\bar{\nu}}^{\pm}$ and $c_{\bar{\nu}}^{-}$ for the ground and first three excited state manifolds for FM tetramers (or the highest four excited state manifolds of AFM tetramers), where $b_1(s_1)=(2304s_1^5-6112s_1^4+5968s_1^3-2650s_1^2+552s_1-45)/[(8s_1-3)(8s_1-7)]$, $b_2(s_1)=(1024s_1^4-2304s_1^3+1808s_1^2-576s_1+63)/[(8s_1-3)(8s_1-7)]$, $c_1(s_1)=256s_1^5-640s_1^4+576s_1^3-240s_1^2+48s_1-3$, and $c_2(s_1)=(2048s_1^6-8960s_1^5+15\ 232s_1^4-13\ 120s_1^4+6096s_1^3-1440s_1+135)/[(8s_1-3)(8s_1-7)]$.

| $s,s_{13},s_{24}$ | $b_{\bar{\nu}}^{+}$ | $b_{\bar{\nu}}^{-}$ | $c_{\bar{\nu}}^{-}$ |
|---|---|---|---|
| $4s_1,2s_1,2s_1$ | $\frac{24s_1^2}{8s_1-1}$ | $-\frac{8s_1^2}{8s_1-1}$ | $\frac{4s_1-1}{2(8s_1-1)}$ |
| $4s_1-1,2s_1,2s_1$ | $\frac{8s_1(5s_1-2)}{8s_1-3}$ | $\frac{8s_1^2}{8s_1-3}$ | $\frac{4s_1-3}{2(8s_1-3)}$ |
| $4s_1-1,2s_1,2s_1-1$ | $\frac{8s_1(5s_1-2)}{8s_1-3}$ | $-\frac{8s_1(3s_1-1)}{8s_1-3}$ | $\frac{8s_1(2s_1-1)^2}{(4s_1-1)^2(8s_1-3)}$ |
| $4s_1-2,2s_1,2s_1$ | $\frac{4(112s_1^3-102s_1^2+22s_1-1)}{(8s_1-1)(8s_1-5)}$ | $\frac{8s_1(24s_1^2-15s_1+1)}{(8s_1-1)(8s_1-5)}$ | $\frac{32s_1^2-44s_1+3}{2(8s_1-1)(8s_1-5)}$ |
| $4s_1-2,2s_1,2s_1-1$ | $\frac{4(14s_1^2-12s_1+1)}{8s_1-5}$ | $-\frac{8s_1(s_1-1)}{8s_1-5}$ | $\frac{c_1(s_1)}{2(2s_1-1)^2(4s_1-1)^2(8s_1-5)}$ |
| $4s_1-2,2s_1,2s_1-2$ | $\frac{4(14s_1^2-12s_1+1)}{8s_1-5}$ | $-\frac{4(10s_1^2-8s_1+1)}{8s_1-5}$ | $\frac{2s_1(4s_1^2-7s_1+3)}{(2s_1-1)^2(8s_1-5)}$ |
| $4s_1-2,2s_1-1,2s_1-1$ | $\frac{4(14s_1^2-10s_1+1)}{8s_1-5}$ | $-\frac{8s_1(5s_1-3)}{8s_1-5}$ | $\frac{4s_1-3}{2(8s_1-5)}$ |
| $4s_1-3,2s_1,2s_1$ | $\frac{12(48s_1^3-74s_1^2+34s_1-5)}{(8s_1-3)(8s_1-7)}$ | $\frac{8s_1(40s_1^2-51s_1+15)}{(8s_1-3)(8s_1-7)}$ | $\frac{(4s_1-1)(8s_1-15)}{2(8s_1-3)(8s_1-7)}$ |
| $4s_1-3,2s_1,2s_1-1$ | $\frac{4b_1(s_1)}{(4s_1-1)(4s_1-3)}$ | $\frac{8s_1b_2(s_1)}{(4s_1-1)(4s_1-3)}$ | $\frac{c_2(s_1)}{2(2s_1-1)^2(4s_1-3)^2}$ |
| $4s_1-3,2s_1,2s_1-2$ | $\frac{12(6s_1^2-8s_1+1)}{8s_1-7}$ | $-\frac{4(6s_1^2-8s_1+1)}{8s_1-7}$ | $\frac{2(s_1-1)(4s_1-1)(16s_1^3-40s_1^2+29s_1-8)}{(2s_1-1)^2(4s_1-3)^2(8s_1-7)}$ |
| $4s_1-3,2s_1,2s_1-3$ | $\frac{12(24s_1^2-50s_1^2+30s_1-5)}{(4s_1-3)(8s_1-7)}$ | $-\frac{4(56s_1^3-114s_1^2+72s_1-15)}{(4s_1-3)(8s_1-7)}$ | $\frac{16s_1(s_1-1)(2s_1-3)}{(4s_1-3)^2(8s_1-7)}$ |
| $4s_1-3,2s_1-1,2s_1-1$ | $\frac{4(18s_1^2-22s_1+5)}{8s_1-7}$ | $-\frac{24s_1(s_1-1)}{8s_1-7}$ | $\frac{4s_1-5}{2(8s_1-7)}$ |
| $4s_1-3,2s_1-1,2s_1-2$ | $\frac{4(72s_1^3-98s_1^2+34s_1-3)}{(4s_1-1)(8s_1-7)}$ | $-\frac{4(56s_1^3-70s_1^2+20s_1-1)}{(4s_1-1)(8s_1-7)}$ | $\frac{16(s_1-1)^2(2s_1-1)}{(4s_1-3)^2(8s_1-7)}$ |

zero, which it reaches at the $B$ value for which $M$ just attains saturation. Note that $\boldsymbol{P}_s \to 0$ at large $B$, since the large $\boldsymbol{B}$ aligns the spins at all sites, causing their vector products to vanish. Some results for the intermediate case $\tilde{J}_g'/\tilde{J}_g=1$ are shown in Fig. 6. In this figure, we plotted $|\boldsymbol{P}_s|$ in arbitrary units versus $\theta/\pi$ for $s_1=1/2$ AFM tetramers with $S_4$ symmetry at $\phi=\pi/4$ where $d/|\tilde{J}_g|=0.01$ and $\gamma B/|\tilde{J}_g|=1.2$ and 1, respectively. The $\boldsymbol{P}_s(\theta)$ curves are antisymmetric about $\theta=\pi/2$. We note that the curves with $\gamma B/|\tilde{J}_g|=1,1.2$ exhibit broad maxima at $\theta/\pi \approx 0.28,0.32$, respectively. These broad curves reflect the strong frustration of the spins with $\tilde{J}_g'=\tilde{J}_g$, for which no preferred $s_{13}$ and $s_{24}$ values exist.

In Figs. 7–9, we plotted analogous curves for $s_1=1$ AFM tetramers, except that $d/|\tilde{J}_g|=0.01$. Curves with $d/|\tilde{J}_g|=0.1$ for $s_1=1$ exhibit steps or peaks that are much broader than the corresponding ones for $s_1=1/2$ pictured in Figs. 4–6. We note that in Fig. 7, the dashed curve for the type-II case $\tilde{J}_g'/\tilde{J}_g=1.5$ has wider steps at $M/\gamma=0$ and 2 than at 1 and 3. This low value of the DM strength $d/|\tilde{J}_g|=0.01$ leads to very sharp peaks in $|\boldsymbol{P}_s|$ for both type-I and II tetramers, as shown in Fig. 8. However, the three peak tails are much broader for AFM type-II tetramers with $\tilde{J}_g'/\tilde{J}_g=1.5$ than for AFM type-I tetramers with $\tilde{J}_g'/\tilde{J}_g=0.5$. In each case, the peak positions correspond to the first three magnetization step $\gamma B/|\tilde{J}_g|$ val-

TABLE VIII. Values of $a_{\bar{\nu}}^{\pm}$ for the ground and first three excited state manifolds for AFM tetramers (or the highest four excited state manifolds of FM tetramers), where $x$ represents any value of $s_{13}$ that satisfies $0 \leqslant s_{13}, s_{24} \leqslant 2s_1$, and $|s_{13}-s_{24}| \leqslant s \leqslant s_{13}+s_{24}$.

| $s,s_{13},s_{24}$ | $a_{\bar{\nu}}^{+}$ | $a_{\bar{\nu}}^{-}$ |
|---|---|---|
| $0,x,x$ | $\frac{(3+4x+4x^2)[3(-1+x+x^2)-4s_1(s_1+1)]}{3(2x+3)(2x-1)}$ | $\frac{(3+4x+4x^2)[x+x^2+4s_1(s_1+1)]}{3(2x+3)(2x-1)}$ |
| $1,x,x$ | $\frac{-3(-1+x+x^2)+4s_1(s_1+1)}{5}$ | $-\frac{x+x^2+4s_1(s_1+1)}{5}$ |
| $1,x,x-1$ | $\frac{-3+6x^2+6x^4-4s_1(s_1+1)(1+2x^2)}{5(4x^2-1)}$ | $\frac{4x^2+2x^4+4s_1(s_1+1)(1+2x^2)}{5(4x^2-1)}$ |
| $2,x,x$ | $\frac{(2x+5)(2x-3)[3(1-x-x^2)+4s_1(s_1+1)]}{21(2x+3)(2x-1)}$ | $-\frac{(2x+5)(2x-3)[x^2+x+4s_1(s_1+1)]}{21(2x+3)(2x-1)}$ |
| $2,x,x-1$ | $\frac{3(5-16x^2+2x^4)-4s_1(s_1+1)(5-2x^2)}{21(4x^2-1)}$ | $\frac{2x^2(7-x^2)+4s_1(s_1+1)(5-2x^2)}{21(4x^2-1)}$ |
| $2,x,x-2$ | $-\frac{3(-3+x+x^2)+4s_1(s_1+1)}{21}$ | $\frac{4-x+x^2+4s_1(s_1+1)}{21}$ |
| $3,x,x$ | $\frac{(-33+4x+4x^2)[-9(-1+x+x^2)+4s_1(s_1+1)]}{45(2x+3)(2x-1)}$ | $-\frac{(-33+4x+4x^2)[x+x^2+4s_1(s_1+1)]}{45(2x+3)(2x-1)}$ |
| $3,x,x-1$ | $\frac{198-729x^2+330x^4-24x^6+8s_1(s_1+1)(33-37x^2+4x^4)}{30(4x^2-1)(4x^2-9)}$ | $-\frac{169x^2-102x^4+8s_1(s_1+1)(33-37x^2+4x^4)}{30(4x^2-1)(4x^2-9)}$ |
| $3,x,x-2$ | $\frac{1}{2}$ | $\frac{1}{6}$ |
| $3,x,x-3$ | $\frac{27-78x+63x^2-24x^3+6x^4-8s_1(s_1+1)x(x-2)}{18(2x-1)(2x-3)}$ | $\frac{9-30x+23x^2-8x^3+2x^4+8s_1(s_1+1)x(x-2)}{18(2x-1)(2x-3)}$ |

ues, and the polarization also vanishes at the $\gamma B/|\tilde{J}_g|$ value at which the fourth magnetization step is completed. Finally, in Fig. 9, we plotted $|\boldsymbol{P}_s|$ in arbitrary units versus $\theta/\pi$ with the same parameters as in Fig. 6, except that the larger field is for $\gamma B/|\tilde{J}_g|=1.5$. The curves with $\gamma B/|\tilde{J}_g|=1,1.5$ exhibit broad maxima at $\theta/\pi \approx 0.28,0.31$, respectively, approximately as for the corresponding curves with $s_1=1/2$, and both $\boldsymbol{P}_s(\theta)$ curves are odd about $\theta=\pi/2$, as are the two curves shown in Fig. 6 for $s_1=1/2$.

### E. First-order antiferromagnetic level-crossing inductions

For AFM tetramers, $\tilde{J}_g<0$. There will be $2s_1+1$ level crossings, as exhibited by the magnetization steps in Figs. 4 and 7 for $s_1=1/2$ and 1, respectively, provided that the lowest energy state in each $s$ manifold does not exhibit level repulsion. In order to specify the level-crossing inductions, we first write $E_{s,m}^{g}(s_{13},s_{24})=E_{\nu,0}^{g}+E_{\nu,1}^{g}$. We then note that the $s_{13}$ and $s_{24}$ values involved in level crossings are those corresponding to the lowest energies for a particular $s$ value. These are different for type-I and II tetramers. For type-I tetramers, the level-crossing inductions occur for

$$E_{s,s}^{g}(2s_1,2s_1)=E_{s-1,s-1}^{g}(2s_1,2s_1), \tag{60}$$

and for type-II tetramers, they occur for

$$E_{s,s}^{g}(s/2,s/2)=E_{s-1,s-1}^{g}[(s-1\pm 1)/2,(s-1\mp 1)/2] \tag{61}$$

for even $s$, and

$$E_{s,s}^{g}[(s\pm 1)/2,(s\mp 1)/2]=E_{s-1,s-1}^{g}[(s-1)/2,(s-1)/2] \tag{62}$$

for odd $s$. In Appendixes G and H, we presented the formulas for the level-crossing induction parameters for both types-I and II tetramers.

For type-I tetramers, the first-order level-crossing inductions $B_{s_1,s}^{g,\mathrm{lc}(1)}$ obtained from Eq. (60) have the remarkably simple form

$$\gamma B_{s_1,s}^{g,\mathrm{lc}(1)}(\theta)=-s(\tilde{J}_g+2s_1^2J_{\mathrm{t},2}^{g})-J_z^g\frac{b^+}{2}-J_{\mathrm{b},1}^{g}d-J_{\mathrm{t},1}^{g}e$$
$$-\frac{c_1^-}{3}\left(J_{\mathrm{eff}}^{g}-\frac{(2s_1-1)}{(4s_1-1)}J_z^g\right)(1-3\cos^2\theta), \tag{63}$$

TABLE IX. Values of $b_{\bar{\nu}}^{+}$ and $c_{\bar{\nu}}^{-}$ for the ground and first three excited state manifolds for AFM tetramers (or the highest four excited state manifolds of FM tetramers), where $\tilde{b}_1(x)=12(15-19x-15x^2+8x^3+4x^4)$, $\tilde{b}_2(x)=3(33-37x-33x^2+8x^3+4x^4)$, $\tilde{b}_3(x)=3(-66+243x^2-110x^4+8x^6)$, and $\tilde{b}_4(x)=-3(9-26x+21x^2-8x^3+2x^4)$.

| $s,s_{13},s_{24}$ | $b_{\bar{\nu}}^{+}$ | $b_{\bar{\nu}}^{-}$ | $c_{\bar{\nu}}^{-}$ |
|---|---|---|---|
| $0,x,x$ | $\frac{8s_1(s_1+1)}{3}$ | $\frac{4x(x+1)-8s_1(s_1+1)}{3}$ | $\frac{3+4x+4x^2}{6}$ |
| $1,x,x$ | $\frac{4[-1+x+x^2+2s_1(s_1+1)]}{5}$ | $\frac{8[x(x+1)-s_1(s_1+1)]}{5}$ | $\frac{3-4x-4x^2}{6}$ |
| $1,x,x-1$ | $\frac{4[1-2x^2-2x^4-2s_1(s_1+1)(1-8x^2)]}{5(4x^2-1)}$ | $\frac{4[-3x^2(1-2x^2)+2s_1(s_1+1)(1-8x^2)]}{5(4x^2-1)}$ | $\frac{3(1-x^2)}{10}$ |
| $2,x,x$ | $\frac{\tilde{b}_1(x)+8s_1(s_1+1)(9+20x+20x^2)}{21(2x+3)(2x-1)}$ | $\frac{-16x(9+x-16x^2-8x^3)-8s_1(s_1+1)(9+20x+20x^2)}{21(2x+3)(2x-1)}$ | $\frac{15-4x-4x^2}{42}$ |
| $2,x,x-1$ | $\frac{4[5-16x^2+2x^4+2s_1(s_1+1)(1+8x^2)]}{7(4x^2-1)}$ | $-\frac{4[7x^2-10x^4+2s_1(s_1+1)(1+8x^2)]}{7(4x^2-1)}$ | $\frac{15+x^2}{42}$ |
| $2,x,x-2$ | $\frac{4[-3+x-x^2+6s_1(s_1+1)]}{7}$ | $\frac{4[1-2x+2x^2-6s_1(s_1+1)]}{7}$ | $\frac{8(2+x-x^2)}{63}$ |
| $3,x,x$ | $\frac{8[\tilde{b}_2(x)+s_1(s_1+1)(87+44x+44x^2)]}{45(2x+3)(2x-1)}$ | $-\frac{4[x(111+43x-136x^2-68x^3)+2s_1(s_1+1)(87+44x+44x^2)]}{45(2x+3)(2x-1)}$ | $\frac{33-4x-4x^2}{90}$ |
| $3,x,x-1$ | $\frac{4[\tilde{b}_3(x)-2s_1(s_1+1)(87+52x^2-64x^4)]}{15(4x^2-1)(4x^2-9)}$ | $\frac{8[x^2(107-151x^2+44x^4)+s_1(s_1+1)(87+52x^2-64x^4)]}{15(4x^2-1)(4x^2-9)}$ | $\frac{132-17x^2}{360}$ |
| $3,x,x-2$ | $\frac{4[-3+2s_1(s_1+1)]}{3}$ | $-\frac{4[x(1-x)+2s_1(s_1+1)]}{3}$ | $\frac{23+4x-4x^2}{72}$ |
| $3,x,x-3$ | $\frac{4[\tilde{b}_4(x)+2s_1(s_1+1)(9-32x+16x^2)]}{9(2x-3)(2x-1)}$ | $-\frac{8[-9+30x-35x^2+20x^3-5x^4+s_1(s_1+1)(9-32x+16x^2)]}{9(2x-3)(2x-1)}$ | $\frac{5(3+2x-x^2)}{72}$ |

$$J_{\rm eff}^{g}=\frac{J_{1,z}^{g}}{2}+\frac{s_1 J_{2,z}^{g}}{4s_1-1}, \tag{64}$$

where $b^{+}=b_I^{s_1,+}(s)$, $c_1^{-}=c_{I,1}^{s_1,-}(s)$, $d=d_I^{s_1}(s)$, and $e=e_I^{s_1}(s)$ are given in Appendix G. We note that this is independent of $\tilde{J}_g'$ and $J_{\rm b,2}^{g}$, $J_{\rm t,2}^{g}$ just renormalizes $\tilde{J}_g$, and that the NN and NNN symmetric anisotropic exchange interactions combine to yield the universal type-I level crossing form $J_{\rm eff}^{g}$. Furthermore, the $\theta$ dependencies of the single-ion and symmetric anisotropic exchange contributions have the same $s$ dependencies for fixed $s_1$. However the $\theta$-independent contributions from $J_z^g$, $J_{\rm eff}^{g}$, $J_{\rm b,1}^{g}$, and $J_{\rm t,1}^{g}$ separately depend on $s$ for fixed $s_1$.

For the type-II AFM tetramer level-crossing inductions, the contributions from the near-neighbor anisotropic exchange interaction $J_{1,z}^{g}$ have a rather simple form. As shown in Appendix H, these contributions $\gamma B_{1,z}^{g,{\rm lc}(1)}=J_{1,z}^{g}f_{1,z}(s,\theta)$ to $\gamma B_{s_1,s}^{g,{\rm lc}(1)}(\theta)$ are independent of $s_1$, where

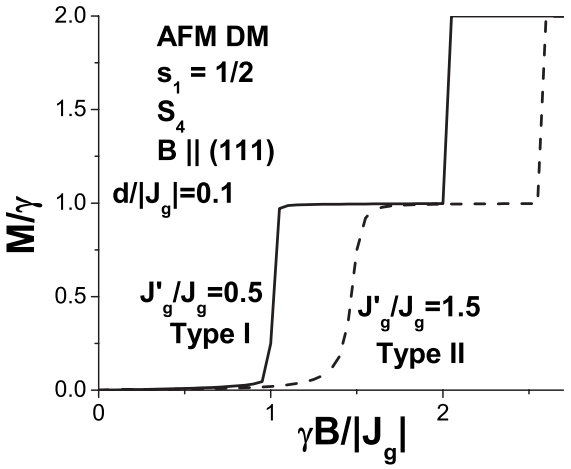


FIG. 4. Plots of the magnetization $M/\gamma$ versus $\gamma B/|\tilde{J}_g|$ of a $s_1=1/2$ tetramer at $T=0$ with $c=a$, $g=S_4$, $d_z^g=d_{1y}^g=d_{2x}^g=d_{2y}^g=d$, $d_{1x}^g=0$, $d/|\tilde{J}_g|=0.1$, and $\boldsymbol{B}\|(111)$. The solid and dashed curves are for the type-I ($\tilde{J}_g'/\tilde{J}_g=0.5$) and type-II ($\tilde{J}_g'/\tilde{J}_g=1.5$) tetramers, respectively.

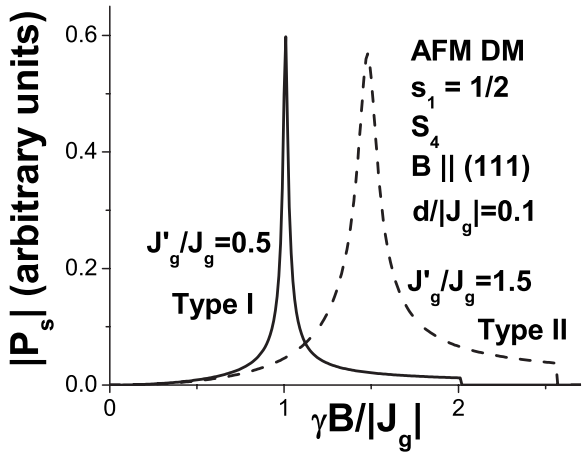


FIG. 5. Plots of the magnitude of the spin-induced polarization $|\boldsymbol{P}_s|$ in arbitrary units versus $\gamma B/|\tilde{J}_g|$ at $T=0$ of a $s_1=1/2$ tetramer with $c=a$, $g=S_4$, $d_z^g=d_{1y}^g=d_{2x}^g=d_{2y}^g=d$, $d_{1x}^g=0$, $d/|\tilde{J}_g|=0.1$, and $\boldsymbol{B}\|(111)$. The solid and dashed curves are for the type-I ($\tilde{J}_g'/\tilde{J}_g=0.5$) and type-II ($\tilde{J}_g'/\tilde{J}_g=1.5$) tetramers, respectively.

$$f_{1,z}(s,\theta)=\begin{cases}\dfrac{(s-1)}{4s}[1+(2s-1)\cos^2\theta] & s \text{ odd}\\ \dfrac{s}{4(s-1)}[1+(2s-3)\cos^2\theta] & s \text{ even}.\end{cases} \tag{65}$$

Note, in particular, that for $s=1$, $f_{1,z}(1,\theta)=0$. However, the single-ion and NNN symmetric anisotropic exchange contributions to the level-crossing inductions depend on both $s$ and $s_1$ in different ways.

#### 1. $s_1=1/2$ *first-order antiferromagnetic level crossings*

For the simplest case $s_1=1/2$, as in AFM $Cu_4$ tetramers, the single-ion interaction $J_z^g$ does not contribute to the first-order eigenstate energies, as for the dimer of equal $s_1=1/2$ spins.[5] By using the results given in Appendixes G and H

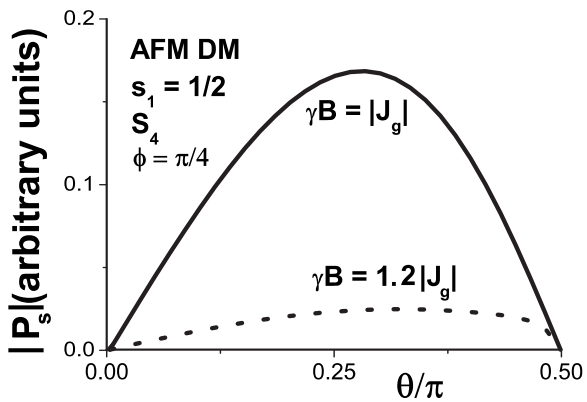


FIG. 6. Plots of the magnitude of the spin-induced polarization $|\boldsymbol{P}_s|$ in arbitrary units versus $\theta/\pi$ at $T=0$ of a $s_1=1/2$ tetramer with $c=a$, $g=S_4$, $\tilde{J}_g'/\tilde{J}_g=1$, $d_z^g=d_{1y}^g=d_{2x}^g=d_{2y}^g=d$, $d_{1x}^g=0$, $d/|\tilde{J}_g|=0.01$, and $\phi=\pi/4$. The solid and dashed curves are for $\gamma B/|\tilde{J}_g|=1$ and 1.2, respectively.

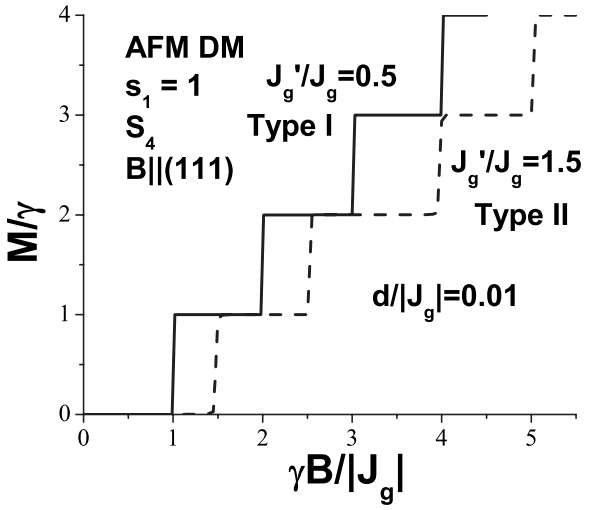


FIG. 7. Plots of the magnetization $M/\gamma$ versus $\gamma B/|\tilde{J}_g|$ of a $s_1=1$ tetramer at $T=0$ with $c=a$, $g=S_4$, $d_z^g=d_{1y}^g=d_{2x}^g=d_{2y}^g=d$, $d_{1x}^g=0$, $d/|\tilde{J}_g|=0.01$, and $\boldsymbol{B}\|(111)$. The solid and dashed curves are for the type-I ($\tilde{J}_g'/\tilde{J}_g=0.5$) and type-II ($\tilde{J}_g'/\tilde{J}_g=1.5$) tetramers, respectively.

and Table IV, the expressions for the $\gamma B_{1/2,s}^{g,\mathrm{lc}(1)}(\theta)$ functions are particularly simple. For $s_1=1/2$ effective-dimer AFM type-I tetramers, $\tilde{J}_g<0$ and $\tilde{J}_g'-\tilde{J}_g>0$,

$$\gamma B_{1/2,1}^{g,\mathrm{lc}(1)}(\theta)=-\tilde{J}_g+\frac{1}{2}(J_{\mathrm{b},1}^g-J_{\mathrm{t},2}^g)+\frac{1}{6}J_{\mathrm{eff}}^g(1-3\cos^2\theta), \tag{66}$$

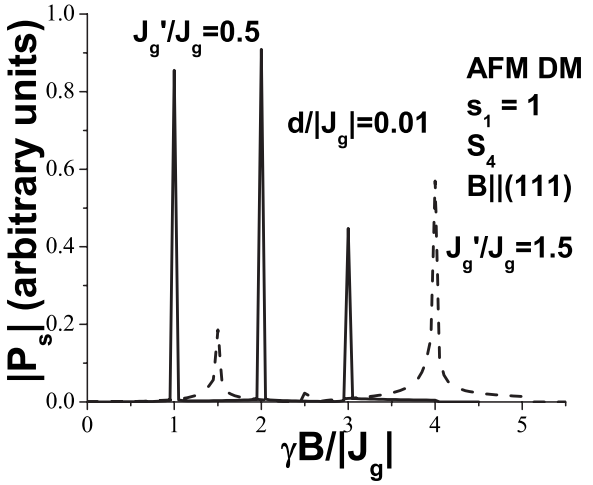


FIG. 8. Plots of the magnitude of the spin-induced polarization $|\boldsymbol{P}_s|$ in arbitrary units versus $\gamma B/|\tilde{J}_g|$ at $T=0$ of a $s_1=1$ tetramer with $c=a$, $g=S_4$, $d_z^g=d_{1y}^g=d_{2x}^g=d_{2y}^g=d$, $d_{1x}^g=0$, $d/|\tilde{J}_g|=0.01$, and $\boldsymbol{B}\|(111)$. The solid and dashed curves are for the type-I ($\tilde{J}_g'/\tilde{J}_g=0.5$) and type-II ($\tilde{J}_g'/\tilde{J}_g=1.5$) tetramers, respectively.

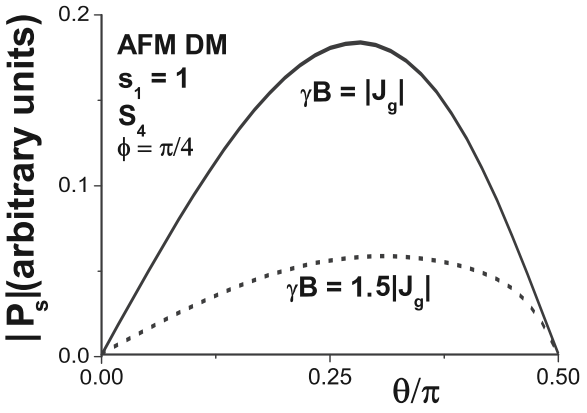


FIG. 9. Plots of the magnitude of the spin-induced polarization $|\boldsymbol{P}_s|$ in arbitrary units versus $\theta/\pi$ at $T=0$ of a $s_1=1$ tetramer with $c=a$, $g=S_4$, $\tilde{J}'_g/\tilde{J}_g=1$, $d^g_z=d^g_{1y}=d^g_{2x}=d^g_{2y}=d$, $d^g_{1x}=0$, $d/|\tilde{J}_g|=0.01$, and $\phi=\pi/4$. The solid and dashed curves are for $\gamma B/|\tilde{J}_g|=1$ and 1.5, respectively.

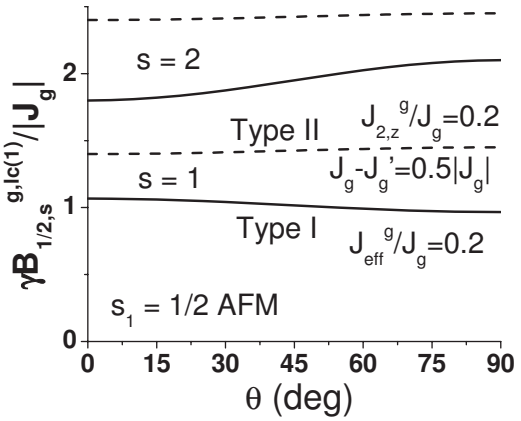


FIG. 10. Plots of the $s_1=1/2$ first-order level crossing $\gamma B^{g,\mathrm{lc}(1)}_{1/2,s}(\theta)/|\tilde{J}_g|$, where $\theta$ is the angle between $\boldsymbol{B}$ and $\hat{\boldsymbol{z}}$, with $J^g_{\mathrm{b},q}=0$, $J^g_{\mathrm{eff}}/\tilde{J}_g=0.2$, $\tilde{J}'_g-\tilde{J}_g>0$ (solid, type I) and $J^g_{2,z}/\tilde{J}_g=0.2$, $\tilde{J}_g-\tilde{J}'_g=0.5|\tilde{J}_g|$ (dashed, type II).

$$\gamma B^{g,\mathrm{lc}(1)}_{1/2,2}(\theta)=-2\tilde{J}_g+J^g_{\mathrm{b},1}-J^g_{\mathrm{t},2}-\frac{1}{2}J^g_{\mathrm{eff}}(1-3\cos^2\theta), \tag{67}$$

where $J^g_{\mathrm{eff}}$ is given by Eq. (64) with $s_1=1/2$. For frustrated type-II AFM tetramers with $s_1=1/2$, $\tilde{J}_g<0$ and $\tilde{J}_g-\tilde{J}'_g>0$,

$$\gamma B^{g,\mathrm{lc}(1)}_{1/2,1}(\theta)=-\tilde{J}'_g-\frac{1}{4}(3J^g_{\mathrm{b},1}-J^g_{\mathrm{t},1})+\frac{J^g_{\mathrm{b},2}}{2}+\frac{1}{4}J^g_{2,z}(1+\cos^2\theta), \tag{68}$$

$$\gamma B^{g,\mathrm{lc}(1)}_{1/2,2}(\theta)=-\tilde{J}_g-\tilde{J}'_g+\frac{5}{4}(J^g_{\mathrm{b},1}-J^g_{\mathrm{t},1})+\frac{1}{2}(J^g_{\mathrm{b},2}-J^g_{\mathrm{t},2})+\frac{1}{4}(2J^g_{1,z}+J^g_{2,z})(1+\cos^2\theta). \tag{69}$$

Even in this simplest of all tetramer cases, there is still a qualitative difference between the level-crossing inductions of type-I and type-II AFM $s_1=1/2$ tetramers. For type-I $s_1=1/2$ tetramers, there are only two parameters, $\tilde{J}_g+(J^g_{\mathrm{t},2}-J^g_{\mathrm{b},1})/2$ and $J^g_{\mathrm{eff}}=(J^g_{1,z}+J^g_{2,z})/2$, that affect the two level crossings. However, for type-II $s_1=1/2$ tetramers, the two level crossings are governed by four effective parameters. These expressions also show that type-II AFM tetramers have a more complex level-crossing induction variation than do type-I $s_1=1/2$ AFM tetramers. For this special $s_1=1/2$ example, the $\theta$ dependencies of the first and second $\gamma B^{g,\mathrm{lc}(1)}_{1/2,s}$ are opposite in sign for type I, but can have the same sign for type II. In Fig. 10, we illustrate these $s_1=1/2$ behaviors for type I with $J^g_{\mathrm{eff}}/\tilde{J}_g=0.2$ and for type II with $J^g_{2,z}/\tilde{J}_g=0.2$ and $\tilde{J}_g-\tilde{J}'_g=0.5|\tilde{J}_g|$.

In the special case of $T_d$ symmetry, we have $\tilde{J}_{T_d}=\tilde{J}'_{T_d}=J$, $J^{T_d}_{\mathrm{b},1}=J^{T_d}_{\mathrm{b},2}=J_b$, $J^{T_d}_{\mathrm{t},1}=J^{T_d}_{\mathrm{t},2}=J_t$, and $J^{T_d}_{q,z}=0$. Since for $s_1=1/2$, $\mathcal{H}^g_b$ and $\mathcal{H}^g_t$ are diagonal, the $J_b$ and $J_t$ dependencies of the eigenstate energies are exact. Hence, the only difference between type-I and type-II $s_1=1/2$ tetramers with $T_d$ symmetry is determined by the sign of $J_b-J_t$, as is evident by comparing Eqs. (66)–(69). In any event, there are no $\theta$ dependencies to the first-order level-crossing inductions for $s_1=1/2$ AFM tetramers with $T_d$ symmetry.

#### 2. $s_1\geq 1$ *first-order antiferromagnetic level crossings*

For $s_1>1/2$, the AFM level crossings become much more complex than for the $s_1=1/2$ case, as single-ion anisotropies $J^g_z$ are allowed, and the biquadratic and three-center quartic interactions $J^g_{\mathrm{b},q}$ and $J^g_{\mathrm{t},q}$ differently affect the various level crossings. We first consider the simplest $s_1>1/2$ case, $s_1=1$, appropriate for AFM $Ni_4$ tetramers. The first-order eigenstate energy parameters are listed in Table V. For the isotropic case $J^g_z=J^g_{q,z}=0$, the Hamiltonian matrix is block diagonal, and the resulting eigenvalues are listed in Table X. Analytic expressions for the $s=1$, 2, 3, and 4 first-order level-crossing inductions $B^{g,\mathrm{lc}(1)}_{1,s}(\theta)$ for type-I and type-II $s_1=1$ tetramers are given in Appendix F. In Figs. 11 and 12, we plotted the $\theta$ dependencies of the first-order level-crossing inductions $\gamma B^{g,\mathrm{lc}(1)}_{1,s}(\theta)/|\tilde{J}_g|$ for $g=C_{4h}$, $D_{4h}$, $C_{4v}$, $S_4$, and $D_{2d}$, for two AFM type-I examples and for three type-II examples with $\tilde{J}_g-\tilde{J}'_g=0.5|\tilde{J}_g|$, respectively. In each curve, we allow only one of the anisotropy interaction strengths to be nonvanishing. In Fig. 11, the solid and dashed curves are for $J^g_z/\tilde{J}_g=0.2$ and $J^g_{\mathrm{eff}}/\tilde{J}_g=0.2$, respectively, where $J^g_{\mathrm{eff}}=J^g_{1,z}/2+J^g_{2,z}/3$ for $s_1=1$. We note from Eq. (63) and from Fig. 11 that for type I, the single-ion and symmetric exchange anisotropies lead to opposite $\theta$ dependencies, both having a change in sign just before the second level crossing, and the dependence of $\gamma B^{g,\mathrm{lc}(1)}_{1,s}$ on $J^g_{\mathrm{b},1}$ decreases with increasing $s$.

In Fig. 12, we illustrate the $s_1=1$ type-II level crossings, setting $\tilde{J}_g-\tilde{J}'_g=0.5|\tilde{J}_g|$. The solid curves are for $J^g_z/\tilde{J}_g=0.2$ for $g=C_{4h}$, $D_{4h}$, $C_{4v}$, $S_4$, and $D_{2d}$, as in Fig. 11. The dashed and dotted curves are for $J^g_{1,z}/\tilde{J}_g=0.4$ and $J^g_{2,z}/\tilde{J}_g=0.4$, respectively. For each curve, the type-II isotropic exchange parameters lead to a larger gap between the $s=2$ and $s=3$ level crossings. The sign of the $\theta$ dependencies of the single-ion (solid) curves changes between $s=2$ and $s=3$. The effects of

TABLE X. Eigenstate energies $E_{\bar{\nu}}$ of $\mathcal{H}=\mathcal{H}_0^{g,r}+\mathcal{H}_b^g+\mathcal{H}_t^g$ for $s_1=1$ as a function of the quantum numbers $\bar{\nu}=s$, $s_{13}$, and $s_{24}$ (prior to the $s$-manifold diagonalizations) in the absence of anisotropy interactions. The two additional $s=2$ eigenstate energies $E_{2\pm}=\frac{1}{2}[a\pm\sqrt{b^2+56(J^g_{b,1})^2}]$, where $a=3\tilde{J}_g-9\tilde{J}'_g-\frac{63}{4}J^g_{b,1}-7J^g_{b,2}+\frac{15}{4}J^g_{t,1}+6J^g_{t,2}$ and $b=3\tilde{J}_g-3\tilde{J}'_g+\frac{17}{4}J^g_{b,1}+3J^g_{b,2}-\frac{33}{4}J^g_{t,1}+6J^g_{t,2}$. The two sets of doubly degenerate $s=1$ eigenstates have $E_{1\pm}=\frac{1}{2}[A+B\pm\sqrt{(A-B)^2+4C^2}]$, where $A=3\tilde{J}_g-4\tilde{J}'_g-\frac{23}{4}J^g_{b,1}-2J^g_{b,2}+\frac{1}{12}J^g_{t,1}$, $B=-\tilde{J}'_g-9J^g_{b,1}-5J^g_{b,2}+\frac{23}{3}J^g_{t,1}$, and $C=\frac{\sqrt{5}}{3}(3J^g_{b,1}-4J^g_{t,1})$, and $E_{0\pm}=\frac{1}{2}[\alpha+\beta\pm\sqrt{(\alpha-\beta)^2+4\gamma^2}]$, where $\alpha=-6\tilde{J}_g+6\tilde{J}'_g-\frac{32}{3}J^g_{b,1}-2J^g_{b,2}-\frac{22}{3}J^g_{t,1}+12J^g_{t,2}$, $\beta=\frac{16}{3}(J^g_{t,1}-J^g_{b,1})-8J^g_{b,2}$, and $\gamma=\frac{4\sqrt{5}}{3}(J^g_{t,1}-J^g_{b,1})$.

| $\bar{\nu}=ss_{13}s_{24}$ | $E_{\bar{\nu}}$ |
|---|---|
| 422 | $-4\tilde{J}_g-6\tilde{J}'_g-4J^g_{b,1}-2J^g_{b,2}-4J^g_{t,1}-8J^g_{t,2}$ |
| 322 | $-6\tilde{J}'_g-4J^g_{b,1}-2J^g_{b,2}$ |
| 312,321 | $-2\tilde{J}_g-4\tilde{J}'_g-\frac{43}{9}J^g_{b,1}-2J^g_{b,2}+\frac{7}{9}J^g_{t,1}$ |
| 212,221 | $\tilde{J}_g-4\tilde{J}'_g-\frac{307}{36}J^g_{b,1}-2J^g_{b,2}+\frac{55}{36}J^g_{t,1}$ |
| 211 | $-\tilde{J}_g-2\tilde{J}'_g-\frac{31}{4}J^g_{b,1}-2J^g_{b,2}+\frac{23}{4}J^g_{t,1}+2J^g_{t,2}$ |
| 222,202,220 | $-3\tilde{J}'_g-4J^g_{b,1}-5J^g_{b,2}, E_{2\pm}$ |
| 122 | $2\tilde{J}_g-3\tilde{J}'_g-\frac{31}{4}J^g_{b,1}-2J^g_{b,2}-\frac{25}{4}J^g_{t,1}+10J^g_{t,2}$ |
| 111 | $\tilde{J}_g-2\tilde{J}'_g-\frac{15}{4}J^g_{b,1}-2J^g_{b,2}-\frac{1}{4}J^g_{t,1}-2J^g_{t,2}$ |
| 121,101 | $E_{1\pm}$ |
| 112,110 | $E_{1\pm}$ |
| 011 | $-2\tilde{J}_g+2\tilde{J}'_g-8J^g_{b,1}-2J^g_{b,2}+6J^g_{t,1}-4J^g_{t,2}$ |
| 022,000 | $E_{0\pm}$ |

the NN symmetric anisotropic exchange interactions vanish for $s=1$, but increase in magnitude with increasing $s$ for $s=2$, 3, and 4. The sign of the $\theta$ dependence of the level crossing due to the NNN symmetric anisotropic exchange interactions does not change, but its magnitude monotonically increases. Thus, type-II AFM $s_1=1$ tetramers have a richer set of first-order level-crossing behaviors than do type-I AFM $s_1=1$ tetramers, and the unpictured biquadratic and three-center quartic interactions increase this richness.

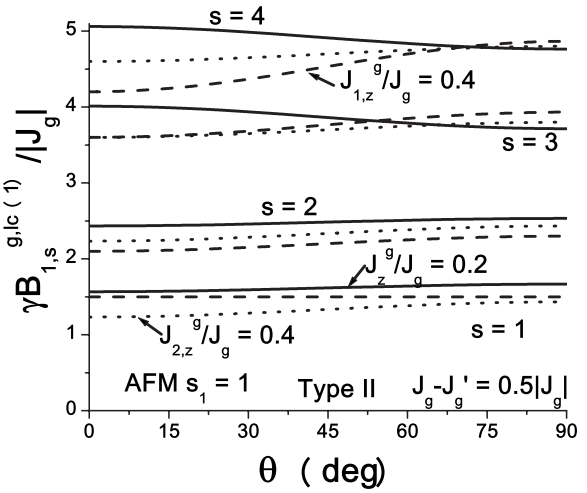


FIG. 12. Plots of the first-order level crossing $\gamma B^{g,\mathrm{lc}(1)}_{1,s}(\theta)/|\tilde{J}_g|$ for type II with $g=C_{4h},D_{4h}$, $C_{4v}$, $S_4$, $D_{2d}$, $\tilde{J}_g-\tilde{J}'_g=0.5|\tilde{J}_g|$, $J^g_{b,q}=0$, and $s_1=1$. Solid curves, $J^g_z/\tilde{J}_g=0.2$. Dashed curves, $J^g_{1,z}/\tilde{J}_g=0.4$. Dotted curves, $J^g_{2,z}/\tilde{J}_g=0.4$.

In Figs. 13 and 14, the analogous type-I and type-II first-order AFM level-crossing inductions are plotted versus $\theta$ for $s_1=3/2$ equal-spin tetramers, such as $Cr_4$. The notation is the same as in Figs. 11 and 12. For type-I $s_1=3/2$ AFM tetramers, the single-ion and symmetric anisotropic exchange interactions lead to different $\theta$ dependencies of the level-crossing inductions, each with a change in sign in the $\theta$ dependence at about the second level crossing, as seen in Fig. 13. For type-II $s_1=3/2$ AFM tetramers, the sign changes appear between the second and third level crossings, as shown in Fig. 14. Although not pictured, the contributions for $s_1=3/2$ to the level-crossing inductions from $J^g_{b,q}$ and $J^g_{t,q}$ can easily be calculated from Eq. (56) and the expressions for $d^{3/2}_{IIo}(s)$, $d^{3/2}_{IIe}(s)$, $e^{3/2}_{IIo}(s)$, and $e^{3/2}_{IIe}(s)$ in Appendix H. They contribute to

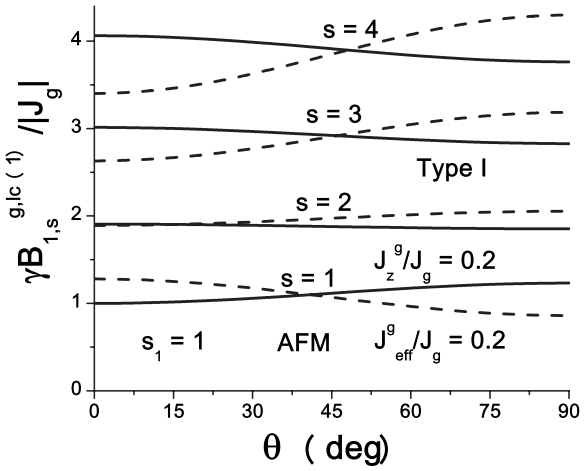


FIG. 11. Plots of the first-order level crossing $B^{g,\mathrm{lc}(1)}_{1,s}(\theta)/|\tilde{J}_g|$ for type I, $\tilde{J}_g-\tilde{J}'_g<0$, $J^g_{b,q}=0$, and $s_1=1$. Solid curves, $J^g_z/\tilde{J}_g=0.2$. Dashed curves, $J^g_{\mathrm{eff}}/\tilde{J}_g=0.2$.

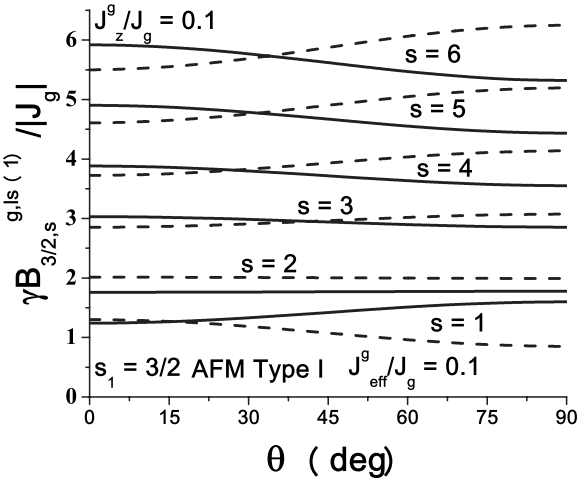


FIG. 13. Plots of the first-order level crossing $\gamma B^{g,\mathrm{lc}(1)}_{3/2,s}(\theta)/|\tilde{J}_g|$ for type I, $\tilde{J}_g-\tilde{J}'_g<0$, $J^g_{b,q}=0$, and $s_1=3/2$. Solid curves, $J^g_z/\tilde{J}_g=0.1$. Dashed curves, $J^g_{\mathrm{eff}}/\tilde{J}_g=0.1$.

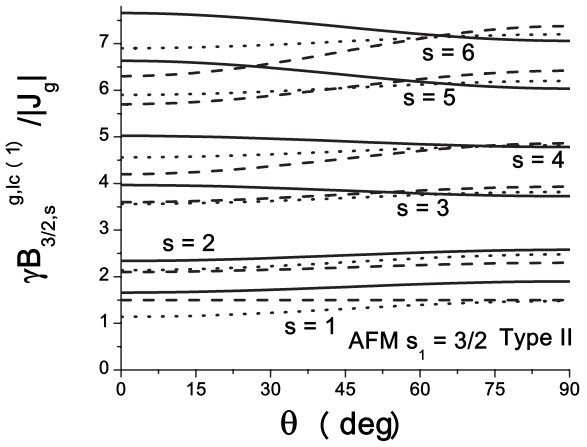


FIG. 14. Plots of the first-order level crossing $\gamma B^{g,\mathrm{lc}(1)}_{3/2,s}(\theta)/|\tilde{J}_g|$ for type II with $g=C_{4h}$, $D_{4h}$, $C_{4v}$, $S_4$, $D_{2d}$, $\tilde{J}_g-\tilde{J}'_g=0.5|\tilde{J}_g|$, $J^g_{\mathrm{b,q}}=0$, and $s_1=3/2$. Solid curves, $J^g_z/\tilde{J}_g=0.2$. Dashed curves, $J^g_{1,z}/\tilde{J}_g=0.4$. Dotted curves, $J^g_{2,z}/\tilde{J}_g=0.4$.

a more complex level-crossing pattern than for $s_1=1$.

For $g=T_d$ with $s_1>1/2$, we still have $J^g_{q,z}=J^g_z=0$, so that the first-order level-crossing inductions $\gamma B^{T_d,\mathrm{lc}(1)}_{s_1,s}(\theta)/|\tilde{J}_{T_d}|$ vary from integral values only by $\theta$-independent constants due to the biquadratic $J^{T_d}_{\mathrm{b},1}=J^{T_d}_{\mathrm{b},2}=J_b$ and three-center quartic $J^{T_d}_{\mathrm{t},1}=J^{T_d}_{\mathrm{t},2}=J_t$ interaction strengths. For $s_1=1$ without any anisotropy interactions, the exact eigenstates are compiled in Table X.

## VII. SELF-CONSISTENT HARTREE APPROXIMATION

### A. Partition function and thermodynamics

The self-consistent Hartree approximation, or strong exchange limit,[37] provides accurate results for the $\boldsymbol{B}$ dependence of the specific heat and magnetization at low $k_BT/|\tilde{J}_g|$ and not too small $\gamma B/|\tilde{J}_g|$,[5] where $k_B$ is Boltzmann's constant. In this approximation, $E^g_\nu=E^g_{\nu,0}+E^g_{\nu,1}$ is given by Eqs. (55) and (57), respectively. We shall present the self-consistent Hartree approximation of four measurable quantities in the induction representation. We first define the trace valid for our eigenstate representation as follows:

$$\mathrm{Tr}_\nu \equiv \sum_\nu = \sum_{s_{13},s_{24}=0}^{2s_1} \sum_{m=-s}^{s} \sum_{s=|s_{13}-s_{24}|}^{s_{13}+s_{24}}. \tag{70}$$

The partition function in the self-consistent Hartree approximation may then be written

$$Z^{(1)}_g = \mathrm{Tr}_\nu\, e^{-\beta E^g_\nu}, \tag{71}$$

where $\beta=1/k_BT$. In this compact notation, the self-consistent Hartree magnetization $M^{(1)}_g(\boldsymbol{B},T)$ and specific heat $C^{(1)}_{g,V}(\boldsymbol{B},T)$ are given by

$$M^{(1)}_g(\boldsymbol{B},T) = \gamma\, \mathrm{Tr}_\nu(m e^{-\beta E^g_\nu})/Z^{(1)}_g, \tag{72}$$

$$\frac{C^{(1)}_{g,V}(\boldsymbol{B},T)}{k_B\beta^2} = \frac{\mathrm{Tr}_\nu[(E^g_\nu)^2 e^{-\beta E^g_\nu}]}{Z^{(1)}_g} - \left[\frac{\mathrm{Tr}_\nu(E^g_\nu e^{-\beta E^g_\nu})}{Z^{(1)}_g}\right]^2. \tag{73}$$

We note that there are strong differences between the low-$T$ behavior of FM and AFM tetramers. We assume $|\tilde{J}_g|>|\tilde{J}'_g-\tilde{J}_g|$. For FM tetramers with $\tilde{J}_g>0$, the low-$T$ thermodynamic behavior is dominated by the $s=4s_1$, $m=-4s_1$ state, leading to

$$M^{(1)}_g(\boldsymbol{B},T) \underset{T\to 0}{\approx} \gamma\hat{\boldsymbol{B}}\mathcal{B}_{4s_1}(\beta\gamma B), \tag{74}$$

where $\mathcal{B}_S(x)$ is the Brillouin function. The universality of this function renders thermodynamic studies useless for the determination of the microscopic parameters. For AFM tetramers with $\tilde{J}_g<0$, however, there will be interesting level-crossing effects, which can be employed to measure the microscopic interaction parameters, as discussed in detail in Sec. VI. As for dimers, $C_V(B,T)$ for AFM tetramers at sufficiently low $T$ exhibits $2s_1$ central minima at the level-crossing inductions $B^{g,\mathrm{lc}}_{s_1,s}(\theta)\approx B^{g,\mathrm{lc}(1)}_{s_1,s}(\theta)$ that vanish as $T\to 0$, which are equally surrounded by peaks of equal height.[5] As for the magnetization, $C_V(B,T)$ for FM tetramers at low $T$ reduces to that of a monomer with spin $4s_1$, yielding a rather uninteresting Schottky anomaly.

### B. Electron paramagnetic resonance

However, the microscopic nature of FM tetramers can be better probed either by EPR or INS techniques. The self-consistent Hartree EPR absorption $\Im\chi^{g,(1)}_{-\sigma,\sigma}(\boldsymbol{B},\omega)$ for clockwise ($\sigma=1$) or counterclockwise ($\sigma=-1$) circularly polarized oscillatory fields normal to $\boldsymbol{B}$ is

$$\Im\chi^{g,(1)}_{-\sigma,\sigma} = \frac{\gamma^2}{Z^{(1)}_g}\mathrm{Tr}_\nu\,\mathrm{Tr}_{\nu'}\, e^{-\beta E^g_\nu}|M_{\nu,\nu'}|^2[\delta(E^g_\nu - E^g_{\nu'}+\omega) - \delta(E^g_{\nu'}-E^g_\nu+\omega)], \tag{75}$$

where $M_{\nu,\nu'}=A^{\sigma m}_s\delta_{m',m+\sigma}\delta_{s',s}\delta_{s'_{13},s_{13}}\delta_{s'_{24},s_{24}}$ and $\mathrm{Tr}_{\nu'}=\Sigma_{\nu'}$. The strong resonant inductions appear at

$$\gamma B^{g,(1)}_{\mathrm{res}} = \pm\omega + \frac{(2m+\sigma)}{2}(1-3\cos^2\theta)\tilde{J}^{g,\bar{\nu}}_z, \tag{76}$$

where $\tilde{J}^{g,\bar{\nu}}_z$ is given by Eq. (58). We note that $\tilde{J}^{g,\bar{\nu}}_z$ contains the three effective microscopic anisotropy interactions, $J^g_z$, $J^g_{1,z}$, and $J^g_{2,z}$, multiplied by the constants $a^+_{\bar{\nu}}$, $-c^-_{\bar{\nu}}$, and $-a^-_{\bar{\nu}}/2$, respectively. In Tables VI and VII, the values of these parameters for the FM ground state and the first three excited state manifolds for arbitrary $s_1$ are given. We note that EPR measurements are insensitive to the Heisenberg, biquadratic, and three-center quartic exchange interactions, which preserve $m$.

For either FM or AFM $s_1=1/2$ tetramers, EPR measurements can only probe the two microscopic symmetric anisotropic exchange interaction parameters $J^g_{1,z}$ and $J^g_{2,z}$, and measurements of the two $s=1$ excited states are sufficient to determine them. For FM tetramers with $s_1\geqslant 1$, it is a bit more difficult. From Tables VI and VII and from Eq. (G1), it is easily seen that the $(s,s_{13},s_{24})=(s,2s_1,2s_1)$ states all provide measurements of the same combination of these three microscopic interactions. This can also be seen from Tables

IV and V for $s_1=1/2$ and 1. Hence, for FM tetramers with $s_1>1/2$, measurements of the ground $s=4s_1$ and the first excited state manifold with $s=4s_1-1$ are insufficient to completely determine the three microscopic interactions. In order to stay within a single $s$ value for FM tetramers, one would need to study the second (or higher) excited state manifold with $s=4s_1-2$ (or lower) in order to obtain sufficient information to determine the three microscopic anisotropy interaction strengths. For AFM tetramers with $s_1 \geqslant 1$, EPR transitions in the ground state are not allowed, but measurements of the first excited $s=1$ state manifold would suffice to determine $J_z^g$ and the $J_{q,z}^g$, as seen from the formulas in Tables VIII and IX.

### C. Inelastic neutron scattering

The Hartree INS cross section $S_g^{(1)}(\boldsymbol{B},\boldsymbol{q},\omega)$ in the induction representation is

$$S_g^{(1)} = \mathrm{Tr}_\nu \, \mathrm{Tr}_{\nu'} \, e^{-\beta E_\nu^g} \sum_{\alpha,\beta} (\delta_{\alpha,\beta} - \hat{q}_\alpha \hat{q}_\beta) \sum_{n,n'} e^{i\boldsymbol{q}\cdot(\boldsymbol{r}_n - \boldsymbol{r}_{n'})} \langle \nu | S_{n',\alpha}^\dagger | \nu' \rangle \times \langle \nu' | S_{n,\beta} | \nu \rangle \delta(\omega + E_\nu^g - E_{\nu'}^g), \tag{77}$$

where $\alpha,\beta=x',y',z'$, $\hat{q}_{x'}=\sin\theta_{b,q}\cos\phi_{b,q}$, $\hat{q}_{y'}=\sin\theta_{b,q}\sin\phi_{b,q}$, and $\hat{q}_{z'}=\cos\theta_{b,q}$; $\theta_{b,q}$ and $\phi_{b,q}$ describe the relative orientations of $\boldsymbol{B}$ and $\boldsymbol{q}$,[5] the $\boldsymbol{r}_n$ are given by Eq. (1), and the $\langle \nu' | S_{n,\alpha} | \nu \rangle$ are given (with $x' \to x$, etc.) by Eqs. (E1) and (E2). The scalar $\boldsymbol{q}\cdot(\boldsymbol{r}_n - \boldsymbol{r}_{n'})$ is invariant under the rotation [Eq. (45)]. After some algebra, we rewrite $S_g^{(1)}(\boldsymbol{q},\omega)$ as

$$S_g^{(1)} = \mathrm{Tr}_\nu \, e^{-\beta E_\nu^g} \sum_{\nu'} \delta(\omega + E_\nu^g - E_{\nu'}^g) \left( \sin^2\theta_{b,q} L_{\nu,\nu'}(\boldsymbol{q}) + \frac{(2-\sin^2\theta_{b,q})}{4} M_{\nu,\nu'}(\boldsymbol{q}) \right), \tag{78}$$

where the Hartree functions $L_{\nu,\nu'}(\boldsymbol{q})$ and $M_{\nu,\nu'}(\boldsymbol{q})$ are given in Appendix I. They are independent of $\boldsymbol{B}$. Since $E_\nu^g$ is well behaved as $\boldsymbol{B} \to 0$, Eq. (78) is accurate for all $\boldsymbol{B}$.

As for the dimer,[5] additional EPR and INS transitions with amplitudes higher order in the anisotropy parameters $J_z^g$, $J_{1,z}^g$, and $J_{2,z}^g$ relative to $\tilde{J}_g$ are obtained in the extended Hartree approximation, but will be presented elsewhere for brevity.[51]

## VIII. DISCUSSION

The quadratic phenomenological total spin anisotropy model widely used in fitting experimental data on SMM's is

$$\mathcal{H}_p = \mathcal{A} - \mathcal{D} S_z^2 - \mathcal{E}(S_x^2 - S_y^2), \tag{79}$$

where $\mathcal{A}$ represents the isotropic total spin interactions, and $\mathcal{D}$ and $\mathcal{E}$ are measures of the axial and azimuthal total spin anisotropies, respectively.[1] Often, additional quartic terms are added.[22,52] The anisotropy is defined relative to the total spin principal axes, which, for equal-spin high-symmetry systems, are the molecular axis vectors. It is easy to evaluate $E_\nu^p = \langle \nu | \tilde{\mathcal{H}}_p | \nu \rangle$ in the induction representation. One obtains Eqs. (55) and (57) provided that

$$\mathcal{A} = \mathcal{A}_0 + \delta\mathcal{A}, \tag{80}$$

$$\mathcal{A}_0 = -\tilde{J}_g s(s+1)/2 - \gamma B m, \tag{81}$$

$$\delta\mathcal{A} = \delta E_{\bar{\nu},0}^g - \delta\tilde{J}_z^{g,\bar{\nu}}, \tag{82}$$

$$\mathcal{D} = \tilde{J}_z^{g,\bar{\nu}}, \tag{83}$$

$$\mathcal{E} = 0, \tag{84}$$

where $\delta E_{\bar{\nu},0}^g$, $\tilde{J}_z^{g,\bar{\nu}}$, and $\delta\tilde{J}_z^{g,\bar{\nu}}$ are given by Eqs. (56), (58), and (59), respectively, which contain the constants $a_{\bar{\nu}}^{\pm}$, $b_{\bar{\nu}}^{\pm}$, $c_{\bar{\nu}}^{-}$, $\mathcal{B}_{\bar{\nu}}$, and $\mathcal{T}_{\bar{\nu}}$. Precise formulas for all of these quantities at arbitrary $\bar{\nu}$ appear in Appendix F, along with Tables VI–IX of the values of $a_{\bar{\nu}}^{\pm}$, $b_{\bar{\nu}}^{\pm}$, and $c_{\bar{\nu}}^{-}$ for arbitrary $s_1$ in the ground and lowest three excited state manifolds for FM and AFM tetramers, respectively. Usually, one assumes the strong exchange limit, so that the isotropic $\mathcal{A}_0$ is sufficiently large that it remains constant for $B=0$ and can be neglected. A nonvanishing $\mathcal{E}$ would lead to a term in Eq. (57) proportional to $\sin^2\theta\cos(2\phi)$, as for the dimer,[5] which does not arise in the first-order calculation for the high-spin tetramers under consideration based on the microscopic parameters alone. Hence, the $\mathcal{D}$ term in $\mathcal{H}_p$ alone correctly describes the $\theta$ and $m$ dependencies of $E_{\nu,0}^g + E_{\nu,1}^g$ provided that the quantum numbers $s_{13}$ and $s_{24}$ remain constant.

More important, the additional constant term $\delta\mathcal{A}$ has generally been neglected. Even to zeroth order, the sign of $\tilde{J}_g - \tilde{J}_g'$ in $\delta E_{\bar{\nu},0}^g$ distinguishes between type-I and type-II tetramers, the distinction of which is absent in the phenomenological model. Moreover, the different first-order dependencies of $\mathcal{A}$ and $\mathcal{D}$ on $\bar{\nu}$ are important in determining the level-crossing inductions for AFM tetramers, each of which involves two values of $s$ and $m$, and for type II, different $s_{13}$ and $s_{24}$ values, as well. The zero-field energy spectrum is thus more complicated than that given by the usual phenomenological model, which could lead to substantially different fits to experiment.

For simplicity, the only higher order interactions we have considered are the isotropic NN and NNN biquadratic and three-center quartic exchange interactions. These isotropic interactions are rotationally invariant, so they are independent of $\theta$ in the induction representation. Hence, they only contribute to $\delta A$. Thus, they modify the positions but neither the $\theta$ dependencies of the AFM level-crossing inductions nor any EPR transitions.

In the ground state of FM tetramers, $\bar{\nu}$ is restricted to the single set of values, $(s,s_{13},s_{24})=(4s_1,2s_1,2s_1)$. In this high-spin case, $\mathcal{H}_p$ can provide a correct phenomenology of the ground state energy. However, if applied to the two low-lying excited states with $s=4s_1-1$, for instance, one would infer two different $\mathcal{A}$ and $\mathcal{D}$ values from those obtained in the ground state. Moreover, as noted above, since all states with $(s_{13},s_{24})=(2s_1,2s_1)$ contain the same combination of $a_{\bar{\nu}}^{\pm}$ and $c_{\bar{\nu}}^{-}$, in order to exploit the $\bar{\nu}$ dependence of $\mathcal{D}$ to obtain an unambiguous EPR measurement of the three microscopic pa-

rameters $J_z^g$, $J_{1,z}^g$, and $J_{2,z}^g$, for $s_1>1/2$, one needs to examine higher eigenstate manifolds, such as the manifold with $s=4s_1-2$. For this manifold, $\mathcal{H}_p$ would require four different $\mathcal{A}$ and $\mathcal{D}$ values. For AFM tetramers, the ground $s=0$ state manifold has $2s_1$ states that are all split in first order, except for tetramers with $T_d$ symmetry and vanishing biquadratic and three-center quartic interactions. Hence, the phenomenological model works best in describing only a single state with fixed $(s,s_{13},s_{24})$. This is more restrictive than the usual assumption of its applicability to all states with fixed $s$.[18,52–55]

We note that the FM $Cu_4$ tetramer $Cu_4OCl_6(TPPO)_6$ was claimed to have $T_d$ symmetry and a $s=2$ ground state.[12–14] It is noteworthy that those authors thought that anisotropic exchange interactions might be responsible for their observed zero-field energy splittings.[12,15] Since tetramers with $T_d$ symmetry do not have either symmetric or antisymmetric anisotropic exchange interactions, another explanation must be considered. From Tables VI and VII, it is evident that the FM ground state is nondegenerate for all $s_1$, even for those SMM's with lower symmetries allowing anisotropic exchange interactions. It therefore appears that the sample may not have been single phase,[12–14] as in a nominally $S_4$ $Ni_4$ tetramer,[22] allowing for an apparent ground state splitting.

We note that for the FM $Fe_4$ SMM, $Fe_4(thme)_2(dpm)_6$, where $H_3$thme is 1,1,1-tris(hydroxymethyl)ethane and Hdpm is dipivaloylmethane,[52–54] the high $D_3$ symmetry also precludes the $\mathcal{E}$ term in $\mathcal{H}_p$. Nevertheless, in fits to INS data, it was assumed that $\mathcal{E}\neq 0$,[52,55] in order to obtain the appropriate anticrossing gaps, so that either the powdered sample did not have pure $D_3$ symmetry or the phenomenological model they used [Eq. (79)], plus two quartic terms obeying $D_3$ symmetry, was not appropriate. Since single-ion interactions appeared to be important,[52] the total spin might not have been a well-defined quantum number, as in at least one $Fe_2$ dimer and in $Fe_8$.[5,6,8,9] However, we note that it might be interesting to investigate whether second-order DM effects might yield an effective finite $\mathcal{E}$ value.

By using a microscopic Hamiltonian, detailed fits to the four magnetization step data obtained in large pulsed fields on powder samples of the AFM $Ni_4$ tetramer $[Mo_{12}^{V}O_{30}(\mu_2\text{-OH})_{10}H_2\{Ni^{II}(H_2O)_3\}_4]$ or $\{Ni_4Mo_{12}\}$ were presented.[46] Although the molecule has $C_{1v}$ symmetry, it is close to exhibiting $C_{3v}$ symmetry. Since the steps with midpoints at 4.5, 8.9, 20.1, and 32 T were unevenly spaced, the authors assumed the molecule to have weak but important biquadratic interactions. The $\Delta M/\Delta B$ versus $B$ data gave full widths to these steps of approximately 2.7, 3.6, 5.0, and 12 T. To limit the number of fitting parameters, they assumed $C_{3v}$ symmetry for the Heisenberg and biquadratic interactions, and $T_d$ symmetry for the single-ion and anisotropic exchange interactions. In addition, they allowed the two Heisenberg interaction strengths to have strong magnetic field dependencies, and solved their Hamiltonian numerically, which can incorporate the site-dependent single-ion interactions for $T_d$ symmetry. This model fits the full magnetization and $\Delta M/\Delta B$ curves nicely. However, subsequent magnetoinfrared studies of that compound were made, revealing only very small differences in the responses at $B=0$ and 14 T,[61] providing little, if any, justification for such strong magnetic field dependencies of the Heisenberg interaction strengths.

More recently, a remarkably simple fit to the four level-crossing midpoints was made by Kostyuchenko.[50] In this fit, the $\{Ni_4Mo_{12}\}$ molecule was assumed to have $T_d$ symmetry, so that $\tilde{J}_{T_d}=\tilde{J}'_{T_d}=-J$, and a plausible argument was presented that the strength $-J_3=J_{t,1}^{T_d}=J_{t,2}^{T_d}$ of the isotropic three-center quartic interactions ought to be comparable in magnitude to that $(-J_2=J_{b,1}^{T_d}=J_{b,2}^{T_d})$ of the biquadratic interactions. We denote this model as the $JJ_2J_3$ model. Since each of these terms preserves the $s$ quantum number, the Hamiltonian matrix in the absence of single-ion and anisotropic exchange interactions is block diagonal, and for $s_1=1$, it is possible to obtain the exact eigenvalues in terms of the three parameters $J,J_2,J_3$. However, in his fit to the magnetization level-crossing midpoint data on $\{Ni_4Mo_{12}\}$, he found $J_2=J_3$, which implies that he claimed to fit the four linear equations for the four unequally spaced level-crossing midpoints with two parameters. Although two of those equations were nearly degenerate, three were clearly nondegenerate, rendering his two-parameter fit inaccurate.

In Appendix F, we extended the calculation of Kostyuchenko to the five lower symmetries, so that there are six isotropic interactions $\tilde{J}_g$, $\tilde{J}'_g$, $J_{b,q}^g$, and $J_{t,q}^g$ for $q=1$ and 2, and our results are listed in Table X. We note that Kostyuchenko took the Heisenberg energies to be $J[s(s+1)-2s_1(s_1+1)]/2$, so each of his eigenstate energies differ from ours for $s_1=1$ by the irrelevant constant $4J$. In the limit of $T_d$ symmetry investigated by Kostyuchenko, our results agree with those of Kostyuchenko for the $s=4$ and $s=0$ state manifolds, and for one state each of the $s=2$ and $s=3$ state manifolds. However, our results do not agree with his for the other $s=1$, 2, and 3 states, except for the special case $J_2=J_3$, which is what he claimed to have obtained in his fit.[50]

Even if one takes the correct forms for the eigenstate energies with $T_d$ symmetry (neglecting the second-order single-ion anisotropy contributions) given in the Appendixes, one still has to solve four equations with three parameters $J$, $J_2$, and $J_3$. In case there remains an accidental remaining degeneracy, we try to do this. We first assumed $J_2\geqslant J_3$, taking the minimum eigenstate energy within each $s$ manifold, but no consistent solution to the equations for the four level crossings could be found. We then assumed $J_3\geqslant J_2$. For each $s$ manifold, the minimum energy is then $E_0=16J_2-8J_3$, $E_{1-}$, $E_2=3J+\frac{39}{4}J_2-\frac{31}{4}J_3$, $E_3=6J+\frac{61}{9}J_2-\frac{7}{9}J_3$, and $E_4=10J+6J_2+12J_3$, respectively, where $E_{1-}=J+\frac{87}{8}J_2-\frac{31}{8}J_3-\frac{1}{24}\sqrt{(91J_3-75J_2)^2+320(3J_2-4J_3)^2}$. In this case, the square root appears with opposite signs in the equations for the first and second level crossings, so that we add those two equations to obtain three linear equations in three unknowns. Solving these three unknowns, we then find the $J$, $J_2$, and $J_3$ values listed in Table XI. These results necessarily fit the midpoints of the third and fourth level crossings precisely. Substituting these values into the equations for the first and second level crossings, we obtain 4.35 and 9.05 T, which are in remarkably good agreement with the experimental values of 4.5 and 8.9 T, respectively. Hence, Kostyuchenko's idea that the three-center terms could be important is valid.[50] It is remarkable that one can obtain a good fit to four level-

TABLE XI. Type-I and type-II fitting parameters for the data of Schnack *et al.* on $\{Ni_4Mo_{12}\}$ (Ref. 46). Upper table: The $JJ_2J_3$ column is the midpoint only fit with $\tilde{J}'_g=\tilde{J}_g=-J$, $J^g_{b,1}=J^g_{b,2}=-J_2$, and $J^g_{t,1}=J^g_{t,2}=-J_3$. The + and − columns refer to least-squares fit to the four widths for the two signs of $J^g_z-3J^g_{\rm eff}$, and the last three columns are for the type-II least-squares fit to the four widths from the $(-+++)$ and $(+---)$ anisotropy interaction sign cases, respectively, with the arbitrary assumptions $\tilde{J}'_g/\tilde{J}_g=1.5$ and $J^g_{t,2}=J^g_{b,2}$. The $JJ_2J_3$ and type-II values for the type-I parameters are listed for comparison. Indeterminate values are left blank. Lower table: Comparison of level-crossing widths in the three models with experiment (see text).

| $-J^g_i/k_B$ | $JJ_2J_3$ | I+ (K) | I− (K) | II(+−−−) (K) | II(−+++) (K) |
|---|---|---|---|---|---|
| $-(\tilde{J}_g+2J^g_{t,2})/k_B$ | 9.45 | 11.21 | 10.60 | 8.06 | 9.08 |
| $-\tilde{J}_g/k_B$ | 7.51 | | | 4.62 | 5.14 |
| $-\tilde{J}'_g/k_B$ | 7.51 | | | 6.94 | 7.71 |
| $-J^g_z/k_B$ | 0 | 2.90 | 4.71 | −0.982 | 0.982 |
| $-J^g_{\rm eff}/k_B$ | 0 | 4.07 | −1.53 | −4.34 | 4.34 |
| $-J^g_{1,z}/k_B$ | 0 | | | −12.8 | 12.8 |
| $-J^g_{2,z}/k_B$ | 0 | | | 6.16 | −6.16 |
| $-J^g_{b,1}/k_B$ | 0.764 | 2.84 | 2.56 | 3.36 | 3.62 |
| $-J^g_{b,2}/k_B$ | 0.764 | | | 1.72 | 1.97 |
| $-J^g_{t,1}/k_B$ | 0.967 | 0.620 | 0.374 | −3.73 | −1.97 |
| $-J^g_{t,2}/k_B$ | 0.967 | | | 1.72 | 1.97 |

| $\gamma\Delta B$(expt) (T) | $\gamma\Delta B(JJ_2J_3)$ (T) | $\gamma\Delta B(I)$ (T) | $\gamma\Delta B(II)$ (T) |
|---|---|---|---|
| 2.7 | 0 | 4.9 | 1.9 |
| 3.6 | 0 | 1.9 | 2.8 |
| 5.0 | 0 | 6.4 | 4.5 |
| 12 | 0 | 10.4 | 12.5 |

crossing midpoints with only three parameters. Nevertheless, these parameters do not give rise to any widths to the transitions, unlike the experiments.[46]

In Appendix F, we listed the type-I and type-II first-order level-crossing inductions for $s_1=1$ AFM tetramers with the six ISPG symmetries under study. Although our quantization scheme is appropriate for the $C_{1v}$ symmetry of $\{Ni_4Mo_{12}\}$, the number of independent parameters for that low symmetry is very large. Nevertheless, one can quantitatively fit the four experimental level-crossing induction midpoints by assuming some approximate symmetry such as $D_{2d}$ or $S_4$, for which $J^g_z$ is nonvanishing. The midpoint of each level crossing occurs at $\theta=\pi/4$ and the width of each level crossing is obtained from the difference between its values at $\theta=0$ and $\theta=\pi/2$. We first tried to fit the data assuming a type-I tetramer. In this case, the widths of the four level crossings are determined by the single parameter $|J^g_z-3J^g_{\rm eff}|$. A least-squares fit of this parameter to the widths of the four level crossings gave $|J^g_z-3J^g_{\rm eff}|=6.94\gamma$ T, which leads to the calculated widths listed in Table XI. There are then two choices for the signs of this parameter. For each sign choice, we fit the four midpoint equations to the remaining four parameters, and our results are listed in Table XI.

Both of these type-I fits have the additional restriction that $\tilde{J}'_g>\tilde{J}_g$, but no restrictions on $J^g_{b,2}$ are obtained. Both of these fits provide reasonable values of the microscopic parameters, which is consistent with the strong-exchange limit. The second (−) fit leads to a smaller magnitude of $J^g_{\rm eff}=J^g_{1,z}/2+J^g_{2,z}/3$, which might be expected physically, but it also leads to a somewhat larger $J^g_z$ magnitude. In either case, an inclusion of the effective anisotropy parameters greatly modifies the Heisenberg, biquadratic, and three-center quartic interaction strengths from those values in the $JJ_2J_3$ model, as seen from Table XI.

With the nine parameters in the four type-II tetramer level-crossing inductions listed in the Appendixes, one might do better by fitting not only the midpoints but also the widths of the level-crossing inductions. For type II, the four widths are given, respectively, by $|(J^g_z+J^g_{2,z})/2|$, $|(J^g_z+J^g_{1,z}+J^g_{2,z})/2|$, $|-3J^g_z/2+5J^g_{1,z}/6+J^g_{2,z}/2|$, and $|-3J^g_z/2+5J^g_{1,z}/3+J^g_{2,z}/2|$. We fit the widths using a standard least-squares procedure, taking into account all possible signs of the four linear combinations of the three parameters. The $(-+++)$ and $(+---)$ combinations gave equivalent best fits, with $J^g_z$, $J^g_{1,z}$, and $J^g_{2,z}$, each having equal and opposite signs in the two combinations. The parameters for these fits are listed in Table XI. The standard deviations for the three types of fits were thus $\sigma_{II}=0.569$ T, $\sigma_I=1.57$ T, and $\sigma_{JJ_2J_3}=6.15$ T, so that the type-II fit to the transition widths is the superior one, although the type-I fit is not too bad, considering the limited number of parameters.

We then had to solve the four midpoint equations with the six parameters, $\tilde{J}_g$, $\tilde{J}'_g$ and $J^g_{b,q}$, $J^g_{t,q}$ for $q=1$ and 2, subject to the type-II assumption $\tilde{J}'_g-\tilde{J}_g<0$. There are an infinite number of ways to do this, as arbitrary choices for two parameters can be made. No type-II solution with $J^g_{t,1}=J^g_{t,2}=0$ could

be found. Hence, to illustrate some of the possible solutions, we arbitrarily chose $\tilde{J}'_g = 1.5\tilde{J}_g$ and $J^g_{b,2} = J^g_{t,2}$. The resulting parameter values for these choices are listed in Table XI.

In Table XI, the anisotropy parameters $J^g_z$ and $J^g_{\rm eff}$ obtained in our (+) type-I and (−+++) type-II fits are in rather good agreement with each other. However, the values for $J^g_{t,1}$ are quite different in these cases. We have examined other type-II fits, using different assumptions for $J^g_{b,2}$ and $J^g_{t,2}$, and the resulting values for $J^g_{b,q}$ and $J^g_{t,q}$ (for $q=1$, and 2) significantly vary with the assumptions, so the particular values of the biquadratic and three-center quartic interactions should not be taken too seriously. We also note that the type-II fit gives very large values for the symmetric anisotropic exchange interaction strengths. However, the $J^g_{1,z}$ and $J^g_{2,z}$, while both very large, are opposite in sign, so that the type-I combination $J^g_{\rm eff}$, while still large, cannot be ruled out for type-II fits. In one type-I and both type-II fits, fitting to the transition widths gave a larger $J^g_{\rm eff}$ than $J^g_z$, which was unexpected. We note that Schnack *et al.*[46] had included single-ion anisotropy, but not symmetric anisotropic exchange. The different physics implied from this work is therefore the evidence for a strong symmetric anisotropic exchange in $\{Ni_4Mo_{12}\}$. We have also shown that it is possible to perform an accurate fit to the data without any field dependencies to the microscopic interaction parameters. However, since the magnitudes of the $J^g_{q,z}$ are comparable to or larger than $\tilde{J}_g$, and $\tilde{J}'_g$, the strong-exchange limit is questionable, and subsequent fits using an exact diagonalization of the full Hamiltonian matrix are warranted.[51]

We note that nonvanishing DM interactions (which vanish in first order) do give some additional widths to the level crossings, and these might provide an additional contribution to the broad third and fourth level crossings observed in experiment.[46] The best fit to experiment may not be either type I or type II, but may involve a more complicated analysis involving other states within some of the constant $s$ manifolds.

However, with only polycrystalline data available, it is difficult to uniquely distinguish the different possible anisotropy interaction strengths. When single crystals of sufficient size for low-temperature magnetization measurements are made, we intend to fit the data by using a more consistent set of parameters, neglecting any field dependencies, if possible.[51]

We note that our formulation of the single-ion matrix elements in terms of a pair of dimers is applicable to low-symmetry systems such as $Mo_{12}O_{30}(\mu_2\text{-OH})_{10}H_2\{Ni(H_2O)_3\}_4$, abbreviated as $\{Ni_4Mo_{12}\}$,[46] systems such as $Ni_4$ tetramers obtained from salts of $[Ni_4(H_2O)_2(PW_9O_{34})_2]^{10-}$ with $C_{2v}$ symmetry,[56] and the unequal-spin systems $Mn^{II}_2Mn^{III}_2$ and $Ni^{II}_2Mn^{III}_2$.[57,58] In the first system with $C_{1v}$ symmetry, one would expect many more single-ion, symmetric anisotropic exchange, and DM interactions, making definitive fits to the existing powder magnetization data problematic.[46] However, to improve the fits to experiments on this compound, one might approximate the ISPG as $C_{3v}$. The study of $C_{3v}$ or $D_3$ symmetry systems, such as the $Fe_4$ compound $Fe_4(thme)_2(dpm)_6$ and the $Cr^{III}Ni^{II}_3$ tetramer with a $s=9/2$ ground state,[52,59] would require a reformulation of the quantization scheme to $|\nu\rangle = |s, m, s_{123}, s_{12}, s_1\rangle$ and the calculation of the appropriate single-ion matrix elements, which are not yet in the literature.[31] Even classical Heisenberg models of such systems show strongly different dynamics than of systems with $T_d$ symmetry.[34,60]

Finally, the DM interactions can also give rise to an electric polarization and, hence, to multiferroic behavior. Our results suggest that this behavior should apply for tetramers with all possible individual spin values, as long as there is no center of inversion symmetry connecting the interacting spin pairs. For tetramers with $S_4$ and $D_{2d}$ or lower symmetry, this should be observable. Our results indicate that these effects should also occur for quantum spins.

## IX. CONCLUSIONS

We presented a theory of high-symmetry single molecule magnets based on the microscopic interactions between the individual spins. We derived a compact form for the exact single-spin matrix elements for four general spins. We used the local axial and azimuthal vector groups to construct the invariant single-ion and symmetric anisotropic exchange Hamiltonians, and the molecular representation to obtain the Dzyaloshinskii-Moriya and biquadratic and three-center quartic interactions for equal-spin $s_1$ tetramers with ionic site point group symmetries $T_d$, $D_{4h}$, $D_{2d}$, $S_4$, $C_{4h}$, or $C_{4v}$. Each vector group introduces site-dependent molecular single-ion and anisotropic exchange interactions. Assuming weak effective site-independent single-ion, symmetric exchange anisotropy, and isotropic biquadratic and three-center quartic exchange interactions, we evaluated the first-order corrections to the eigenstate energies. Depending on the relative strengths of the near-neighbor and next-nearest-neighbor Heisenberg exchange interactions, there are generally two types of high-symmetry tetramers. For the single-ion and symmetric exchange anisotropy interactions, we provided analytic results and illustrations of the antiferromagnetic level-crossing inductions. We used our first-order results to provide preliminary fits to the low-temperature magnetization data on an AFM $Ni_4$ tetramer, and we found evidence for strong symmetric anisotropic exchange interactions in that material. We also provided Hartree expressions for the magnetization, specific heat, EPR absorption, and INS cross section, which are accurate at low temperatures and arbitrary magnetic fields. For ferromagnetic tetramers, we provided a procedure for a precise EPR determination of three of the microscopic anisotropy parameters. We predict that geometrically frustrated tetramers with symmetries $S_4$ and $D_{2d}$, as well as $C^{13}_{2v}$, are likely candidate materials for multiferroic states. Our procedure is extendable to more general systems.

## ACKNOWLEDGMENTS

We thank N. S. Dalal, D. Khomskii, J. L. Musfeldt, M. R. Pederson, J. Schnack, and J. van den Brink for helpful comments and discussions. This work was supported in part by the NSF under Contract No. NER-0304665.

## APPENDIX A: SYMMETRY OPERATION MATRICES

Rotations of $\pm\pi/2$ about the $z$ axis are represented by

$$\mathcal{O}_{1,2}=\begin{pmatrix} 0 & \pm 1 & 0 \\ \mp 1 & 0 & 0 \\ 0 & 0 & 1 \end{pmatrix}. \tag{A1}$$

Rotations of $\pi$ about the $x$ and $y$ axes are represented by

$$\mathcal{O}_{3,4}=\begin{pmatrix} \pm 1 & 0 & 0 \\ 0 & \mp 1 & 0 \\ 0 & 0 & -1 \end{pmatrix}. \tag{A2}$$

Rotations of $\pi$ about the $z$ axis and reflections in the $xy$ plane are respectively represented by

$$\mathcal{O}_{5,6}=\begin{pmatrix} \mp 1 & 0 & 0 \\ 0 & \mp 1 & 0 \\ 0 & 0 & \pm 1 \end{pmatrix}. \tag{A3}$$

Rotations of $\pi$ about the $y=\pm x$ diagonal axes are represented by

$$\mathcal{O}_{7,8}=\begin{pmatrix} 0 & \pm 1 & 0 \\ \pm 1 & 0 & 0 \\ 0 & 0 & -1 \end{pmatrix}. \tag{A4}$$

Reflections in the $xz$ and $yz$ mirror planes are represented by

$$\mathcal{O}_{9,10}=\begin{pmatrix} \pm 1 & 0 & 0 \\ 0 & \mp 1 & 0 \\ 0 & 0 & 1 \end{pmatrix}. \tag{A5}$$

Reflections in the mirror planes containing the $z$ axis and the diagonals $y=\pm x$ are represented by

$$\mathcal{O}_{11,12}=\begin{pmatrix} 0 & \pm 1 & 0 \\ \pm 1 & 0 & 0 \\ 0 & 0 & 1 \end{pmatrix}. \tag{A6}$$

Reflections in the mirror planes containing the $y$ axis and the lines $z=\pm x$ are represented by

$$\mathcal{O}_{13,14}=\begin{pmatrix} 0 & 0 & \pm 1 \\ 0 & 1 & 0 \\ \pm 1 & 0 & 0 \end{pmatrix}. \tag{A7}$$

Reflections in the mirror planes containing the $x$ axis and the lines $y=\pm z$ are represented by

$$\mathcal{O}_{15,16}=\begin{pmatrix} 1 & 0 & 0 \\ 0 & 0 & \pm 1 \\ 0 & \pm 1 & 0 \end{pmatrix}. \tag{A8}$$

For $T_d$, clockwise rotations of $2\pi/3$ about the cube diagonals are represented by

$$\mathcal{O}_{17,18}=\begin{pmatrix} 0 & \pm 1 & 0 \\ 0 & 0 & 1 \\ \pm 1 & 0 & 0 \end{pmatrix} \tag{A9}$$

and

$$\mathcal{O}_{19,20}=\begin{pmatrix} 0 & \pm 1 & 0 \\ 0 & 0 & -1 \\ \mp 1 & 0 & 0 \end{pmatrix}. \tag{A10}$$

Counterclockwise rotations of $2\pi/3$ about the cube diagonals are represented by $\mathcal{O}_\lambda^T=\mathcal{O}_\lambda^{-1}$ for $\lambda=17,\ldots,20$. Finally, there are six $S_4$ improper rotations consisting of rotations about a high-symmetry axis of $\pm\pi/2$ followed by a reflection in the plane perpendicular to the rotation axis. For $S_4$ symmetry, $z$ is the high-symmetry axis and the operations are represented by

$$\mathcal{O}_{21,22}=\begin{pmatrix} 0 & \pm 1 & 0 \\ \mp 1 & 0 & 0 \\ 0 & 0 & -1 \end{pmatrix}. \tag{A11}$$

For $T_d$ symmetry, we also have

$$\mathcal{O}_{23,24}=\begin{pmatrix} -1 & 0 & 0 \\ 0 & 0 & \pm 1 \\ 0 & \mp 1 & 0 \end{pmatrix} \tag{A12}$$

and

$$\mathcal{O}_{25,26}=\begin{pmatrix} 0 & 0 & \pm 1 \\ 0 & -1 & 0 \\ \mp 1 & 0 & 0 \end{pmatrix}. \tag{A13}$$

All ISPG symmetries allow the identity operation, which we omit for brevity, listing only the following:[33]

For $C_{4h}$ symmetry, $\mathcal{O}^{C_{4h}}=\{\mathcal{O}_1,\mathcal{O}_2,\mathcal{O}_6\}$;

for $D_{4h}$ symmetry, $\mathcal{O}^{D_{4h}}=\{\mathcal{O}_1,\mathcal{O}_2,\mathcal{O}_3,\mathcal{O}_4,\mathcal{O}_6,\mathcal{O}_7,\mathcal{O}_8\}$;

for $C_{4v}$ symmetry, $\mathcal{O}^{C_{4v}}=\{\mathcal{O}_1,\mathcal{O}_2,\mathcal{O}_9,\mathcal{O}_{10},\mathcal{O}_{11},\mathcal{O}_{12}\}$;

for the lowest ISPG symmetry under study, $S_4$, $\mathcal{O}^{S_4}=\{\mathcal{O}_{21},\mathcal{O}_{22}\}$;

for $D_{2d}$ symmetry, $\mathcal{O}^{D_{2d}}=\{\mathcal{O}_3,\mathcal{O}_4,\mathcal{O}_6,\mathcal{O}_{11},\mathcal{O}_{12}\}$; finally, for the highest symmetry under study, $T_d$,

$$\mathcal{O}^{T_d}=\{\mathcal{O}_3,\mathcal{O}_4,\mathcal{O}_6,\mathcal{O}_{11},\mathcal{O}_{12},\mathcal{O}_{13},\mathcal{O}_{14},\mathcal{O}_{15},\mathcal{O}_{16},\mathcal{O}_{17},\mathcal{O}_{18},\mathcal{O}_{19},\mathcal{O}_{20},\mathcal{O}_{17}^{-1},\mathcal{O}_{18}^{-1},\mathcal{O}_{19}^{-1},\mathcal{O}_{20}^{-1},\mathcal{O}_{21},\mathcal{O}_{22},\mathcal{O}_{23},\mathcal{O}_{24},\mathcal{O}_{25},\mathcal{O}_{26}\}. \tag{A14}$$

## APPENDIX B: MOLECULAR SINGLE-ION INTERACTIONS

The site-independent interactions in the molecular representation are

$$J_z^g = \begin{cases} J_a^g & \text{for } g = C_{4h} \text{ and } D_{4h} \\ \frac{1}{2}[J_a^g(3\cos^2\theta_1^g - 1) + 3J_e^g \sin^2\theta_1^g] & \text{for } g = C_{4v} \text{ for } D_{2d}, \end{cases} \tag{B1}$$

$$J_z^{S_4} = \frac{J_a^{S_4}}{2}(3\cos^2\theta_1^{S_4} - 1) - \frac{3}{2}J_e^{S_4}\sin^2\theta_1^{S_4}\cos(2\psi_1^{S_4}), \tag{B2}$$

$$J_z^{T_d} = 0. \tag{B3}$$

For $g=D_{4h}$, the only nonvanishing site-dependent single-ion interaction is

$$K_{xy}^{D_{4h}}(n) = (-1)^{n+1}J_e^{D_{4h}}. \tag{B4}$$

For $g=C_{4h}$, the two nonvanishing site-dependent single-ion interactions are

$$J_{xy}^{C_{4h}} = J_e^{C_{4h}}\cos(2\chi_1^{C_{4h}}), \tag{B5}$$

$$K_{xy}^{C_{4h}}(n) = (-1)^{n+1}J_e^{C_{4h}}\sin(2\chi_1^{C_{4h}}). \tag{B6}$$

For $g=C_{4v}, D_{2d}$, the three nonvanishing site-dependent single-ion interactions in Eq. (32) are

$$K_{xy}^g(n) = \frac{(-1)^{n+1}}{2}[J_a^g\sin^2\theta_1^g + J_e^g(1+\cos^2\theta_1^g)], \tag{B7}$$

$$K_{xz}^g(n) = \frac{1}{2}\cos\left[(2n-1)\frac{\pi}{4}\right]\sin(2\theta_1^g)(J_a^g - J_e^g), \tag{B8}$$

$$K_{yz}^g(n) = \frac{1}{2}\sin\left[(2n-1)\frac{\pi}{4}\right]\sin(2\theta_1^g)(J_a^g - J_e^g). \tag{B9}$$

For $S_4$, the single-ion site-dependent interactions are

$$J_{xy}^{S_4} = -J_1\cos(2\phi_1^{S_4}) + J_2\sin(2\phi_1^{S_4}), \tag{B10}$$

$$K_{xy}^{S_4}(n) = (-1)^n[J_1\sin(2\phi_1^{S_4}) + J_2\cos(2\phi_1^{S_4})], \tag{B11}$$

$$K_{xz}^{S_4}(n) = (-1)^{n+1}\left[J_3\cos\left(\phi_1^{S_4} - \frac{n\pi}{2}\right) - J_4\sin\left(\phi_1^{S_4} - \frac{n\pi}{2}\right)\right], \tag{B12}$$

$$K_{yz}^{S_4}(n) = (-1)^{n+1}\left[J_3\sin\left(\phi_1^{S_4} - \frac{n\pi}{2}\right) + J_4\cos\left(\phi_1^{S_4} - \frac{n\pi}{2}\right)\right], \tag{B13}$$

$$J_1 = \frac{1}{2}[J_a^{S_4}\sin^2\theta_1^{S_4} - J_e^{S_4}(1+\cos^2\theta_1^{S_4})\cos(2\psi_1^{S_4})], \tag{B14}$$

$$J_2 = J_e^{S_4}\cos\theta_1^{S_4}\sin(2\psi_1^{S_4}), \tag{B15}$$

$$J_3 = \frac{1}{2}\sin(2\theta_1^{S_4})[J_a^{S_4} + J_e^{S_4}\cos(2\psi_1^{S_4})], \tag{B16}$$

$$J_4 = J_e^{S_4}\sin\theta_1^{S_4}\sin(2\psi_1^{S_4}). \tag{B17}$$

The site-dependent single-ion interactions for $T_d$ symmetry are easily obtained from Eqs. (B7)–(B9) by setting $\theta_1^{D_{2d}} \to \tan^{-1}(\sqrt{2})$ and $J_e^{T_d} \to 0$,

$$K_{xy}^{T_d}(n) = \frac{(-1)^n}{3}J_a^{T_d}, \tag{B18}$$

$$K_{xz}^{T_d}(n) = \frac{\sqrt{2}}{3}\cos\left[(2n-1)\frac{\pi}{4}\right]J_a^{T_d}, \tag{B19}$$

$$K_{yz}^{T_d}(n) = \frac{\sqrt{2}}{3}\sin\left[(2n-1)\frac{\pi}{4}\right]J_a^{T_d}. \tag{B20}$$

## APPENDIX C: MOLECULAR ANISOTROPIC EXCHANGE INTERACTIONS

We first consider the symmetric anisotropic exchange interactions, letting $q=1$ and 2 and $p=q+1$. For simplicity of presentation, we write

$$J_{q,\pm}^g = \frac{1}{2}(J_{c,q}^g \pm J_{f,q}^g). \tag{C1}$$

Then, the isotropic exchange renormalizations may be written as

$$\delta J_g = \delta J_g' = 0 \quad \text{for } g = C_{4h}, D_{4h}, C_{4v}, \text{ and } T_d, \tag{C2}$$

$$\delta J_{D_{2d}} = -J_{1,-}^{D_{2d}}\sin^2\theta_{12}^{D_{2d}}, \tag{C3}$$

$$\delta J'_{D_{2d}} = -J_{2,-}^{D_{2d}}, \tag{C4}$$

$$\delta J_{S_4}, \delta J'_{S_4} = \frac{\sin^2\theta_{1p}^{S_4}}{2}[J_{f,q}^{S_4} + J_{c,q}^{S_4}\cos(2\psi_{1p}^{S_4})]. \tag{C5}$$

In Eq. (C5), $q=1$ and 2 corresponds to $\delta J_{S_4}$ and $\delta J'_{s_4}$, respectively.

The nonvanishing site-independent symmetric anisotropic exchange interactions in the molecular representation are

$$J^g_{q,z} = -J^g_{f,q} \quad \text{for } g = C_{4h}, D_{4h}, \text{ and } C_{4v}, \tag{C6}$$

$$J^{D_{2d}}_{1,z} = \frac{J^{D_{2d}}_{f,1}}{2}(1 - 3\cos^2\theta^{D_{2d}}_{12}) - \frac{3J^{D_{2d}}_{c,1}}{2}\sin^2\theta^{D_{2d}}_{12}, \tag{C7}$$

$$J^{D_{2d}}_{2,z} = -J^{D_{2d}}_{2,-} - J^{D_{2d}}_{c,2}, \tag{C8}$$

$$J^{S_4}_{q,z} = \frac{J^{S_4}_{f,q}}{2}(1 - 3\cos^2\theta^{S_4}_{1p}) + \frac{3J^{S_4}_{c,q}}{2}\sin^2\theta^{S_4}_{1p}\cos(2\psi^{S_4}_{1p}). \tag{C9}$$

For $g=C_{4h}$, the nonvanishing site-dependent symmetric anisotropic exchange interactions in Eq. (37) have strengths

$$K^{C_{4h}}_{q,xy} = J^{C_{4h}}_{c,q}\sin(2\chi^{C_{4h}}_{1p}), \tag{C10}$$

$$J^{C_{4h}}_{q,xy} = -J^{C_{4h}}_{c,q}\cos(2\chi^{C_{4h}}_{1p}), \tag{C11}$$

where $\chi^g_{1p} = \phi^g_{1p} + \psi^g_{1p}$. For $g=D_{4h}$ and $C_{4v}$, the nonvanishing site-dependent symmetric anisotropic exchange interaction strengths are

$$J^g_{1,xy} = -J^g_{c,1}, \tag{C12}$$

$$K^g_{2,xy} = -J^g_{c,2}. \tag{C13}$$

Again, the more interesting group is $g=S_4$. We find

$$J^{S_4}_{q,xy} = -\tilde{J}_1\cos(2\phi^{S_4}_{1p}) + \tilde{J}_2\sin(2\phi^{S_4}_{1p}), \tag{C14}$$

$$K^{S_4}_{q,xy} = \tilde{J}_1\sin(2\phi^{S_4}_{1p}) + \tilde{J}_2\cos(2\phi^{S_4}_{1p}), \tag{C15}$$

$$K^{S_4}_{q,xz}(n) = -\tilde{J}_3\cos\left(\phi^{S_4}_{1p} - \frac{n\pi}{2}\right) + \tilde{J}_4\sin\left(\phi^{S_4}_{1p} - \frac{n\pi}{2}\right), \tag{C16}$$

$$K^{S_4}_{q,yz}(n) = -\tilde{J}_3\sin\left(\phi^{S_4}_{1p} - \frac{n\pi}{2}\right) - \tilde{J}_4\cos\left(\phi^{S_4}_{1p} - \frac{n\pi}{2}\right), \tag{C17}$$

$$\tilde{J}_1 = \frac{1}{2}[J^{S_4}_{f,q}\sin^2\theta^{S_4}_{1p} - J^{S_4}_{c,q}(1 + \cos^2\theta^{S_4}_{1p})\cos(2\psi^{S_4}_{1p})], \tag{C18}$$

$$\tilde{J}_2 = J^{S_4}_{c,q}\cos\theta^{S_4}_{1p}\sin(2\psi^{S_4}_{1p}), \tag{C19}$$

$$\tilde{J}_3 = \frac{1}{2}\sin(2\theta^{S_4}_{1p})[J^{S_4}_{f,q} + J^{S_4}_{c,q}\cos(2\psi^{S_4}_{1p})], \tag{C20}$$

$$\tilde{J}_4 = J^{S_4}_{c,q}\sin\theta^{S_4}_{1p}\sin(2\psi^{S_4}_{1p}). \tag{C21}$$

For $g=D_{2d}$, the nonvanishing site-dependent anisotropic exchange interaction strengths are

$$J^{D_{2d}}_{1,xy} = -\frac{J^{D_{2d}}_{f,1}}{2}\sin^2\theta^{D_{2d}}_{12} - \frac{J^{D_{2d}}_{c,1}}{2}(1 + \cos^2\theta^{D_{2d}}_{12}), \tag{C22}$$

$$K^{D_{2d}}_{1,xz}(n) = \cos(n\pi/2)J^{D_{2d}}_{1,+}\sin 2\theta^{D_{2d}}_{12}, \tag{C23}$$

$$K^{D_{2d}}_{1,yz}(n) = -\sin(n\pi/2)J^{D_{2d}}_{1,+}\sin 2\theta^{D_{2d}}_{12}, \tag{C24}$$

$$K^{D_{2d}}_{2,xy} = -J^{D_{2d}}_{2,+}. \tag{C25}$$

For $g=T_d$, there are no symmetric or antisymmetric anisotropic exchange interactions.

The antisymmetric anisotropic exchange interactions in the molecular representation are given for $g=C_{4h}, D_{4h}, S_4$, and $D_{2d}$ by

$$d^g_z(n) = d^g_z \quad \text{for } g = C_{4h} \text{ and } D_{4h}, \tag{C26}$$

$$\boldsymbol{d}^g_q = 0 \quad \text{for } g = C_{4h} \text{ and } D_{4h}, \tag{C27}$$

$$d^g_z(n) = d^g_z(-1)^{n+1} \quad \text{for } g = S_4 \text{ and } D_{2d}, \tag{C28}$$

$$\boldsymbol{d}^{D_{2d}}_1 = d^{D_{2d}}_{y1}\hat{\mathbf{y}}, \tag{C29}$$

$$\boldsymbol{d}^{D_{2d}}_2 = d^{D_{2d}}_{x2}(\hat{\mathbf{x}} + \hat{\mathbf{y}}), \tag{C30}$$

$$\boldsymbol{d}^{S_4}_1 = d^{S_4}_{x1}\hat{\mathbf{x}} + d^{S_4}_{y1}\hat{\mathbf{y}}, \tag{C31}$$

$$\boldsymbol{d}^{S_4}_2 = d^{S_4}_{x2}\hat{\mathbf{x}} + d^{S_4}_{y2}\hat{\mathbf{y}}. \tag{C32}$$

Tetramers with the lowest-symmetry $S_4$ require five parameters to describe the full DM interactions, those with $D_{2d}$ symmetry require three parameters, those with either $C_{4h}$ or $D_{4h}$ symmetry require just one parameter, and tetramers with $T_d$ or $C_{4v}$ symmetry have no DM interactions.

## APPENDIX D: $C^{13}_{2v}$ DZYALOSHINSKII-MORIYA INTERACTIONS

For the $[2\times2]$ grid compounds with approximate $C^{13}_{2v}$ symmetry, the four spins lie on the corners of a rhombus of side $a$ with the position vectors relative to the origin given by

$$\boldsymbol{r}_n = \frac{a}{\sqrt{2}}[\hat{\mathbf{x}}(\sin[(2n-1)\pi/4] + \cos[(2n-1)\pi/4]\cos\theta_0) + \hat{\mathbf{y}}\cos[(2n-1)\pi/4]\sin\theta_0], \tag{D1}$$

where the acute angle $\theta_0$ satisfies $\pi/2 > \theta_0 > \pi/3$ for the $[2\times2]$ grid compounds.[47,48] There are three $C^{13}_{2v}$ symmetry operations,[49] $\mathcal{O}^{C^{13}_{2v}} = \{\mathcal{O}_5, \mathcal{O}_{27}, \mathcal{O}_{28}\}$, where

$$\mathcal{O}_{27,28} = \begin{pmatrix} \pm\cos\theta_0 & \pm\sin\theta_0 & 0 \\ \pm\sin\theta_0 & \mp\cos\theta_0 & 0 \\ 0 & 0 & 1 \end{pmatrix}. \tag{D2}$$

The NNN and next-next-nearest-neighbor DM interactions, corresponding to pairs across the diagonals, vanish due to Moriya rule (3) and invariance under $\mathcal{O}_{27,28}$. However, as for

$C_{4h}$ and $D_{4h}$ symmetries, the DM interactions between NN spins do not vanish for $C_{2v}^{13}$ symmetry, but are given by

$$\mathcal{H}_{DM}^{C_{2v}^{13}} = \sum_{n=1}^{4} [d_z(-1)^{n+1}\hat{z} + \boldsymbol{d}\sin(n\pi/2) - \tilde{\boldsymbol{d}}\cos(n\pi/2)] \cdot (\boldsymbol{S}_n \times \boldsymbol{S}_{n+1}), \tag{D3}$$

$$\tilde{\boldsymbol{d}} = \mathcal{O}_2^{C_{2v}^{13}} \cdot \boldsymbol{d} = \mathcal{O}_{27} \cdot \boldsymbol{d}, \tag{D4}$$

for a general two-vector $\boldsymbol{d}$ in the $xy$ plane. We note that Eq. (D3) is invariant under all three symmetries of $C_{2v}^{13}$.

## APPENDIX E: COMPACT SINGLE-ION MATRIX ELEMENTS

By using the Schwinger boson technique of representing a spin by two noninteracting bosons and checking our results by using the standard Clebsch–Gordan algebra with the assistance of symbolic manipulation software, we find the single-spin matrix elements with general $\{s_n\}=(s_1,s_2,s_3,s_4)$ to be

$$\langle \nu'|S_{n,z}|\nu\rangle = \delta_{m',m}(m\delta_{s',s}\Gamma^{\{s_n\},s,n}_{s_{13},s'_{13},s_{24},s'_{24}} + \delta_{s',s+1}C^m_{-s-1}\Delta^{\{s_n\},-s-1,n}_{s_{13},s'_{13},s_{24},s'_{24}} + \delta_{s',s-1}C^m_s\Delta^{\{s_n\},s,n}_{s_{13},s'_{13},s_{24},s'_{24}}), \tag{E1}$$

$$\langle \nu'|S_{n,\sigma}|\nu\rangle = \delta_{m',m+\sigma}(A^{\sigma m}_s\delta_{s',s}\Gamma^{\{s_n\},s,n}_{s_{13},s'_{13},s_{24},s'_{24}} - \delta_{s',s+1}D^{\sigma,m}_{-s-1}\Delta^{\{s_n\},-s-1,n}_{s_{13},s'_{13},s_{24},s'_{24}} + \delta_{s',s-1}D^{\sigma,m}_s\Delta^{\{s_n\},s,n}_{s_{13},s'_{13},s_{24},s'_{24}}), \tag{E2}$$

$$C^m_s = \sqrt{s^2-m^2}, \tag{E3}$$

$$D^{\sigma,m}_s = \sigma\sqrt{(s-\sigma m)(s-\sigma m-1)}, \tag{E4}$$

$$\Gamma^{\{s_n\},s,n}_{s_{13},s'_{13},s_{24},s'_{24}} = \delta_{s'_{24},s_{24}}\epsilon^-_n\alpha^{s_{24},s,n}_{s_1,s_3}(s_{13},s'_{13}) + \delta_{s'_{13},s_{13}}\epsilon^+_n\alpha^{s_{13},s,n}_{s_2,s_4}(s_{24},s'_{24}), \tag{E5}$$

$$\Delta^{\{s_n\},s,n}_{s_{13},s'_{13},s_{24},s'_{24}} = \delta_{s'_{24},s_{24}}\epsilon^-_n\beta^{s_{24},s,n}_{s_1,s_3}(s_{13},s'_{13}) + \delta_{s'_{13},s_{13}}\epsilon^+_n\beta^{s_{13},s,n}_{s_2,s_4}(s_{24},s'_{24}), \tag{E6}$$

$$\alpha^{s_{24},s,n}_{s_1,s_3}(s_{13},s'_{13}) = \frac{1}{4}(1+\xi_{s,s_{13},s_{24}})\delta_{s'_{13},s_{13}} - \sqrt{2}\sin[(2n-1)\pi/4] \times (F^{s_{13},s_{24}}_{s_1,s_3,s}\delta_{s'_{13},s_{13}-1} + F^{s_{13}+1,s_{24}}_{s_1,s_3,s}\delta_{s'_{13},s_{13}+1}), \tag{E7}$$

$$\beta^{s_{24},s,n}_{s_1,s_3}(s_{13},s'_{13}) = -\frac{(-1)^n}{4}\eta_{s,s_{13},s_{24}}\delta_{s'_{13},s_{13}} + \sqrt{2}\sin[(2n-1)\pi/4](G^{s_{13},s_{24}}_{s_1,s_3,s}\delta_{s'_{13},s_{13}-1} + G^{s_{13}+1,s_{24}}_{s_1,s_3,-s}\delta_{s'_{13},s_{13}+1}), \tag{E8}$$

$$F^{s_{13},s_{24}}_{s_1,s_3,s} = \frac{\eta_{s_{13},s_1,s_3}A^{s_{24}}_{s+s_{13}}A^{s-s_{13}}_{s_{24}}}{4s(s+1)}, \tag{E9}$$

$$G^{s_{13},s_{24}}_{s_1,s_3,s} = \frac{\eta_{s_{13},s_1,s_3}A^{s_{24}}_{s+s_{13}}A^{s_{24}}_{s+s_{13}-1}}{4s\sqrt{4s^2-1}}, \tag{E10}$$

$$\eta_{z,x,y} = \frac{A^y_{x+z}A^{x-z}_y}{\sqrt{z^2(4z^2-1)}}, \tag{E11}$$

$$\xi_{z,x,y} = \frac{x(x+1)-y(y+1)}{z(z+1)}, \tag{E12}$$

$$\epsilon^{\pm}_n = \frac{1}{2}[1\pm(-1)^n], \tag{E13}$$

where $A^m_s$ is given by Eq. (51). The prefactors $m$, $A^{\sigma m}_s$, $C^m_s$, $C^m_{-s-1}$, $D^{\sigma,m}_s$, and $D^{\sigma,m}_{-s-1}$ are consequences of the Wigner–Eckart theorem for a vector operator.[33] The challenge was to obtain the coefficients $\Gamma^{\{s_n\},s,n}_{s_{13},s'_{13},s_{24},s'_{24}}$ and $\Delta^{\{s_n\},s,n}_{s_{13},s'_{13},s_{24},s'_{24}}$. Their hierarchical structure based on the unequal-spin dimer suggests that analogous coefficients with $n>4$ may be obtainable.[5] Details will be presented elsewhere.[51]

## APPENDIX F: FIRST-ORDER EIGENSTATE ENERGY CONSTANTS

The constants appearing in the first-order eigenstate energies (57) are

$$c^{\pm}_{\bar{\nu}} = \frac{1}{4}(1\pm\xi^2_{s,s_{13},s_{24}} - \eta^2_{s,s_{13},s_{24}} - \eta^2_{s+1,s_{13},s_{24}}), \tag{F1}$$

$$a^{\pm}_{\bar{\nu}} = c^{+}_{\bar{\nu}} \pm 2\Bigg\{\sum_{\sigma=\pm1}\Bigg[(F^{s_{13}+(\sigma+1)/2,s_{24}}_{s_1,s_1,s})^2 - \sum_{\sigma'=\pm1}(G^{s_{13}+(1+\sigma)/2,s_{24}}_{s_1,s_1,\sigma\sigma' s+\sigma(1+\sigma')/2})^2\Bigg] + (s_{13}\leftrightarrow s_{24})\Bigg\}, \tag{F2}$$

$$b^{\pm}_{\bar{\nu}} = \frac{1}{8}\sum_{\sigma'=\pm1}(2s+1+\sigma')^2\Bigg\{\eta^2_{s+(1+\sigma')/2,s_{13},s_{24}} \pm 8\sum_{\sigma=\pm1}[(G^{s_{13}+(1+\sigma)/2,s_{24}}_{s_1,s_1,\sigma\sigma' s+\sigma(1+\sigma')/2})^2 + (s_{13}\leftrightarrow s_{24})]\Bigg\}, \tag{F3}$$

where the $F^{s_{13},s_{24}}_{s_1,s_3,s}$, $G^{s_{13},s_{24}}_{s_1,s_3,s}$, $\eta_{z,x,y}$, and $\xi_{z,x,y}$, are given by Eqs. (E9)–(E12), respectively.

In order to calculate the matrix elements $\langle\nu'|\mathcal{H}^g_{b,1}|\nu\rangle$ and $\langle\nu'|\mathcal{H}^g_{t,1}|\nu\rangle$, we first write them as

$$\langle\nu'|\mathcal{H}^g_{b,1}|\nu\rangle = -\frac{J^g_{b,1}}{4}\sum_{n=1}^{4}\sum_{\nu''}\langle\nu'|\boldsymbol{S}_n\cdot\boldsymbol{S}_{n+1}+\boldsymbol{S}_{n+1}\cdot\boldsymbol{S}_n|\nu''\rangle \times\langle\nu''|\boldsymbol{S}_n\cdot\boldsymbol{S}_{n+1}+\boldsymbol{S}_{n+1}\cdot\boldsymbol{S}_n|\nu\rangle, \tag{F4}$$

$$\langle \nu' | \mathcal{H}^g_{\mathrm{t},1} | \nu \rangle = -\frac{J^g_{\mathrm{t},1}}{4} \sum_{n=1,3} \sum_{n'=2,4} \sum_{\nu''} \langle \nu' | \boldsymbol{S}_n \cdot \boldsymbol{S}_{n+1} + \boldsymbol{S}_{n+1} \cdot \boldsymbol{S}_n | \nu'' \rangle \times \langle \nu'' | \boldsymbol{S}_{n'} \cdot \boldsymbol{S}_{n'+1} + \boldsymbol{S}_{n'+1} \cdot \boldsymbol{S}_{n'} | \nu \rangle, \tag{F5}$$

so that we need to calculate the intermediate matrix elements $\langle \nu' | \boldsymbol{S}_n \cdot \boldsymbol{S}_{n+1} + \boldsymbol{S}_{n+1} \cdot \boldsymbol{S}_n | \nu \rangle$. We note that for any $n$, $\boldsymbol{S}_n \cdot \boldsymbol{S}_{n+1}$ commutes with the Hamiltonian consisting of the Heisenberg, biquadratic, and three-center quartic terms and, thus, should preserve the quantum number $s$. It is also easy to see that it should preserve the quantum number $m$. We have explicitly checked that our single-ion matrix element forms yield these results.

We then performed two additional checks of our matrix element forms. First, we evaluated

$$\begin{aligned}\langle \nu' | \boldsymbol{S}_1 \cdot \boldsymbol{S}_3 | \nu \rangle = \delta_{\nu,\nu'} \Bigg\{ & s(s+1) \left[ \frac{1}{16} (1 + \xi_{s,s_{13},s_{24}})^2 - (F^{s_{13},s_{24}}_{s_1,s_1,s})^2 - (F^{s_{13}+1,s_{24}}_{s_1,s_1,s})^2 \right] + s(2s-1) \left[ \frac{1}{16} \eta^2_{s,s_{13},s_{24}} - (G^{s_{13},s_{24}}_{s_1,s_1,-s})^2 - (G^{s_{13}+1,s_{24}}_{s_1,s_1,-s})^2 \right] + (s+1)(2s+3) \\ & \times \left[ \frac{1}{16} \eta^2_{s+1,s_{13},s_{24}} - (G^{s_{13},s_{24}}_{s_1,s_1,s+1})^2 - (G^{s_{13}+1,s_{24}}_{s_1,s_1,s+1})^2 \right] \Bigg\} \\ = & \left[ \frac{1}{2} s_{13}(s_{13}+1) - s_1(s_1+1) \right] \delta_{\nu,\nu'}, \end{aligned} \tag{F6}$$

as required, where $\delta_{\nu,\nu'}$ is defined in Eq. (54). Similarly, $\langle \nu' | \boldsymbol{S}_2 \cdot \boldsymbol{S}_4 | \nu \rangle$ is found from the above by setting $s_{13} \leftrightarrow s_{24}$, as required. Then, we found

$$\sum_{n=1}^{4} \langle \nu' | \boldsymbol{S}_n \cdot \boldsymbol{S}_{n+1} | \nu \rangle = \frac{g_0(\bar{\nu})}{4} \delta_{\nu,\nu'}, \tag{F7}$$

where

$$\begin{aligned} g_0(\bar{\nu}) &= s(s+1)(1 - \xi^2_{s,s_{13},s_{24}}) - s(2s-1)\eta^2_{s,s_{13},s_{24}} - (s+1)(2s+3)\eta^2_{s+1,s_{13},s_{24}} \\ &= 2[s(s+1) - s_{13}(s_{13}+1) - s_{24}(s_{24}+1)], \end{aligned} \tag{F8}$$

as required. We may then write

$$\langle \nu' | \boldsymbol{S}_n \cdot \boldsymbol{S}_{n+1} + \boldsymbol{S}_{n+1} \cdot \boldsymbol{S}_n | \nu \rangle = \delta_{s,s'} \delta_{m,m'} M^{s_{24},s'_{24}}_{s_{13},s'_{13}}(\bar{\nu}, n), \tag{F9}$$

where

$$\begin{aligned} M^{s_{24},s'_{24}}_{s_{13},s'_{13}}(\bar{\nu}, n) = {} & \delta_{s'_{13},s_{13}} \delta_{s'_{24},s_{24}} \frac{g_0(\bar{\nu})}{8} + (-1)^{n+1} \times \sum_{\sigma,\sigma'=\pm 1} \delta_{s'_{24},s_{24}+\sigma} \delta_{s'_{13},s_{13}+\sigma'} h_{\sigma,\sigma'}(\bar{\nu}) \\ & - \sqrt{2} \sin\left[ (2n-1)\frac{\pi}{4} \right] \times \sum_{\sigma=\pm 1} \delta_{s'_{13},s_{13}} \delta_{s'_{24},s_{24}+\sigma} \frac{g_\sigma(\bar{\nu})}{4} \\ & - \sqrt{2} \sin\left[ (2n+1)\frac{\pi}{4} \right] \times \sum_{\sigma=\pm 1} \delta_{s'_{13},s_{13}+\sigma} \delta_{s'_{24},s_{24}} \frac{\tilde{g}_\sigma(\bar{\nu})}{4}, \end{aligned} \tag{F10}$$

with

$$\begin{aligned} g_\sigma = \sum_{\sigma_1=\pm 1} \Bigg[ & s(s+1)(1 + \xi_{s,s_{13},s_{24}+\sigma(1+\sigma_1)/2}) F^{s_{24}+(1+\sigma)/2,s_{13}}_{s_1,s_1,s} + \frac{1}{2}(2s+1+2\sigma_1)(2s+1+\sigma_1) \\ & \times \sum_{\sigma_2=\pm 1} \eta_{s+(\sigma_1+1)/2,s_{13},s_{24}+(\sigma+\sigma_2)/2} G^{s_{24}+(1+\sigma)/2,s_{13}}_{s_1,s_1,\sigma_1\sigma_2 s+\sigma_2(1+\sigma_1)/2} \Bigg], \end{aligned} \tag{F11}$$

$$\begin{aligned} h_{\sigma,\sigma} = {} & s(s+1) F^{s_{13}+(\sigma+1)/2,s_{24}}_{s_1,s_1,s} F^{s_{24}+(1+\sigma)/2,s_{13}+\sigma}_{s_1,s_1,s} + \frac{1}{2} \sum_{\sigma_1=\pm 1} [(2s+1+\sigma_1)(2s+1+2\sigma_1) \\ & \times G^{s_{13}+(1+\sigma)/2,s_{24}}_{s_1,s_1,\sigma_1\sigma s+\sigma(1+\sigma_1)/2} G^{s_{24}+(1+\sigma)/2,s_{13}+\sigma}_{s_1,s_1,-\sigma_1\sigma s-\sigma(1+\sigma_1)/2}] + (s_{13} \leftrightarrow s_{24}), \end{aligned} \tag{F12}$$

$$\begin{aligned} h_{+,-} = \sum_{\sigma=\pm 1} \Bigg[ & s(s+1) F^{s_{13}+1,s_{24}-(1-\sigma)/2}_{s_1,s_1,s} F^{s_{24},s_{13}+(1+\sigma)/2}_{s_1,s_1,s} + \frac{1}{2} \sum_{\sigma_1=\pm 1} (2s+\sigma_1+1)(2s+2\sigma_1+1) \\ & \times G^{s_{13}+1,s_{24}-(1-\sigma)/2}_{s_1,s_1,\sigma\sigma_1 s+\sigma(1+\sigma_1)/2} G^{s_{24},s_{13}+(1+\sigma)/2}_{s_1,s_1,\sigma\sigma_1 s+\sigma(1+\sigma_1)/2} \Bigg], \end{aligned} \tag{F13}$$

where $\tilde{g}_\sigma(\bar{\nu})$ and $h_{-,+}(\bar{\nu}) = \tilde{h}_{+,-}(\bar{\nu})$ are respectively obtained from $g_\sigma(\bar{\nu})$ and $h_{+,-}(\bar{\nu})$ by setting $s_{13} \leftrightarrow s_{24}$.

Letting $x = s_{13}$ and $y = s_{24}$, these expressions may be simplified to yield

$$\begin{aligned} h_{\sigma,\sigma}(s,x,y) = {} & -\delta_{s,0}\delta_{x,y} \frac{(2x+1+\sigma)}{2} \eta^2_{x+(1+\sigma)/2,s_1,s_1} \times \sqrt{(2x+2+\sigma)(2x+\sigma)} - (1-\delta_{s,0}) \frac{(x-y)^2}{s(s+1)} \\ & \times \eta_{x+(1+\sigma)/2,s_1,s_1} \eta_{y+(1+\sigma)/2,s_1,s_1} \end{aligned}$$

$$\times\sqrt{(x+y+1+\sigma)^2-s^2}$$
$$\times\sqrt{(x+y+1+\sigma)^2-(s+1)^2}, \tag{F14}$$

$$h_{+,-}(s,x,y)=\frac{(x+y+1)^2}{s(s+1)}\eta_{x,s_1,s_1}\eta_{y+1,s_1,s_1}$$
$$\times\sqrt{(s+1)^2-(x-y-1)^2}\sqrt{s^2-(x-y-1)^2}, \tag{F15}$$

$$g_\sigma(s,x,y)=\eta_{x+(1+\sigma)/2,s_1,s_1}\sqrt{[x+(1+\sigma)/2]^2-(y-s)^2}$$
$$\times\sqrt{(y+s+1)^2-[x+(1+\sigma)/2]^2}. \tag{F16}$$

The diagonal matrix elements of $\mathcal{H}^g_{\mathrm{b},1}$ and $\mathcal{H}^g_{\mathrm{t},1}$ are then easily found to be

$$\langle\nu|\mathcal{H}^g_{\mathrm{b},1}|\nu\rangle=-J^g_{\mathrm{b},1}\mathcal{B}_{\bar{\nu}}, \tag{F17}$$

$$\langle\nu|\mathcal{H}^g_{\mathrm{t},1}|\nu\rangle=-J^g_{\mathrm{t},1}\mathcal{T}_{\bar{\nu}}, \tag{F18}$$

where

$$\mathcal{B}_{\bar{\nu}}=\sum_{\sigma=\pm1}\left(h^2_{\sigma,\sigma}(\bar{\nu})+\frac{1}{16}[g^2_\sigma(\bar{\nu})+\tilde{g}^2_\sigma(\bar{\nu})]\right)+h^2_{+,-}(\bar{\nu})+\tilde{h}^2_{+,-}(\bar{\nu})$$
$$+\frac{1}{64}g^2_0(\bar{\nu}), \tag{F19}$$

$$\mathcal{T}_{\bar{\nu}}=\frac{g^2_0(\bar{\nu})}{64}-h^2_{+,-}(\bar{\nu})-\tilde{h}^2_{+,-}(\bar{\nu})-\sum_{\sigma=\pm1}h^2_{\sigma,\sigma}(\bar{\nu}), \tag{F20}$$

where we made use of the fact that

$$\sum_{n=2,4}\sin[(2n\pm1)\pi/4]=\sum_{n=1,3}\sin[(2n\pm1)\pi/4]=0, \tag{F21}$$

so that there are no contributions from $g_\sigma$ and $\tilde{g}_\sigma$ in Eq. (F20).

For $s_1=1/2$, the matrix $\langle\nu'|\mathcal{H}^g_{\mathrm{b},1}+\mathcal{H}^g_{\mathrm{t},1}|\nu\rangle$ is diagonal, so these interactions can be treated exactly, and are listed in Table IV. The analogous list of first-order parameters for $s_1=1$ is given in Table V. For $s_1\geqslant1$, since these quartic interactions preserve $s$ to the extent that the single-ion and exchange anisotropy interactions can be neglected or treated in first order only, the resulting matrix is block diagonal, as noted by Kostyuchenko.[50] In Table X, we present the exact eigenstates for $s_1=1$ of the Hamiltonian $\mathcal{H}^{g,r}_0+\mathcal{H}^g_{\mathrm{b}}+\mathcal{H}^g_{\mathrm{t}}$ for the six symmetries under consideration. Inclusion of the anisotropy interactions to first order can be made by using Table V.

In Tables VI and VII and Tables VIII and IX, we listed analytic formulas for the first-order anisotropy coefficients $a^\pm_{\bar{\nu}}$, $b^\pm_{\bar{\nu}}$, and $c^\pm_{\bar{\nu}}$ for the lowest four eigenstate manifolds of FM and AFM tetramers, respectively. In both cases, the manifolds are restricted by $0\leqslant s_{13}$, $s_{24}\leqslant 2s_1$ and $|s_{13}-s_{24}|\leqslant s\leqslant s_{13}+s_{24}$. In addition, the coefficients are symmetric under $s_{13}\leftrightarrow s_{24}$, as illustrated for $s_1=1/2,1$ in Tables IV and V. These tables provide the complete first-order set of anisotropy parameters for $s_1\leqslant 3/2$. Of the 54 distinct $s_1=2$ states, these formulas provide the anisotropy parameters for all but the nine $s=4$ states. General formulas for the anisotropy parameters and $\mathcal{B}_{\bar{\nu}}$ and $\mathcal{T}_{\bar{\nu}}$ are given by Eqs. (F1)–(F3), (F19), and (F20).

For type-I and II tetramers, the $s$th AFM level-crossing induction in the first-order approximation may be written as

$$\gamma B^{g,\mathrm{lc}(1)}_{s_1,s}(\theta)=-\tilde{J}_g s-\Theta(\tilde{J}'_g-\tilde{J}_g)2ss_1^2J^g_{\mathrm{t},2}+\Theta(\tilde{J}_g-\tilde{J}'_g)\Bigg\{[\tilde{J}_g-\tilde{J}'_g$$
$$+2s_1(s_1+1)J^g_{\mathrm{b},2}]E\left(\frac{s+1}{2}\right)-J^g_{\mathrm{b},2}\left[E\left(\frac{s+1}{2}\right)\right]^3$$
$$-J^g_{\mathrm{t},2}E\left(\frac{s}{2}\right)\left[sE\left(\frac{s+1}{2}\right)-2s_1(s_1+1)\right]\Bigg\}$$
$$-\frac{J^g_z}{2}(a^+_2+2b^++a^+_1\cos^2\theta)$$
$$+\frac{J^g_{1,z}}{2}\left[c^-_2+\frac{1}{2}(b^++b^-)+c^-_1\cos^2\theta\right]$$
$$+\frac{J^g_{2,z}}{4}(a^-_2+b^-+a^-_1\cos^2\theta)-J^g_{\mathrm{b},1}d-J^g_{\mathrm{t},1}e, \tag{F22}$$

where $\Theta(s)$ is the standard Heaviside step function, $E(x)$ is the largest integer in $x$, and the level-crossing parameters $a^\pm_j$, $b^\pm$, and $c^-_j$ for $j=1$, 2 and $d$ and $e$ are functions of $s$, $s_1$, and the tetramer type. For type II, the functions are different for even and odd $s$.

The AFM level-crossing parameters are defined according to

$$a^\pm_1=s(2s-1)a^{s_1,\pm}_{s,s_{13},s_{24}}-(s-1)(2s-3)a^{s_1,\pm}_{s-1,s'_{13},s'_{24}}, \tag{F23}$$

$$a^\pm_2=sa^{s_1,\pm}_{s,s_{13},s_{24}}-(s-1)a^{s_1,\pm}_{s-1,s'_{13},s'_{24}}, \tag{F24}$$

$$b^\pm=b^{s_1,\pm}_{s,s_{13},s_{24}}-b^{s_1,\pm}_{s-1,s'_{13},s'_{24}}, \tag{F25}$$

$$c^-_1=s(2s-1)c^{s_1,-}_{s,s_{13},s_{24}}-(s-1)(2s-3)c^{s_1,-}_{s-1,s'_{13},s'_{24}}, \tag{F26}$$

$$c^-_2=sc^{s_1,-}_{s,s_{13},s_{24}}-(s-1)c^{s_1,-}_{s-1,s'_{13},s'_{24}}, \tag{F27}$$

$$d=\mathcal{B}_{\bar{\nu}}-\mathcal{B}_{\bar{\nu}'}, \tag{F28}$$

$$e=\mathcal{T}_{\bar{\nu}}-\mathcal{T}_{\bar{\nu}'}, \tag{F29}$$

where

$$\bar{\nu}'=\{s-1,s'_{13},s'_{24}\} \tag{F30}$$

and the $s'_{13}$ and $s'_{24}$ values depend on the tetramer type. In Appendixes G and H, we evaluate $a^\pm_j$, $b^\pm$, $c^-_j$, $d$, and $e$ for type-I and type-II AFM tetramers.

For $s_1=1/2$, type-I and II first-order level-crossing inductions $\gamma B^{g,\mathrm{lc}(1)}_{1/2,s}(\theta)$ are given in the text. In that simplest ex-

ample, there are no effects of single-ion anisotropy. Hence, to illustrate the full dependencies on all of the microscopic parameters under study, we list the $s_1=1$ first-order level-crossing inductions. For type I, we have

$$\gamma B_{1,1}^{g,\mathrm{lc}(1)}(\theta) = -\widetilde{J}_g + \frac{1}{12}(35J_{\mathrm{b},1}^g + 13J_{\mathrm{t},1}^g) - 2J_{\mathrm{t},2}^g - J_z^g\left(\frac{7}{6} - \frac{7}{10}\cos^2\theta\right) + \frac{7}{10}J_{\mathrm{eff}}^g(1-3\cos^2\theta), \tag{F31}$$

$$\gamma B_{1,2}^{g,\mathrm{lc}(1)}(\theta) = -2\widetilde{J}_g + 2J_{\mathrm{b},1}^g + 4J_{\mathrm{t},1}^g - 4J_{\mathrm{t},2}^g + J_z^g\left(\frac{31}{42} - \frac{19}{70}\cos^2\theta\right) - \frac{19}{70}J_{\mathrm{eff}}^g(1-3\cos^2\theta), \tag{F32}$$

$$\gamma B_{1,3}^{g,\mathrm{lc}(1)}(\theta) = -3\widetilde{J}_g + \frac{1}{4}(7J_{\mathrm{b},1}^g - 9J_{\mathrm{t},1}^g) - 6J_{\mathrm{t},2}^g + J_z^g\left(\frac{181}{210} - \frac{13}{14}\cos^2\theta\right) - \frac{13}{14}J_{\mathrm{eff}}^g(1-3\cos^2\theta), \tag{F33}$$

$$\gamma B_{1,4}^{g,\mathrm{lc}(1)}(\theta) = -4\widetilde{J}_g - 4J_{\mathrm{t},1}^g - 8J_{\mathrm{t},2}^g + J_z^g\left(\frac{83}{70} - \frac{3}{2}\cos^2\theta\right) - \frac{3}{2}J_{\mathrm{eff}}^g(1-3\cos^2\theta). \tag{F34}$$

The type-II first-order level-crossing inductions for $s_1=1$ are

$$\gamma B_{1,1}^{g,\mathrm{lc}(1)}(\theta) = -\widetilde{J}_g' - \frac{1}{3}(11J_{\mathrm{b},1}^g + 9J_{\mathrm{t},1}^g) + 3J_{\mathrm{b},2}^g - \frac{J_z^g}{6}(5-3\cos^2\theta) + \frac{J_{2,z}^g}{6}(1+3\cos^2\theta), \tag{F35}$$

$$\gamma B_{1,2}^{g,\mathrm{lc}(1)}(\theta) = -\widetilde{J}_g - \widetilde{J}_g' + \frac{1}{12}(15J_{\mathrm{b},1}^g + 23J_{\mathrm{t},1}^g) + 3J_{\mathrm{b},2}^g + 2J_{\mathrm{t},2}^g + \frac{J_z^g}{2}(5+\cos^2\theta) + \frac{J_{1,z}^g}{2}(1+\cos^2\theta) + \frac{J_{2,z}^g}{6}(1+3\cos^2\theta), \tag{F36}$$

$$\gamma B_{1,3}^{g,\mathrm{lc}(1)}(\theta) = -\widetilde{J}_g - 2\widetilde{J}_g' + \frac{1}{36}(107J_{\mathrm{b},1}^g + 179J_{\mathrm{t},1}^g) - 2J_{\mathrm{t},2}^g + J_z^g\left(\frac{43}{30} - \frac{3}{2}\cos^2\theta\right) + \frac{J_{1,z}^g}{6}(1+5\cos^2\theta) + \frac{J_{2,z}^g}{2}(1+\cos^2\theta), \tag{F37}$$

$$\gamma B_{1,4}^{g,\mathrm{lc}(1)}(\theta) = -2\widetilde{J}_g - 2\widetilde{J}_g' + \frac{1}{9}(7J_{\mathrm{b},1}^g - 29J_{\mathrm{t},1}) - 8J_{\mathrm{t},2}^g + J_z^g\left(\frac{83}{70} - \frac{3}{2}\cos^2\theta\right) + \frac{J_{1,z}^g}{3}(1+5\cos^2\theta) + \frac{J_{2,z}^g}{2}(1+\cos^2\theta). \tag{F38}$$

## APPENDIX G: TYPE-I FIRST-ORDER ANTIFERROMAGNETIC LEVEL-CROSSING CONSTANTS

The type-I constants are relevant for both $\widetilde{J}_g'-\widetilde{J}_g>0$ AFM level-crossing inductions and for some low energy FM manifold states (with $\widetilde{J}_g'>\widetilde{J}_g>0$). We let $a_{s,s_{13},s_{24}}^{s_1,\pm}\equiv a_{\bar{\nu}}^{\pm}$. For general $s$ and $s_1$, we have

$$a_{s,2s_1,2s_1}^{s_1,\pm} = c_{s,2s_1,2s_1}^{s_1,-}\left(1 \mp \frac{1}{4s_1-1}\right), \tag{G1}$$

$$b_{s,2s_1,2s_1}^{s_1,\pm} = \frac{1}{2(2s+3)(2s-1)}\Big[s(s+1) + [2s(s+1)-1] \times [8s_1(2s_1+1) - s(s+1)] \pm \frac{1}{4s_1-1}\{2[16s_1^2 + s(s+1)][s(s+1)-1] - 8s_1[2s(s+1)-1]\}\Big], \tag{G2}$$

$$c_{s,2s_1,2s_1}^{s_1,-} = \frac{3[s(s+1)-1] - 8s_1(2s_1+1)}{2(2s-1)(2s+3)}, \tag{G3}$$

$$\mathcal{B}_{s,2s_1,2s_1}^{s_1} = \frac{1}{16}[s(s+1) - 4s_1(2s_1+1)]^2 + \frac{s(s+1)(4s_1-s)(s+4s_1+1)}{8(4s_1-1)} + \frac{s_1^2(4s_1+1)}{(4s_1-1)}\delta_{s,0}, \tag{G4}$$

$$\mathcal{T}_{s,2s_1,2s_1}^{s_1} = \frac{1}{16}[s(s+1) - 4s_1(2s_1+1)]^2 - \frac{s_1^2(4s_1+1)}{(4s_1-1)}\delta_{s,0}. \tag{G5}$$

From these expressions, we may evaluate the type-I first-order level-crossing inductions for AFM tetramers. From Eq.

(60) and the definitions of the level-crossing constants in Eqs. (F23)–(F30), we rewrite them to explicitly indicate the $s_1$, $s$, and type dependencies, and for type I, it is easy to show that

$$a_{I,j}^{s_1,\pm}(s) = c_{I,j}^{s_1,-}(s)\left(1 \mp \frac{1}{4s_1 - 1}\right), \tag{G6}$$

$$b_I^{s_1,\pm}(s) = -\frac{2s[8s_1(2s_1+1) + 4s^4 - 10s^2 + 3]}{(4s^2-1)(4s^2-9)}\left(1 \mp \frac{1}{4s_1 - 1}\right), \tag{G7}$$

$$c_{I,1}^{s_1,-}(s) = \frac{3[4s^3 + 5s^2 - 3s - 3 - 8s_1(2s_1+1)]}{2(2s+1)(2s+3)}, \tag{G8}$$

$$c_{I,2}^{s_1,-}(s) = \frac{3(4s^4 - 9s^2 - s + 3) + (4s^2 - 4s + 3)8s_1(2s_1+1)}{2(4s^2-1)(4s^2-9)}, \tag{G9}$$

$$d_I^{s_1}(s) = \frac{s[s^2(4s_1 - 3) + 8s_1(s_1 + 1 - 4s_1^2)]}{4(4s_1 - 1)} - \frac{s_1^2(4s_1+1)}{(4s_1-1)}\delta_{s,1}, \tag{G10}$$

$$e_I^{s_1}(s) = \frac{s}{4}[s^2 - 4s_1(2s_1+1)] + \frac{s_1^2(4s_1+1)}{(4s_1-1)}\delta_{s,1}, \tag{G11}$$

for $j=1$ and 2. For $s_1=1/2$, it is easy to see that $a_{I,j}^{1/2,+}(s) = b_I^{1/2,+}(s)=0$ for $s=1$ and 2, as expected.

Letting $a_{I,j}^{s_1,\pm}(s)=a_j^{\pm}$, $b_I^{s_1,\pm}(s)=b^{\pm}$, and $c_{I,j}^{s_1,-}(s)=c_j^-$, it is easy to show that for type-I tetramers,

$$c_2^- + \frac{1}{2}(b^+ + b^-) = -\frac{1}{3}c_1^-, \tag{G12}$$

$$a_2^- + b^- = -\frac{1}{3}a_1^- = -\frac{4s_1}{3(4s_1-1)}c_1^-. \tag{G13}$$

This implies that for type I, the axial NN and NNN anisotropic exchange interactions may be combined to yield an effective axial anisotropic exchange interaction given by Eq. (64).

For the single-ion contributions to the level-crossing inductions, no such simple relation can be found. We note that

$$a_2^+ + b^+ = -\frac{1}{3}a_1^+, \tag{G14}$$

but the overall quantity $a_2^+ + 2b^+ + a_1^+ \cos^2\theta$ in Eq. (F22) contains the extra quantity $b^+$, which depends on $s$ and $s_1$.

## APPENDIX H: TYPE-II FIRST-ORDER ANTIFERROMAGNETIC LEVEL-CROSSING CONSTANTS

For type-II AFM tetramers with even $s$, the relevant parameters are

$$a_{s,s/2,s/2}^{s_1,\pm} = \frac{1}{2(2s-1)}\left(s - 1 \mp \frac{[16s_1(s_1+1) - s^2 - 2s + 6]}{2(s+3)}\right), \tag{H1}$$

$$b_{s,s/2,s/2}^{s_1,\pm} = \frac{1}{2(2s-1)}\left(s^2 \pm \frac{[16s_1(s_1+1)(s^2+2s-1) - s(s^3+4s^2+s-4)]}{s+3}\right), \tag{H2}$$

$$c_{s,s/2,s/2}^{-} = \frac{s-1}{2(2s-1)}, \tag{H3}$$

$$\mathcal{B}_{s,s/2,s/2}^{s_1} = \frac{s^4}{64} + \frac{s(s+1)[16s_1(s_1+1) - s(s+4)]}{16(s+3)} + (1-\delta_{s,0})\frac{(s+1)[16s_1(s_1+1) - s^2 + 4]}{128s(s+3)}(s+2)[16s_1(s_1+1) - s(s+4)] + \delta_{s,0}\frac{4s_1^2(s_1+1)^2}{3}, \tag{H4}$$

$$\mathcal{T}_{s,s/2,s/2}^{s_1} = \frac{s^4}{64} - \delta_{s,0}\frac{4s_1^2(s_1+1)^2}{3} - (1-\delta_{s,0})\frac{(s+1)[16s_1(s_1+1) - s^2 + 4]}{128s(s+3)}(s+2)[16s_1(s_1+1) - s(s+4)]. \tag{H5}$$

For odd $s$, the relevant parameters are

$$a_{s,(s+1)/2,(s-1)/2}^{s_1,\pm} = \frac{1}{2s(2s-1)}\left(s^2 - s + 1 \mp \frac{[16s_1(s_1+1)(s^2+3s-1) - s^4 - 5s^3 + 11s - 11]}{2(s+2)(s+4)}\right), \tag{H6}$$

$$b_{s,(s+1)/2,(s-1)/2}^{s_1,\pm} = \frac{1}{2(2s-1)}\left(s^2 - 1 \pm \frac{[16s_1(s_1+1)(s^3+5s^2+4s-3) - (s+1)(s^4+6s^3+7s^2-3s+1)]}{(s+2)(s+4)}\right), \tag{H7}$$

$$c^{-}_{s,(s+1)/2,(s-1)/2} = \frac{(s+1)(s-1)^2}{2s^2(2s-1)}, \tag{H8}$$

$$\mathcal{B}^{s_1}_{s,(s+1)/2,(s-1)/2} = \frac{(s^2-1)^2}{64} + \frac{(s+1)^2}{32(s+2)}[16s_1(s_1+1)-(s+3)(s-1)] + [16s_1(s_1+1)-(s+3)(s-1)]^2\frac{(s+1)^4}{256s^2(s+2)^2}$$
$$+ [16s_1(s_1+1)-(s+3)(s-1)][16s_1(s_1+1)-(s+5)(s+1)]\frac{(2s+3)(s^2-2s-1)^2}{256s^3(s+1)(s+4)(2s+1)^2}, \tag{H9}$$

$$\mathcal{T}^{s_1}_{s,(s+1)/2,(s-1)/2} = \frac{(s^2-1)^2}{64} - \frac{(s+1)^4}{256s^2(s+2)^2}[16s_1(s_1+1)-(s+3)(s-1)]^2 - [16s_1(s_1+1)-(s+3)(s-1)]$$
$$\times[16s_1(s_1+1)-(s+5)(s+1)]\frac{(2s+3)(s^2-2s-1)^2}{256s^3(s+1)(s+4)(2s+1)^2}. \tag{H10}$$

From these expressions, we may obtain the type-II AFM level-crossing induction parameters by using Eqs. (61), (62), and (F23)–(F30). For even $s$, we find

$$a^{s_1,\pm}_{II\mathrm{e},1}(s) = \frac{2s-3}{2} \mp \frac{48s_1(s_1+1)-2s^3-5s^2+6s+18}{4(s+1)(s+3)}, \tag{H11}$$

$$a^{s_1,\pm}_{II\mathrm{e},2}(s) = \frac{1}{2(2s-1)(2s-3)}\left[2s^2-6s+3 \pm \frac{16s_1(s_1+1)(2s^2-4s+3)+2s^4+2s^3-9s^2-18s+18}{2(s+1)(s+3)}\right], \tag{H12}$$

$$b^{s_1,\pm}_{II\mathrm{e}}(s) = \frac{s}{(2s-1)(2s-3)}\left[s-1 \pm \frac{16s_1(s_1+1)(s-2)-4s^4-7s^3+20s^2+14s-18}{2(s+1)(s+3)}\right], \tag{H13}$$

$$c^{-}_{II\mathrm{e},1}(s) = \frac{s(2s-3)}{2(s-1)}, \tag{H14}$$

$$c^{-}_{II\mathrm{e},2}(s) = \frac{s(2s^2-4s+1)}{2(s-1)(2s-1)(2s-3)}, \tag{H15}$$

$$d^{s_1}_{II\mathrm{e}}(s) = \mathcal{B}^{s_1}_{s,s/2,s/2} - \mathcal{B}^{s_1}_{s-1,s/2,(s-2)/s}, \tag{H16}$$

$$e^{s_1}_{II\mathrm{e}}(s) = \mathcal{T}^{s_1}_{s,s/2,s/2} - \mathcal{T}^{s_1}_{s-1,s/2,(s-2)/s}. \tag{H17}$$

Combining $a^{s_1,-}_{II\mathrm{e},2}(s)$ and $b^{s_1,-}_{II\mathrm{e}}(s)$, we find

$$a^{s_1,-}_{II\mathrm{e},2} + b^{s_1,-}_{II\mathrm{e}} = \frac{1}{2} - \frac{16s_1(s_1+1)-(2s^3+7s^2+2s-6)}{4(s+1)(s+3)}. \tag{H18}$$

We note that this expression substantially differs from that for $a^{s_1,-}_{II\mathrm{e},1}(s)$, except for $s_1=1/2$ and $s=2$. Similarly, it is elementary to combine $c^{-}_{II\mathrm{e},2}(s)$ and $[b^{s_1,+}_{II\mathrm{e}}(s)+b^{s_1,-}_{II\mathrm{e}}(s)]/2$. We find

$$c^{-}_{II\mathrm{e},2}(s) + \frac{1}{2}[b^{s_1,+}_{II\mathrm{e}}(s) + b^{s_1,-}_{II\mathrm{e}}(s)] = \frac{s}{2(s-1)}. \tag{H19}$$

This simple expression differs from that for $c^{-}_{II\mathrm{e},1}(s)$ by a factor $2s-3$. However, at $s=2$, the only even $s$ value for $s_1=1/2$, they are equivalent. In addition, as for type I, there is no simple relation between the single-ion parameters $a^{s_1,+}_{II\mathrm{e},2}(s)+2b^{s_1,+}_{II\mathrm{e}}(s)$ and $a^{s_1,+}_{II\mathrm{e},1}(s)$.

For odd $s$, the type-II level-crossing induction parameters are

$$a^{s_1,\pm}_{II\mathrm{o},1}(s) = \frac{2s-1}{2} \mp \frac{48s_1(s_1+1)-2s^3-11s^2-10s+17}{4(s+2)(s+4)}, \tag{H20}$$

$$a^{s_1,\pm}_{II\mathrm{o},2}(s) = \frac{1}{2(2s-1)(2s-3)}\left[2s^2-2s-1 \pm \frac{16s_1(s_1+1)(2s^2+1)+2s^4+10s^3+9s^2-22s-5}{2(s+2)(s+4)}\right], \tag{H21}$$

$$b_{IIo}^{s_1,\pm}(s)=\frac{1}{(2s-1)(2s-3)}\left[(s-1)(s-2)\pm\frac{16s_1(s_1+1)(s^2-4s+1)-4s^5-19s^4+54s^2-2s-5}{2(s+2)(s+4)}\right], \tag{H22}$$

$$c_{IIo,1}^{-}(s)=\frac{(s-1)(2s-1)}{2s}, \tag{H23}$$

$$c_{IIo,2}^{-}(s)=\frac{(s-1)(2s^2-4s+3)}{2s(2s-1)(2s-3)}, \tag{H24}$$

$$d_{IIo}^{s_1}(s)=\mathcal{B}_{s,(s+1)/2,(s-1)/2}^{s_1}-\mathcal{B}_{s-1,(s-1)/2,(s-1)/2}^{s_1}, \tag{H25}$$

$$e_{IIo}^{s_1}(s)=\mathcal{T}_{s,(s+1)/2,(s-1)/2}^{s_1}-\mathcal{T}_{s-1,(s-1)/2,(s-1)/2}^{s_1}, \tag{H26}$$

where, for $s=1$, the last two equations reduce to

$$d_{IIo}^{s_1}(1)=\frac{s_1}{6}(4s_1^3+8s_1^2+7s_1+3), \tag{H27}$$

$$e_{IIo}^{s_1}(1)=-\frac{s_1}{6}(4s_1^3+8s_1^2+3s_1-1). \tag{H28}$$

We note that $a_{IIe,j}^{1/2,+}(2)=a_{IIo,j}^{1/2,+}(1)=b_{IIe}^{1/2,+}(2)=b_{IIo}^{1/2,+}(1)=0$ for $j=1$ and 2, as expected. However, by combining $a_{IIo,2}^{s_1,-}(s)$ and $b_{IIo}^{s_1,-}(s)$, we have

$$a_{IIo,2}^{s_1,-}+b_{IIo}^{s_1,-}=\frac{1}{2}-\frac{16s_1(s_1+1)-(2s^3+13s^2+22s+5)}{4(s+2)(s+4)}, \tag{H29}$$

which substantially differs from the version with $s_1=1/2$. In addition, it is elementary to combine $c_{IIo,2}^{-}(s)+[b_{IIo}^{s_1,+}(s)+b_{IIo}^{s_1,-}(s)]/2$. We find

$$c_{IIo,2}^{-}(s)+\frac{1}{2}[b_{IIo}^{s_1,+}(s)+b_{IIo}^{s_1,-}(s)]=\frac{(s-1)}{2s}, \tag{H30}$$

which differs from $c_{IIo,1}^{-}(s)$ by a factor $2s-1$. At $s=1$, the only relevant odd $s$ value for $s_1=1/2$, these are equivalent. In addition, as for type I and the even crossings of type II, there is no simple relation between the single-ion parameters $a_{IIo,2}^{s_1,+}(s)+2b_{IIo}^{s_1,+}(s)$ and $a_{IIo,1}^{s_1,+}(s)$.

## APPENDIX I: HARTREE INELASTIC NEUTRON SCATTERING FUNCTIONS

The functions $L_{\nu,\nu'}(\boldsymbol{q})$ and $M_{\nu,\nu'}(\boldsymbol{q})$ in the self-consistent Hartree INS $S_g^{(1)}(\boldsymbol{q},\omega)$ in the induction representation are given by

$$L_{\nu,\nu'}(\boldsymbol{q})=\delta_{m',m}\delta_{s'_{24},s_{24}}\Bigg[m^2\delta_{s',s}\Bigg(\delta_{s'_{13},s_{13}}f_{\bar{\nu},0}(\boldsymbol{q})+\sum_{\sigma''=\pm1}\delta_{s'_{13},s_{13}+\sigma''}f_{\bar{\nu},1}^{\sigma''}(\boldsymbol{q})\Bigg)+\sum_{\sigma'=\pm1}\delta_{s',s+\sigma'}(C_{-\sigma's-(\sigma'+1)/2}^{m})^2\Bigg(\delta_{s'_{13},s_{13}}f_{\bar{\nu},2}^{\sigma'}(\boldsymbol{q})+\sum_{\sigma''=\pm1}\delta_{s'_{13},s_{13}+\sigma''}f_{\bar{\nu},3}^{\sigma',\sigma''}(\boldsymbol{q})\Bigg)\Bigg]+\begin{pmatrix}s_{13}\leftrightarrow s_{24}\\ s'_{13}\leftrightarrow s'_{24}\\ q_y\rightarrow -q_y\end{pmatrix}, \tag{I1}$$

$$M_{\nu,\nu'}(\boldsymbol{q})=\sum_{\sigma=\pm1}\delta_{m',m+\sigma}\delta_{s'_{24},s_{24}}\Bigg[(A_s^{\sigma m})^2\delta_{s',s}\Bigg(\delta_{s'_{13},s_{13}}f_{\bar{\nu},0}(\boldsymbol{q})+\sum_{\sigma''=\pm1}\delta_{s'_{13},s_{13}+\sigma''}f_{\bar{\nu},1}^{\sigma''}(\boldsymbol{q})\Bigg)+\sum_{\sigma'=\pm1}\delta_{s',s+\sigma'}(D_{-\sigma's-(\sigma'+1)/2}^{\sigma,m})^2\Bigg(\delta_{s'_{13},s_{13}}f_{\bar{\nu},2}^{\sigma'}(\boldsymbol{q})+\sum_{\sigma''=\pm1}\delta_{s'_{13},s_{13}+\sigma''}f_{\bar{\nu},3}^{\sigma',\sigma''}(\boldsymbol{q})\Bigg)\Bigg]+\begin{pmatrix}s_{13}\leftrightarrow s_{24}\\ s'_{13}\leftrightarrow s'_{24}\\ q_y\rightarrow -q_y\end{pmatrix}, \tag{I2}$$

$$f_{\bar{\nu},0}(\boldsymbol{q})=\frac{1}{8}[f_+(\boldsymbol{q})+\xi_{s,s_{13},s_{24}}^2f_-(\boldsymbol{q})-2\xi_{s,s_{13},s_{24}}\sin(q_xa)\sin(q_ya)], \tag{I3}$$

$$f_{\bar{\nu},1}^{\sigma''}(\boldsymbol{q})=2\{1-\cos[a(q_x+q_y)]\}(F_{s_1,s_1,s}^{s_{13}+(\sigma''+1)/2,s_{24}})^2, \tag{I4}$$

$$f_{\bar{\nu},2}^{\sigma'}(\boldsymbol{q})=\frac{1}{8}f_-(\boldsymbol{q})\,\eta_{s+(\sigma'+1)/2,s_{13},s_{24}}^2, \tag{I5}$$

$$f_{\bar{\nu},3}^{\sigma',\sigma''}(\boldsymbol{q})=2\{1-\cos[a(q_x+q_y)]\}(G_{s_1,s_1,\sigma'\sigma''s+\sigma''(\sigma'+1)/2}^{s_{13}+(\sigma''+1)/2,s_{24}})^2, \tag{I6}$$

$$f_\pm(\boldsymbol{q})=1+\cos(q_xa)\cos(q_ya)\pm\cos(q_zc)[\cos(q_xa)+\cos(q_ya)], \tag{I7}$$

where $A_s^m$, $C_s^m$, $D_s^{\tilde{\sigma},m}$, $F_{s_1,s_3,s}^{s_{13},s_{24}}$, $G_{s_1,s_3,s}^{s_{13},s_{24}}$, $\eta_{z,x,y}$, and $\xi_{z,x,y}$ are given by Eqs. (51), (E3), (E4), and (E9)–(E12), respectively.

*klemm@physics.ucf.edu
†efremov@theory.phy.tu-dresden.de

[1] R. Sessoli, D. Gatteschi, A. Caneschi, and M. Novak, Nature (London) **365**, 141 (1993); W. Wernsdorfer and R. Sessoli, Science **284**, 133 (1999).
[2] M. N. Leuenberger and D. Loss, Nature (London) **410**, 789 (2001).
[3] D. V. Efremov and R. A. Klemm, Phys. Rev. B **66**, 174427 (2002).
[4] R. A. Klemm and D. V. Efremov, in *24th International Conference on Low Temperature Physics*, edited by Y. Takano *et al.*, AIP Conf. Proc. No. 850 (AIP, New York, 2006), p. 1151.
[5] D. V. Efremov and R. A. Klemm, Phys. Rev. B **74**, 064408 (2006).
[6] Y. Shapira, M. T. Liu, S. Foner, C. E. Dubé, and P. J. Bonitatebus Jr., Phys. Rev. B **59**, 1046 (1999).
[7] C. Mennerich, H.-H. Klauss, M. Broekelmann, F. J. Litterst, C. Golze, R. Klingeler, V. Kataev, B. Büchner, S.-N. Grossjohann, W. Brenig, M. Goiran, H. Rakoto, J.-M. Broto, O. Kataeva, and D. J. Price, Phys. Rev. B **73**, 174415 (2006).
[8] D. Zipse, J. M. North, N. S. Dalal, S. Hill, and R. S. Edwards, Phys. Rev. B **68**, 184408 (2003).
[9] S. Carretta, E. Liviotti, N. Magnani, P. Santini, and G. Amoretti, Phys. Rev. Lett. **92**, 207205 (2004).
[10] D. Zipse, N. S. Dalal, R. M. Achey, J. M. North, S. Hill, and R. S. Edwards, Appl. Magn. Reson. **27**, 151 (2004).
[11] S. Hill, R. S. Edwards, J. M. North, S. Maccagnano, and N. S. Dalal, Polyhedron **22**, 1897 (2003).
[12] R. S. Rubins, T. D. Black, and J. Barak, J. Chem. Phys. **85**, 3770 (1985).
[13] T. D. Black, R. S. Rubins, D. K. De, R. C. Dickinson, and W. A. Baker, Jr., J. Chem. Phys. **80**, 4620 (1984).
[14] R. C. Dickinson, W. A. Baker, Jr., T. D. Black, and R. S. Rubins, J. Chem. Phys. **79**, 2609 (1983).
[15] E. Buluggiu, J. Chem. Phys. **84**, 1243 (1986).
[16] A. Bino, D. C. Johnston, D. P. Goshorn, T. R. Halbert, and E. I. Stiefel, Science **241**, 1479 (1988).
[17] E.-C. Yang, D. N. Hendrickson, W. Wernsdorfer, M. Nakano, L. N. Zakharov, R. D. Sommer, A. L. Rheingold, M. Ledezma-Gairaud, and G. Christou, J. Appl. Phys. **91**, 7382 (2002).
[18] A. Sieber, C. Boskovic, R. Bircher, O. Waldmann, W. T. Ochsenbein, G. Chaboussant, H. U. Güdel, N. Kirchner, J. van Slageren, W. Wernsdorfer, A. Neels, H. Stoeckli-Evans, S. Jannsen, F. Juranyi, and H. Mutka, Inorg. Chem. **44**, 4315 (2005), and references therein.
[19] M. Moragues-Cánovas, M. Helliwell, L. Ricard, Éric Rivière, W. Wernsdorfer, E. Brechin, and T. Mallah, Eur. J. Inorg. Chem. **2004**, 2219.
[20] R. S. Edwards, S. Maccagnano, E.-C. Yang, S. Hill, W. Wernsdorfer, D. Hendrickson, and G. Christou, J. Appl. Phys. **93**, 7807 (2003).
[21] E. del Barco, A. D. Kent, E.-C. Yang, and D. N. Hendrickson, Polyhedron **24**, 2695 (2005).
[22] D. N. Hendrickson, E.-C. Yang, R. M. Isidro, C. Kirman, J. Lawrence, R. S. Edwards, S. Hill, A. Yamaguchi, H. Ishimoto, W. Wernsdorfer, C. Ramsey, N. Dalal, and M. M. Olmstead, Polyhedron **24**, 2280 (2005).
[23] C. Boskovic, R. Bircher, P. L. W. Tregenna-Piggott, H. U. Güdel, C. Paulsen, W. Wernsdorfer, A.-L. Barra, E. Khatsko, A. Neels, and H. Stoeckli-Evans, J. Am. Chem. Soc. **125**, 14046 (2003).
[24] K. Park, M. R. Pederson, and C. S. Hellberg, Phys. Rev. B **69**, 014416 (2004).
[25] J. Ribas-Arino, T. Baruah, and M. R. Pederson, J. Chem. Phys. **123**, 044303 (2005).
[26] A. V. Postnikov, J. Kortus, and M. R. Pederson, Phys. Status Solidi B **243**, 2533 (2006).
[27] S. Stolbov, R. A. Klemm, and T. S. Rahman, arXiv:cond-mat/0501178 (unpublished).
[28] K. Park, M. R. Pederson, and N. Bernstein, J. Phys. Chem. Solids **65**, 805 (2004).
[29] M. R. Pederson (private communication).
[30] D. W. Boukhvalov, M. Al-Sager, E. Z. Kurmaev, A. Moewes, V. R. Galakhov, L. D. Finkelstein, S. Chiuzbaian, M. Neumann, V. V. Dobrovitski, M. I. Katsnelson, A. I. Lichtenstein, B. N. Harmon, K. Endo, J. M. North, and N. S. Dalal, Phys. Rev. B **75**, 014419 (2007).
[31] R. Boča, *Theoretical Foundations of Molecular Magnetism* (Elsevier, Amsterdam, 1999).
[32] O. Waldmann and H. U. Güdel, Phys. Rev. B **72**, 094422 (2005).
[33] M. Tinkham, *Group Theory and Quantum Mechanics* (McGraw-Hill, New York, 1964).
[34] R. A. Klemm and M. Ameduri, Phys. Rev. B **66**, 012403 (2002).
[35] D. M. Barnhart, D. L. Clark, J. C. Gordon, J. C. Huffman, J. G. Watkin, and B. D. Zwick, J. Am. Chem. Soc. **115**, 8461 (1993).
[36] R. A. Klemm and M. Luban, Phys. Rev. B **64**, 104424 (2001).
[37] A. Bencini and D. Gatteschi, *Electron Paramagnetic Resonance of Exchange Coupled Systems* (Springer, Berlin, 1990).
[38] T. Moriya, Phys. Rev. **120**, 91 (1960).
[39] I. Dzyaloshinskii, J. Phys. Chem. Solids **4**, 241 (1958).
[40] J. D. Jackson, *Classical Electrodynamics*, 3rd ed. (Wiley, Hoboken, NJ, 1999), p. 186.
[41] H. Goldstein, *Classical Mechanics* (Addison-Wesley, Reading, MA, 1965), p. 109.
[42] M. A. Ortigoza, R. A. Klemm, and T. S. Rahman, Phys. Rev. B **72**, 174416 (2005).
[43] R. Valenti, C. Gros, and W. Brenig, Phys. Rev. B **62**, 14164 (2000).
[44] H. Katsura, N. Nagaosa, and A. V. Balatsky, Phys. Rev. Lett. **95**, 057205 (2005).
[45] S.-W. Cheong and M. Mostovoy, Nat. Mater. **6**, 13 (2007).
[46] J. Schnack, M. Brüger, M. Luban, P. Kögerler, E. Morosan, R. Fuchs, R. Modler, H. Nojiri, R. C. Rai, J. Cao, J. L. Musfeldt, and X. Wei, Phys. Rev. B **73**, 094401 (2006).
[47] O. Waldmann, J. Hassmann, P. Müller, D. Volkmer, U. S. Schubert, and J.-M. Lehn, Phys. Rev. B **58**, 3277 (1998).
[48] O. Waldmann, Coord. Chem. Rev. **249**, 2550 (2005).
[49] R. A. Klemm, C. T. Rieck, and K. Scharnberg, Phys. Rev. B **61**, 5913 (2000).
[50] V. V. Kostyuchenko, Phys. Rev. B **76**, 212404 (2007).
[51] D. V. Efremov and R. A. Klemm (unpublished).
[52] S. Carretta, P. Santini, G. Amoretti, T. Guidi, R. Caciuffo, A. Candini, A. Cornia, D. Gatteschi, M. Plazanet, and J. A. Stride, Phys. Rev. B **70**, 214403 (2004).
[53] A. Cornia, A. C. Fabretti, P. Garrisi, C. Mortalò, D. Bonacchi, D. Gatteschi, R. Sessoli, L. Sorace, W. Wernsdorfer, and A.-L. Barra, Angew. Chem., Int. Ed. **43**, 1136 (2004).
[54] E. Rastelli and A. Tossi, Phys. Rev. B **75**, 134414 (2007).
[55] G. Amoretti, S. Carretta, R. Caciuffo, H. Casalta, A. Cornia, M. Affronte, and D. Gatteschi, Phys. Rev. B **64**, 104403 (2001).
[56] J. M. Clemente-Juan, H. Andres, J. J. Borrás-Almenar, E. Coro-

nado, H. U. Güdel, M. Aebersold, G. Kearly, H. Büttner, and M. Zolliker, J. Am. Chem. Soc. **121**, 10021 (1999).
[57] L. Lecren, W. Wernsdorfer, Y.-G. Li, O. Roubeau, H. Miyasaka, and R. Clérac, J. Am. Chem. Soc. **127**, 11311 (2005).
[58] M. Koikawa, M. Ohba, and T. Tokii, Polyhedron **24**, 2257 (2005).
[59] J.-N. Rebilly, L. Catala, E. Rivière, R. Guillot, W. Wernsdorfer, and T. Mallah, Inorg. Chem. **44**, 8194 (2005).
[60] M. Ameduri and R. A. Klemm, J. Phys. A **37**, 1095 (2004).
[61] J. Cao, J. L. Musfeldt, M. Pederson, R. A. Klemm, and P. Kögerler (unpublished).